DETERMINANTS OF OSTEON GEOMETRIC PARAMETERS AND THEIR RELATION WITH AGE IN CORTICAL BONE

A Thesis Submitted to the College

of Graduate Studies and Research

in Partial Fulfilment of the Requirements

for the Degree of Masters of Science

in the Department of Anatomy and Cell Biology

University of Saskatchewan

Saskatoon

By

CHERYL HENNIG

PERMISSION TO USE

In presenting this thesis in partial fulfilment of the requirements for a Postgraduate degree from the University of Saskatchewan, I agree that the Libraries of this University may make it free available for inspection. I further agree that permission for copying of this thesis in any manner in whole or in part, for scholarly purposes may be granted by the professor of professors who supervised my thesis work or, in their absence, the Head of the Department or Dean of the College in which my thesis work was done. It is understood that due recognition shall be given to me and the University of Saskatchewan in any scholarly use which may be made of any material in my thesis

Request for permission to copy or to make other use of material in this thesis in whole or in part should be addressed to:

Head of the Department of Anatomy and Cell Biology

University of Saskatchewan

Saskatoon, Saskatchewan S7N 5E5

Canada

ABSTRACT

It is recognized that utilizing 3D technology can provide greater insights into the dynamics of bone tissue. Past studies investigating the microstructure of cortical bone have predominantly used histology, a 2D form of analysis, to evaluate the age-related differences that occur within the histological structures of bone. Many of these studies have developed age-regression formulae to estimate age at death from the observed differences within the microstructure. The objective of this thesis was to integrate histology with high-resolution micro-CT to assess the age-related differences of cortical bone to produce an age-regression formula and evaluate the relation of the osteon geometry (circularity, aspect ratio, and osteon angle - theta) to osteon orientation (measured through phi). Upon investigation, it was determined that the reported precision (measured through Standard Error of the Estimate [SEE]) for age regression formulae is greatly affected by sample size, consequently, developing an age-estimation formula was not pursued due to the limited sample size available for this study. Therefore, the focus of this was to describe the age-related differences within 2D geometry of osteons and their relation to 3D osteon orientation (measured through phi). Twenty-seven, anterior, mid-femoral, female, specimens were analyzed. An unexpected negative correlation was found between osteon orientation (phi) to osteon circularity and aspect ratio, signifying that the orientation of osteons in 3D cannot be used to predict the geometry of osteons visualized in 2D. Nevertheless, these relations can likely be explained through the more dominant relations between osteon circularity and aspect ratio to age. My results demonstrate that osteons become more circular in their cross-sections with advancing age independent of osteon orientation (phi). Interestingly, osteon orientation was also found to become oblique with age and not increasingly longitudinal as was

expected. However, my results also suggest that osteons are being rotated two axes. As osteon orientation (phi) is rotated about the z-axis, my results indicate that the osteon angle (theta) is also being rotated about the x-axis. This was demonstrated through the negative correlation between osteon orientation (phi) and osteon angle (theta). This relation can potentially account for the negative correlation between osteon orientation (phi) and circularity since the appearance of increased circularity can be explained through the projection of the elliptical cross-section on to the imaging/sectioning plane. All together, my results establish that osteons are not cylindrical structures, especially in younger individuals, but are rather elliptical structures that become increasingly circular with advancing age.

DEDICATION

For my grandparents (Ronald and Alice Hennig). I am lucky to have such an amazing source of support. I could not have done any of this without you. I will forever be grateful for all you have done for me. I love you always

ACKNOWLEDGEMENTS

First, I want to extend my eternal gratitude to my family. I truly cannot express how grateful I am for all the support you have provided me throughout the course of my academic career. I will forever be grateful for all you have done to help me pursue this goal. Your support has kept me going through the good and the bad times. Papa bear, there are no words. You have been the most constant source of support. I could not have made it this far without you. I love you so much! Jack (Jackie), I am so grateful for your love. I am truly blessed to have you in my life. Mom and Dean, you have done so much for me. I would not be here if it were not for your support. Michael, you always have my back when I need it the most, thank you! Lastly, and most definitely not least, I would like to thank my Grams and Gramps. Simply put, I have the best grandparents EVER! You have done so much for me so I can achieve my Masters. I love you and I am so grateful that you are here to see me succeed.

I do need to acknowledge of few other select individuals for their specific contributions. Matthew Courchene, your artistic skills are impeccable. I also need express my gratitude for all your support and encouragement throughout this entire process. I cannot thank you enough for the countless hours you spent listening to me go on and on...and on about my thesis. You are an amazing friend. Robert St. Pierre, thank you, your math and excel spreadsheet skills were a blessing. Justin Shultenkamper...thanks for all the computer help and the for nerd sessions with your microscope! Philippe St. Pierre, thank you for all your time and efforts. Your time and skills are very much appreciated! Candace Gellert, thank you for allowing me to bounce so many ideas off you and for the encouragement and support when I needed it most. Natasha Streeter and Zachary Powers (you probably know my thesis as well as I do by now) and Fredrick

Krammer...THANK YOU!!! I have some pretty awesome cousins!!! Hudson Byblow, thank you for all you help! Emma Turner and Nikki McLean thank you for your help in editing. Lisa Gillis, what can I say? You are an amazing friend. You have been an incredible source of support for me. I am incredibly lucky to have a friend like you. Jeff Galon, I owe you special thanks, I will forever be grateful to you.

There are far too many others to thank by name for all the love and support over the years. My apologies for the generic/catch all shout out. I am grateful to have such an amazing group of friends. I love you all. I hope you know who you are and how you have contributed to my success. To my friends/family back home: I miss you. Life has not been easy being away from home, but I appreciate all encouragement you continue to give me; your support keeps me going through the hard times. I would not have made it this far without you. To my friends/family here in Saskatoon: I am so thankful to have met you. The friendships I have encountered here have made my time here so much better than I could have hoped for. I will forever be grateful for having met you. You have all truly changed my life for the better. THANK YOU!

I would also like to acknowledge my lab mates both past and present. Hayley Britz, Brain Bewer, Yasmin Carter, Isaac Pratt, and Treena Swanston. Thank you for the support and letting me bounce so many ideas off you. I particularly need to thank my supervisor Dr. David Cooper and committee members Drs Angela Lieverse, Helen Nichol, and Ernie Walker. A special thank you must be given to my collaborators Drs David Thomas and John Clement for providing the specimens. Without their generosity, this thesis would not have been possible.

TABLE OF CONTENTS

LIST OF FIGURES

CHAPTER TWO

CHAPTER THREE

CHAPTER FOUR

APPENDIX II

APPENDIX IV

LIST OF EQUATIONS

CHAPTER THREE

CHAPTER FOUR

LIST OF TABLES

LIST OF ABBREVIATIONS

Standard Error of the Estimate: SEE
Two-dimensional: 2D
Three-dimensional: 3D
Micro-computed tomography: micro-CT
Osteon population density: OPD
Regions of Interest: ROI
Melbourne Femur Collection: MFC
Victorian Institute of Forensic Medicine: VIFM
Osteon circularity: On.Cr.
Aspect Ratio: AR
Osteon Orientation: phi
Osteon Angle: theta

CHAPTER ONE
INTRODUCTION

1.1 Introduction

Bone is a three-dimensional (3D) structure that continually renews itself throughout life and is capable of adapting to different mechanical stimuli, thereby adding a fourth dimension. Two-dimensional (2D) techniques cannot fully capture the true extent of the interconnections within the networks of the microstructure of cortical bone. It is clear that the process of bone maintenance (remodelling) is extremely complex and not fully understood. While we may not know exactly how this process works, as bone remodels several differences have been identified that can be analyzed microscopically. Histology, the microscopic study of tissues, is generally achieved through 2D analysis, and has been the predominant means of exploring the age-related differences observed in cortical bone. Age-related differences in histological features have been used to estimate the age at death of individuals; however, histomorphometric aging techniques require large sample sizes that are not always available (Hennig and Cooper 2011)(results presented in Chapter 3). Currently, there is a large gap in our understanding of the microstructure of cortical bone. I propose that 3D investigations used in conjunction with 2D histological analysis will help to narrow this gap. Only recently has the use of 3D imaging of cortical bone become accessible using micro-computed tomography (micro-CT). Since bone remodels in 3D, investigations using 3D imaging can potentially provide information on the complexity of the internal architecture of cortical bone that cannot be visualized with 2D techniques. Given the complexity of the remodelling processes and the technological limitations that have historically hindered our ability to investigate this process in 3D, it is clear further investigation is needed now that 3D techniques are available.

1.2 Objective of Thesis

One of the initial goals of this thesis was to develop an age prediction formula through the combination of 2D and 3D techniques. Through an independent study investigating the relation of precision (measured through standard error of the estimate - SEE) to sample size (discussed in Chapter 3), it was concluded that, given the limited sample size of this study, developing an age regression formula to predict age at death could not pursued. Nonetheless, evaluating the relation between 2D osteon geometry and 3D osteon orientation as well as their relation to age was possible and is presented in Chapter 4.

While both 2D and 3D techniques have their limitations, these different techniques can also complement each other. I intend to demonstrate that a more comprehensive understanding of the microstructure of cortical bone will be gained through the integration of histology and high-resolution micro-CT by providing new insights into how bone remodelling varies throughout an individual's lifetime. Therefore, this thesis aims to gain a better understanding of the age-related differences that have been observed in cortical bone by investigating whether the 3D orientation of the microstructure explains the variation found in the 2D geometrical parameters (circularity and aspect ratio).

While the use of micro-CT will help us achieve a higher level of understanding the organization of the microstructure in cortical bone, desktop micro-CT is not currently capable of consistently providing detailed information on the geometric parameters of the histological structures, which are best captured through 2D imaging. Thus, 2D imaging is still a necessary method for studying age-related differences in bone.

1.2.1 Overview of Chapters

Chapter 2 provides an introduction to bone biology and provides a brief overview and

background about the application of 2D and 3D imaging to cortical bone.

Chapter 3 explores the relation of sample size to reported standard error of the estimates (SEE) for histomorphometric aging techniques. Histomorphometric aging techniques are used in fields such as archaeology and forensic anthropology. The reported degree of precision (measured through SEE) is highly variable (see Table 3.1 - Chapter 3) and it remains unclear which method or skeletal element is the best predictor of age at death. Despite the fact that several age-related differences have been detected in cortical bone, these differences have predominantly been discussed in terms of their 2D parameters. Few studies have discussed the age-related differences using 3D imaging (Cooper *et al.* 2007a; Cooper *et al.* 2003), and no studies have been published attempting to predict age from 3D data.

After reviewing the literature and noting the small sample sizes used to develop these methods, as well as the degree of variation in the reported SEE, an independent study was launched to determine the impact sample size has on the SEE. While several authors have noted the need for larger sample sizes (Bouvier and Ubelaker 1977; Crowder 2005; Lazenby 1984; Pfeiffer 1985; Walker, Lovejoy and Meindl 1994), the relation between sample size and SEE has not been previously discussed in the literature in reference to histomorphometric aging techniques. Upon investigation, it was concluded that a sample size of at least 150 specimens would be needed if I were to precisely predict age at death within ±10 years. These results are presented and discussed in Chapter 3. The results presented in this chapter have been published, in collaboration with Dr. David Cooper, supervisor, in the *American Journal of Physical Anthropology* (Hennig and Cooper 2011). Written permission for the use of this from John Wiley and Sons is presented in Appendix I.

Chapter 4 discusses the relation of 3D osteon orientation to 2D geometric parameters of

osteons. *A*s a result of the study investigating the relation between sample size and SEE, it was decided that developing an age estimation formula would not be feasible due to both time constraints (duration of a master's program) and the inadequate sample size available (n = 32). Therefore, the remainder of this thesis focused on incorporating histology and micro-CT to evaluate the relation of osteon geometry (2D) to osteon orientation (3D), and their relation to age. Two-dimensional studies continue to be a useful way of investigating the histological structures of cortical bone that cannot always be visualized using 3D imaging, such as shape and size of the osteon (basic structural unit of bone). Conversely, micro-CT can provide information on the canals of osteons, such as their orientation, that cannot be investigated using 2D techniques due to a limited depth of field. Nevertheless, many questions remain about the associated differences that have been observed in the geometry of osteons and attributed to age as well as what role osteon orientation plays.

Recently, Britz *et al.* (2009) investigated the relation between strain and geometric parameters of osteons, using weight as a proxy for strain. They found that osteon size (diameter and area) was inversely related to weight. They also found a relation between geometric parameters (diameter, area, and circularity) and age, where diameter and area decreased with age and circularity increased with age. While the results presented by Britz *et al.* (2009) provide valuable insights into relations of osteon geometry, their study was a 2D investigation, and cannot provide information on whether the observed differences within the geometry of osteons resulted from differences in the orientation of osteons or true age-related differences. It is clear from the results they presented that a detailed and thorough analysis of these relations is required using 3D techniques to assess how osteon orientation may be related to osteon geometry. Following their study, two questions were developed and analyzed:

(1) Does the orientation of osteons in 3D determine their geometric parameters visualized in 2D?

(2) Do the differences in osteon orientation explain the age-related differences seen in the geometrical parameters of cortical bone?

With the current technological limitations of both methods, studying the age-related differences through the combination of 2D and 3D techniques is likely the most beneficial way of gaining a complete understanding of the differences within the microstructure of cortical bone associated with age.

Chapter 5 concludes the thesis with a summary of the results presented in Chapters 3 and 4 and a discussion of future directions.

CHAPTER TWO
BONE BIOLOGY AND BACKGROUND

2.1 Basic Bone Biology

At the gross level, there are two structural types of bone, trabecular and cortical. Trabecular, bone also referred to as spongy or cancellous bone, is a lightweight porous structure composed of a lattice-work known as trabeculae. Trabecular bone is predominantly found in the epiphyses (ends) of long bones, under protuberances of tendon attachments, and in the body of short bones. Cortical bone, also referred to as compact bone, is a solid dense structure predominantly found in the diaphysis (shaft) of long bones.

Trabecular and cortical bone go through the same developmental and renewal processes. Growth and maintenance of the skeletal system takes place through two distinct processes - modelling and remodelling. Modelling is the dominant process that occurs during growth of the skeleton. Immature bone (primary bone) is produced during modelling and is characterized by coarsely bundled and woven bone (Frost 1963), that encompass the primary vascular pores that ultimately develop into primary osteons (Cooper *et al.* 2004). As growth continues, immature bone is replaced with mature bone (lamellar bone). The structure of mature bone is much more organized than immature bone as it is composed of layers of lamellae penetrated by Haversian systems (secondary osteons - hereafter called osteons - Figure 2.1)(Frost 1963). Once skeletal maturity is reached, modelling is reduced significantly and remodelling becomes the dominant means of skeletal maintenance (Frost 1973).

Remodelling is achieved through a specific process of 'activation → resorption → formation.' Once an activation signal is received, the renewal process commences by the resorption of microscopic packets of bone by osteoclasts (bone destroying cells). It is completed

by osteoblasts (bone forming cells) that replace the resorption spaces with osteoid, which subsequently mineralizes to form new bone. Collectively, osteoclasts and osteoblasts form basic multicellular units (BMU); the resulting product is the osteon (Frost 1963; Frost 1973).

The osteon is the basic structural unit of bone and is approximately 200 μm to 300 μm in diameter in humans (Bousson *et al.* 2000; Britz *et al.* 2009; Robling, Castillo and Turner 2006). Within each osteon, concentric lamellae enclose the Haversian canal where blood vessels, lymph, and nerve fibers pass through. Volkmann's canals transversely connect osteons to one another, and, ultimately, the periosteal and endosteal surfaces of bone. Collectively these canals create an interconnected network whereby blood and lymph are supplied to the osteocytes (living bone cells) housed within the lacunae. Osteocytes communicate with each other via a network of radiating canaliculi - tiny fluid-filled channels (Figure 2.2)(White 2005).

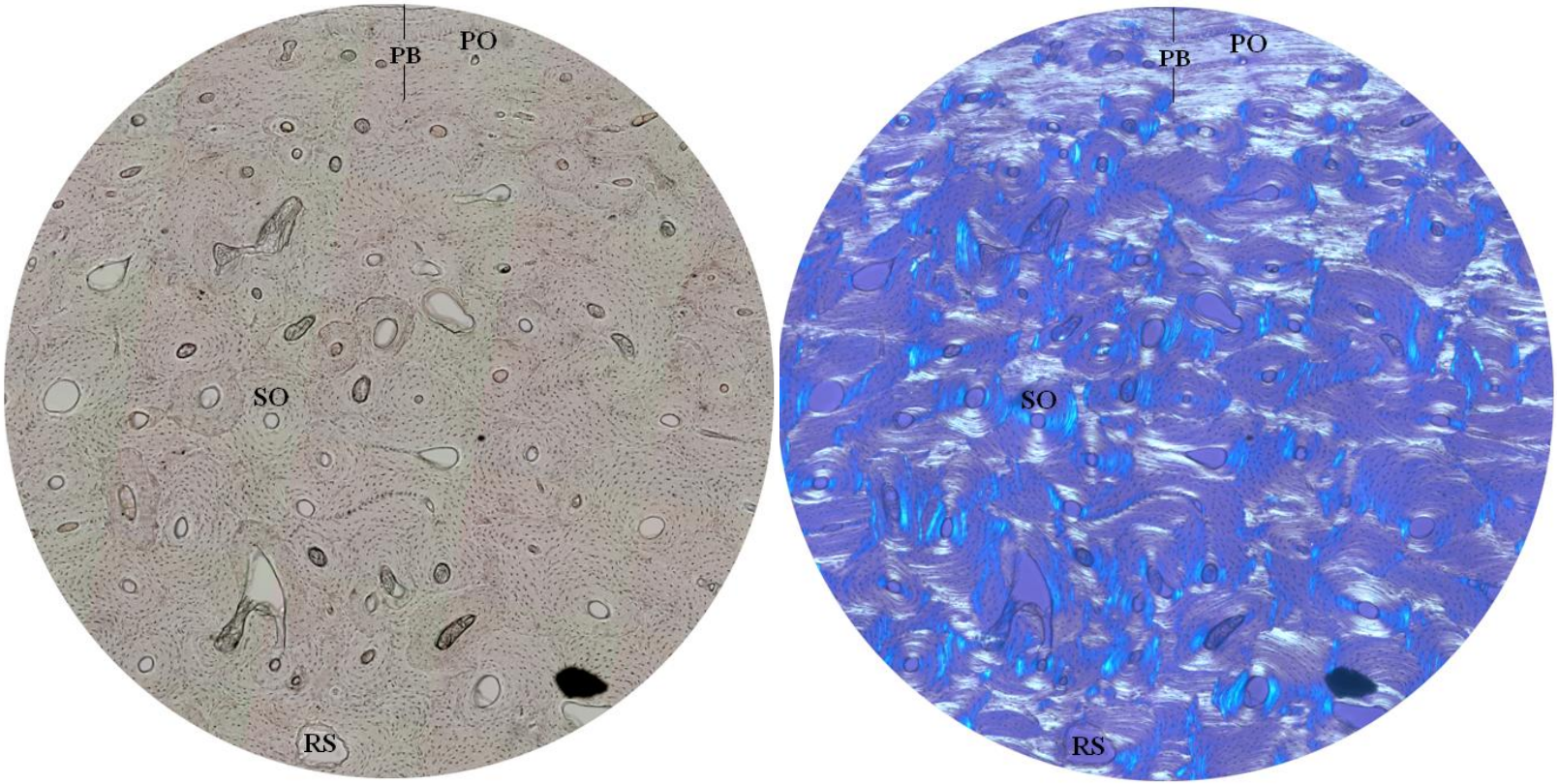

Figure 2.1: Histology ground section from a human femur 20X (left: polarized light, right: transmitted non-polarized light). Female 33 years old. PB: primary bone, PO: primary osteon, SO: secondary osteon, RS: resorption space

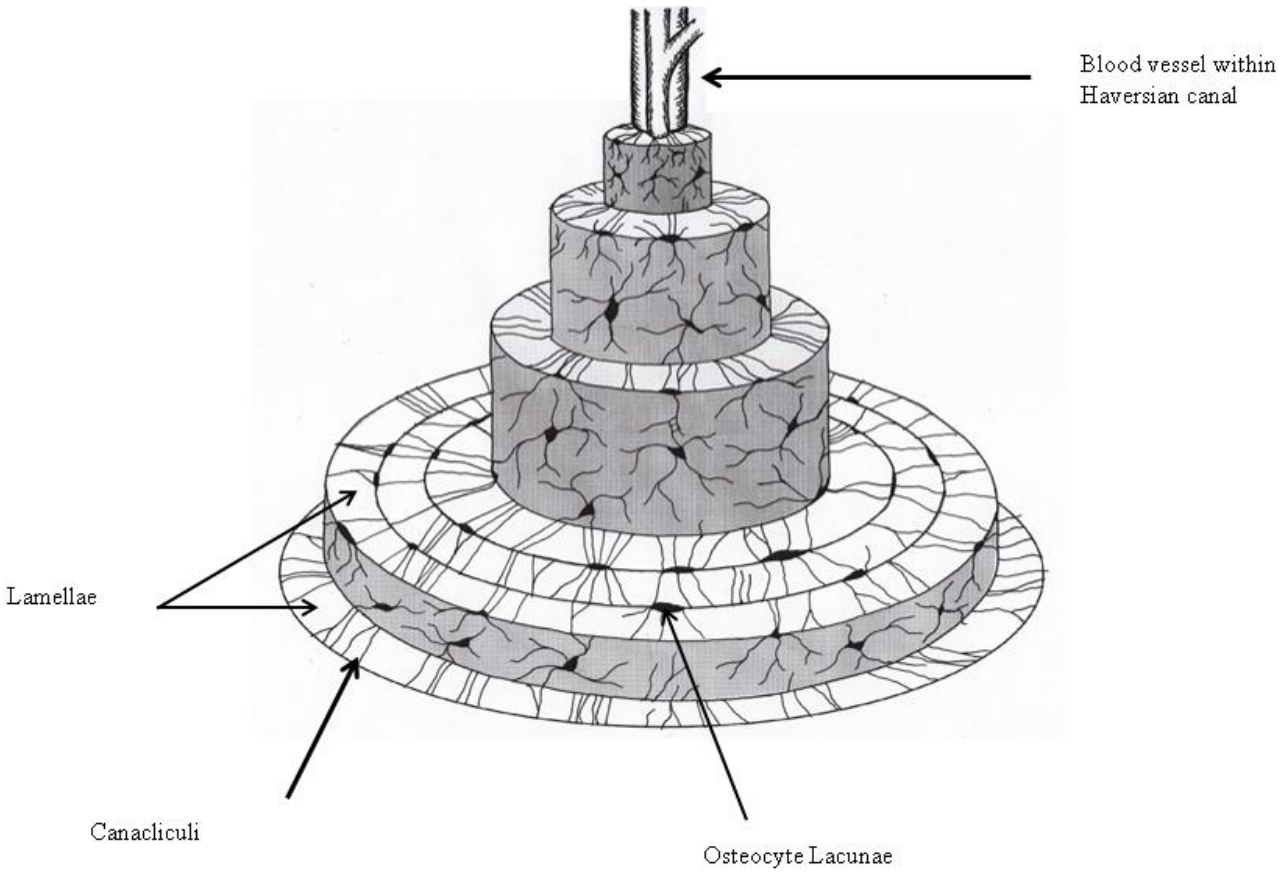

Figure 2.2: Osteon schematic showing the microscopic view of the basic structural unit (secondary osteon) of bone. Note: not drawn to scale (image adapted from White (2005))

2.1.1 Theories of Bone Adaptation

In 1893, Julius Wolff proposed a theory to explain the adaptation of bone stating that changes in the function of bone will alter the internal structure of bone, in essence, form follows function (Wolff 1893). This has become known as "Wolff's Law" and in its strictest sense is inaccurate; however, in its most general sense, the theory that mechanical loading influences the architecture of bone is generally well accepted (Bertram and Swartz 1991; Ruff, Holt and Trinkaus 2006).

Though the mechanisms that regulate bone adaptation are still not fully understood, several theories have been put forth in an attempt to explain how adaptation is initiated and maintained. Frost, proposed the "mechanostat" theory as a mechanism to explain modelling and remodelling of bone. The theory states that similar to a thermostat, the mechanisms regulating bone adaptation will turn "ON" as a response to stimuli such as mechanical loading and "OFF" in the absence of stimuli. In situations of "gross overloading" bone mass would be adapted through modelling whereas in situations of "gross underloading" BMU based remodelling would occur (Frost 1987).

Turner has similarly proposed three rules for bone adaption: (1) Bone adaptation is driven by dynamic loading (a load applied with motion), not static loading (an external load applied in a fixed position). (2) Extensive loading is not necessary, only a short period of mechanical loading (any load applied to the body) is necessary to induce a response, while increasing the duration of loading can have a diminishing effect. And (3) bone cells will become accustomed, and therefore less responsive, to routine (habitual) loading (Turner 1998).

Numerous studies investigating the geometry of bone have found support for both Frost's

(1987) and Turner's (1998) theories. I*n vivo* studies using sheep have demonstrated that a short duration of dynamic loading leads to increases in cortical area, whereas static loading or unloading leads to decreases in cortical area (Lanyon and Rubin 1984; Rubin and McLeod 1994).

Mechanotransduction is a theory to describe how adaptation is initiated at the microstructural level. The exact process of how adaptation proceeds at the cellular level is unknown, but several theories have been put forth to explain how cells sense and respond to external forces. In general, mechanotransduction is the process where osteocytes sense mechanical loads and transmit a signal to initiate an appropriate response (Pearson and Lieberman 2004). Osteocytes act as the receptors and transducers of strain (Marotti 1996). Once a signal is initiated, the osteocytes communicate with one another via the canaliculi, essentially providing a nervous system within each bone (Pearson and Lieberman 2004). Martin (2000) has suggested that remodelling is automatically initiated unless an inhibitory signal is received from osteocytes. When osteocytes sense mechanical stimuli, an inhibitory signal is sent and remodelling is withdrawn whereas, when a signal of reduced mechanical loading is received, the lack of response from osteocytes initiates remodelling. Furthermore, strain magnitude has been suggested to affect the direction of the BMU (van Oers *et al.* 2008a) and ultimately the orientation, geometric size and shape of the BMU tunnel (van Oers *et al.* 2008b), thereby dictating the orientation and the geometry of the osteon.

2.2 Two-Dimensional Analyses

2.2.1 Histomorphometry

Remodelling is the primary means of renewal in the adult skeleton and plays an integral role in the process of adaptation of bone (Frost 1973). The differences associated with remodelling are best observed through histomorphometric analysis. Histomorphometry is the quantitative analysis of the microscopic differences of the histological structures within cortical bone. These histological features can be quantified, by counting the osteon population density (OPD - osteons per unit of area^2) and/or measuring geometric parameters such as osteon area, or osteon circularity to characterize the and identify differences that that take place as bone is remodelled (Stout and Crowder 2012).

Many of the differences that have been observed within the geometry of osteons have been correlated with age. For example, a number of authors report a decrease in osteon size with age (Britz *et al.* 2009; Burr, Ruff and Thompson 1990; Currey 1964; Ericksen 1991; Iwamoto, Oonuki and Konishi 1978; Kerley 1965; Martin, Pickett and Zinaich 1980; Singh and Gunberg 1970; Thompson and Galvin 1983; Ural and Vashishth 2006; Watanabe *et al.* 1998; Yoshino *et al.* 1994). Studies have also found an increase in circularity with age (Britz *et al.* 2009; Currey 1964; Goliath 2010), an increase in osteon population density (Burr, Ruff and Thompson 1990; Currey 1964; Ericksen 1991; Iwamoto, Oonuki and Konishi 1978; Kerley 1965; Kimura 1992; Martin, Pickett and Zinaich 1980; Singh and Gunberg 1970; Thompson and Galvin 1983; Ural and Vashishth 2006; Watanabe *et al.* 1998; Yoshino *et al.* 1994) as well as an increase in Haversian canal diameter with age (Burr, Ruff and Thompson 1990; Martin, Pickett and Zinaich 1980; Ural and Vashishth 2006; Yoshino *et al.* 1994).

Based on some of the observed differences found in the histological structures of cortical bone, age at death predictions have been attempted using regression formulae (see Table 3.1-Chapter 3). The noted increase in OPD is the most commonly used age-related difference to develop age regression formulae, where the number of whole and/or fragmentary osteons is counted and used to estimate age (Figure 2.3). While many formulae and techniques have been developed since Kerley (1965) first developed a histomorphometric aging technique, it is unclear which method and skeletal element yields the most precise predictions (discussed in Chaper 3).

It is also important to note that there is a lack of consensus within the literature regarding some of the observed age-related differences, given that several studies report having found no significant relation between osteon size and age (Bell *et al.* 2001; Black, Mattson and Korostoff 1974; Jowsey 1966; Jowsey 1968; Kimura 1992; Mulhern and Van Gerven 1997; Pfeiffer 1998; Pfeiffer *et al.* 2006). Further complicating issues of histomorphometric analyses and potentially the source of the lack of agreement within the literature is the inconsistent use and application of the terminology. For example, Goliath (2010) only included osteons in his study in which at least 90% of the Haversian canals showed no signs of remodelling, whereas Britz *et al.* (2009) included osteons in which the cement line was ≥75% complete. Another inconsistency within the literature includes the definition of osteon size. Some studies refer to size as the 'total area included within the outlined region' (Britz *et al.* 2009; Goliath 2010; Pfeiffer *et al.* 2006); other studies describe size as the 'perimeter of the osteon' (Jowsey 1966). Ural and Vashishth (2006) used two different definitions of area; one is defined as the 'total area including canals' and the other is defined as the 'total area excluding canals'; however, the relation with age was different between their two definitions. The use of multiple definitions within the literature makes

meaningful comparisons difficult and potentially erroneous. Furthermore, the use of various definitions makes it difficult to detect and understand if true meaningful relations exist among these variables being studied.

It is clear that inconsistent approaches and applications of terminology complicate our understanding of bone remodelling. Despite the fact that histological studies provide valuable information regarding the microstructure, the techniques employed in these studies are ultimately destructive to bone. To process a specimen for histology, the bone is often destroyed and therefore a detailed analysis and description of the specimen must be recorded before the processing begins.

Moreover 2D analyses often requires large sample sizes upwards of 150 specimens are needed to characterize and generate meaningful statistics for quantitative evaluations (results of this study are discussed in Chapter 3) (Hennig and Cooper 2011). When available, these large sample sizes often come from archaeological populations. At best, archaeological populations can only provide limited medical or occupational histories. Furthermore, the biological information such as, sex and age is most likely estimated, truly limiting their usefulness in making meaningful comparisons.

Yet, another drawback in the investigations on the microstructure of cortical bone is that these evaluations, both past and present, predominantly use 2D techniques, such as histology, to evaluate a 3D structure. Given that the architecture of bone is multi-dimensional, 2D evaluations can only provide a limited perspective of section being analyzed.

While 3D reconstructions can be made from serial sectioning, it is very a tedious process (DeHoff 1983) and can often only provide qualitative data. Furthermore, the sectioning plane of

the histological slice can also affect the shape and dimensions of the geometrical parameters being measured (Recker 1983; Stout *et al.* 1999). Therefore, I suggest that by using 3D techniques, such as micro-CT, a better understanding of the remodelling process and the age-related differences that accompany it will be gained.

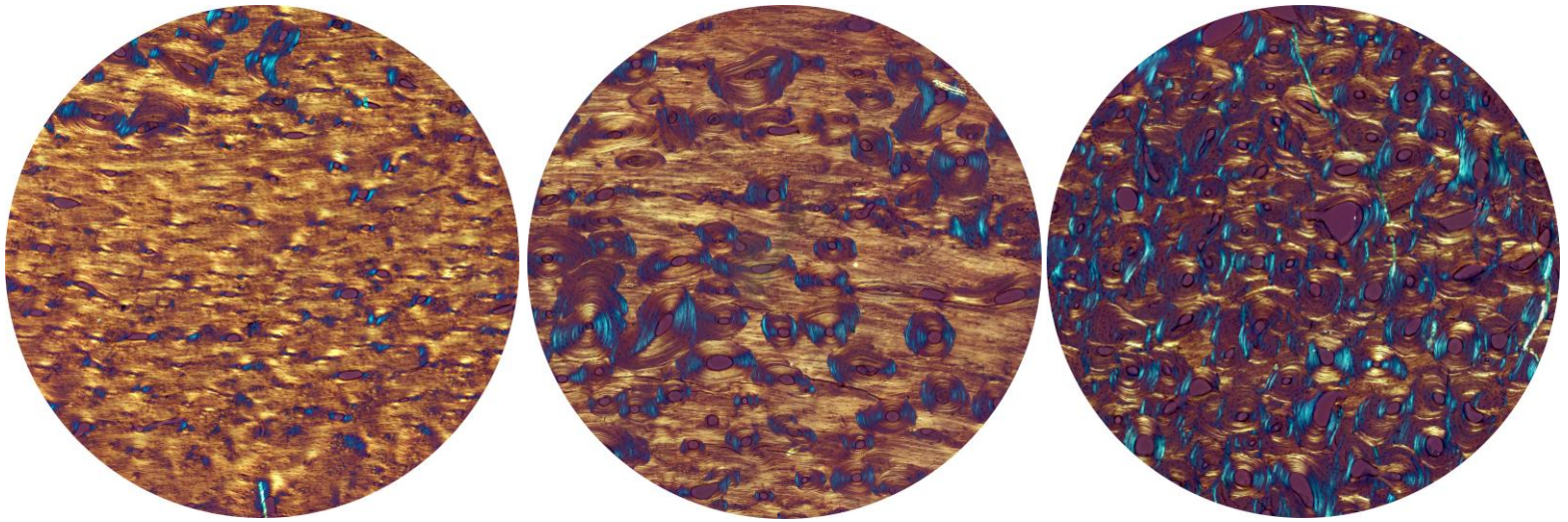

Figure 2.3: An example demonstrating the increase in osteon population density with age. Left: young adult (female, 21 yrs), middle: middle adult (female, 41 yrs) and right: old adult (female, 81 years). The periosteal surface: top of each image.

2.3 Three-Dimensional Analyses

Due to technological limitations, very few studies in the past have investigated the microstructure of bone in 3D. Those studies in which 3D applications were completed were either reconstructions made from the microstructure from serial sections (Cohen and Harris 1958; Stout *et al.* 1999; Tappen 1977), or using the split line method and injecting India ink into the canals to look at the orientation of osteons (Hert, Fiala and Petrtyl 1994; Petrtýl, Heřt and Fiala 1996). Improvements to micro-CT scan resolutions in the past decade have now made it possible for investigations of cortical bone in 3D. Computed tomography makes 3D reconstructions from 2D X-ray images and is a minimally-destructive. Micro-CT is the application of computed tomography at the microscopic level. The few studies that apply micro-CT to cortical bone have largely focused on the mid-femoral diaphysis (Cooper *et al.* 2011; Cooper *et al.* 2004; Cooper *et al.* 2006; Cooper *et al.* 2007a; Cooper *et al.* 2003; Jones *et al.* 2004), the femoral neck (Bousson *et al.* 2006; Bousson *et al.* 2004; Chen *et al.* 2010) and the mandible (Renders *et al.* 2007).

Studies using 3D techniques have provided new insights into the arrangement and complexity of the microstructure of cortical bone and demonstrated the need for further investigation. For example, Stout *et al.* (1999) produced the first computer simulated 3D rendition of cortical bone using serial sections from Tappen (1977) and found Haversian systems to be a complex pattern of interconnecting branches. In fact, they noted the "dumbbell-shaped" osteon, often discussed in the literature, was actually two separate branching osteons. The pattern found by Stout *et al.* was much more complex and difficult to characterize than originally hypothesized by earlier non-computerized 3D analyses (Cohen and Harris 1958; Hert, Fiala and

Petrtyl 1994; Petrtýl, Heřt and Fiala 1996; Tappen 1977). Recent studies using micro-CT also have noted the complexity of the interconnecting branches of Haversian systems (Basillais *et al.* 2007; Cooper *et al.* 2007a; Cooper *et al.* 2003; Mohsin, Taylor and Lee 2002; Tanck *et al.* 2006).

Despite the fact that 3D techniques have begun to be applied as an investigatory tool of the microstructure of cortical bone, to my knowledge no studies using micro-CT have evaluated the orientation of osteons in human bone. Prior to the application of micro-CT, osteon orientation was described at length in the literature, yet these descriptions have largely been qualitative. Nevertheless, the conclusion reached by these studies is that osteons are aligned along the dominant loading trajectories of long bones (Ascenzi, Andreuzzi and Kabo 2004; Black, Mattson and Korostoff 1974; Black *et al.* 1980; Cohen and Harris 1958; de Boef and Larsson 2007; Hert, Fiala and Petrtyl 1994; Lanyon and Bourn 1979; Nomura *et al.* 2003; Petrtýl, Heřt and Fiala 1996; Rho, Kuhn-Spearing and Zioupos 1998; Wasserman *et al.* 2008). Several investigations have also used computer-simulated models to explain the regulation orientation of osteons (Burger, Klein-Nulend and Smit 2003; Martin 2007; Smit, Burger and Huyghe 2002; Ural and Vashishth 2007; van Oers *et al.* 2008a; van Oers *et al.* 2008b).

It is generally accepted that age is correlated to the size and shape of the 2D histological structures (Britz *et al.* 2009); yet no study has investigated the relation of the orientation of osteons to the 2D geometric parameters. Britz *et al.* (Britz *et al.* 2009) have proposed that the age-related differences seen in circularity may be the result from different osteon orientations, which suggests that the differences in osteon shape (and size) that have been associated with age are, in fact, reflections of differences in osteon orientation with age. Given that their study was 2D, this theory could not be explored, further demonstrating the need for the application of 3D

techniques.

While access and availability to desktop micro-CT is not always possible, 3D techniques are important for furthering our understanding of bone remodelling. A few current limitations of 3D imaging must be acknowledged. There is a diminishing gain when using micro-CT; increasing the resolution of a scan will unfortunately decrease the field of view that can be scanned. Despite advancements in the ability to capture 3D images of the microstructure of cortical bone, the geometrical parameters of secondary osteons have not been consistently visualized using desktop micro-CT (Cooper *et al.* 2004); however recent work by Arhatari *et al.* (2011) have demonstrated that visualizing the geometric parameters using desktop micro-CT is possible . Thus, histological techniques are still extremely useful.

While several age prediction formulae have been developed using the age-related differences seen in the histological structures of cortical bone, no studies have attempted this using 3D imaging. An initial goal of this thesis was to develop a formula by combining these methodologies. Upon, conducting a literature review of the histomorphometric aging techniques, the varying degrees of precision and the small sample sizes were noted. An investigation was therefore launched to evaluate the relation between precision (SEE) and sample size in order to determine what the recommended/appropriate minimum sample size should be when developing histomorphometric formulae. The results of this study are presented in Chapter 3.

CHAPTER THREE
THE RELATION BETWEEN STANDARD ERROR OF THE ESTIMATE AND SAMPLE SIZE OF HISTOMORPHOMETRIC AGING METHODS

3.1 Introduction

Kerley (1965) developed the first histomorphometric aging technique that employed linear regression to predict age from differences observed in cortical bone. He reported that by using the femur, tibia, or fibula, a precise age (measured through standard error of the estimate, or SEE) could be predicted within ±9.39, 6.69, and 5.27 years, respectively. Shortly after, Ahlqvist and Damsten (1969) introduced a modification of Kerley's method for the femur, reporting a smaller SEE of ±6.71years. While the precisions reported by these pioneers were extremely promising, looking back after nearly a half century (Table 3.1) it is unclear how precise histomorphometric aging actually is and which methodology or skeletal element yields the best results.

Standard error of the estimate tells us how well the prediction equation fits the sample data by measuring the dispersion of predicted (*y'*) values from the known values (*y*):

$$\mathrm{SEE} = \sqrt{\frac{\sum(\mathrm{y} - \mathrm{y}')^2}{\mathrm{n} - 2}}$$

Equation 3.1

Where *n* is the sample size. As such, SEE is an indicator of how precise the prediction equation actually is (Aykroyd *et al.* 1997; Hinton 2004). In the case of histomorphometric age prediction, error between the predicted and known values can potentially arise from numerous sources including variation within and between individuals as well as the methodology used to

characterize histological features. When comparing approaches it seems intuitive to dismiss the method with the larger SEE as being less precise; however, the issue of sample size complicates such a comparison. For example, Kerley's reported precision for the femur, noted above, although larger than that reported by Ahlqvist and Damsten, was derived from a sample over three times larger (n = 67 vs. 20). In addition to the fact that the need for larger sample sizes has been discussed by many (Bouvier and Ubelaker 1977; Crowder 2005; Lazenby 1984; Pfeiffer 1985; Walker, Lovejoy and Meindl 1994), the question of which technique should be considered the better method remains unanswered. Given the importance of histomorphometric aging in physical anthropology, it is important that the impact of sample size on SEE be explored and discussed. This chapter explores this relation through a review of the literature, predictions based upon sampling theory, and a simulation.

3.2 Materials and Methods

3.2.1 Literature Review

A review of the literature (abstracts, articles, book chapters, theses, and dissertations) was completed for histomorphometric aging techniques which reported sample size (n) and SEE in units of years from individuals of known age (from gravestone markers or autopsy reports). Studies that reported SEE in other units such as natural log (ln) years (e.g. Stout and Paine 1992; Stout, Porro and Perotti 1996) were not included in this study as these SEE values cannot be directly converted back into units of years from the information provided within the publication. Forty studies, which reported SEE for 63 skeletal elements, met these criteria and were included in our analysis (Table 3.1). Standard errors of the estimates reported for more than one skeletal element in an individual study were recorded separately as individual cases. In the case of

multiple equations, the lowest reported SEE values were included in our analysis. In studies where SEE was provided separately for males and females, each SEE was recorded as an individual case. If SEE was provided for the pooled sexes as well as individually for males and females, the pooled SEE was selected as the SEE to be included. Pooled SEE was chosen because identifying sex is not always possible and therefore we suggest that pooled SEE (when provided) is a more accurate measure of the expected precision. Two studies (Table 3.1) that did not include SEE in their results but included sufficient raw data (known and predicted age) to calculate SEE were included in our study (Thompson 1981; Watanabe *et al.* 1998).

Table 3.1: Sample Descriptions and Reported Standard Error of the Estimates for Histomorphometric Aging Techniques

Bone	Study	Sample Size	Age Range Average Age	Sex ♂:♀:?	SEE Range
Femur	Ahlqvist and Damsten (1969)	20	N/A (55.4)	N/A	6.71 - 6.79
Femur	Aiello and Molleson (1993)	20	15 - 91 (54.7)	10:10:00	8.3 - 17.4
Femur	Bouvier and Ubelaker (1977)	40	11 - 82 (48.6)	N/A	11.65
Rib	Cho *et al.* (2002)	154	17 - 95 (50.4)	N/A	12.679
Frontal	Curtis (2003)	90	29 - 99 (75.2)	43:46:00	13.132
Femur	Drusini (1987)	20	19 - 50 (28.8)	N/A	3.92
Mandible	Drusini *et al.* (1990)	50	18 - 97 (35.3)	32:18:00	6.42 - 11.45
Rib	Dudar *et al.* (1993)	55	17 - 95 (61.8)	24:43:00	11.4
Femur	Ericksen (1997)	58	14 - 60 (41)	27:31:00	9.14
Femur	Ericksen (1991)	328	14 - 97 (62.8)	174:154:00	10.08 - 12.21
Femur	Han *et al.* (2009)	72	35 - 94 (68.5)	44:28:00	6.65 - 6.99
Femur	Hauser *et al.* (1980)	96	21 - 87	N/A	10.7 - 11.4
Tibia		31	18 - 88	N/A	13.5 -16
Femur	Hummel and Schutkowski (1993)	18	19 - 76 (52)	N/A	10.9 - 14.5
Humerus	Iwamoto *et al.* (1978) [*1]	42	41 - 102 (69.1)	42:00:00	5.49 - 12.79
Femur	Keough *et al.* (2009)	146	19 - 82 (51.7)	104:41:00	13.31 - 16.3
Femur	Kerley (1965)	67	0 - 95 (41.6)	43:17:07	9.39 - 13.85
Fibula		25	0 - 83 (34.5)	19:05:01	5.27 - 10.85
Tibia		33	0 - 85	24:08:01	6.69 - 13.62
Femur	Kerley and Ubelaker (1978)	67	0 - 95 (41.6)	43:17:07	6.98 - 12.52
Fibula		25	0 - 83 (34.5)	19:05:01	3.66 - 14.62
Tibia		33	0 - 85	24:08:01	8.42 - 14.28
Rib	Kim *et al.* (2007)	64	22 - 67 (44.8)	36:28:00	4.82 - 4.97
2nd metacarpal	Kimura (1992)	227	30 - 98 (68.8)	114:113:00	11.10 - 14.82
Femur	Maat *et al.* (2006)	162	15 - 96	86:76:00	9.162 - 14.786
Femur	Narasaki (1990)	28	43 - 98 (77.5)	28:00:00	9.28
Femur		24	43 - 98 (77.5)	00:24:00	9.95
Femur	Nor *et al.* (2006)[*2]	36	N/A (53)	N/A	14.04
Humerus		5	N/A (38.7)	N/A	11.75
Multiple		64	21 - 91 (42.3)	50:14:00	12.62 - 13.86
Radius		15	N/A (37.4)	N/A	9.46
Tibia		9	N/A (53)	N/A	12.28
Femur	Pfeiffer (1992)	6	25 - 98 (58.3)	18:00:00	9.24
Femur		10	17 - 76 (51.5)	00:11:00	8.23
Rib	Pratte and Pfeiffer (1999)	51	24 - 95 (63.6)	N/A	3.256

Table 3.1: Continued. Sample Descriptions and Reported Standard Error of the Estimates for Histomorphometric Aging Techniques

Bone	Study	Sample Size	Age Range Average Age	Sex ♂:♀:?	SEE Range
Rib	Ren *et al.* (2001)	67	N/A	00:67:00	4.08
Clavicle	Rogers (1996) *3	95	22 - 88 (54.8)	50:45:00	13.69 - 24.75
Clavicle	Rogers (1996)	95	22 - 88 (54.8)	50:45:00	16.48 - 21.10
Humerus	Rother *et al.* (1978)	70	20 - 81	42:28:00	8.45 - 9.7
Femur	Samson and Branigan (1987)	31	16 - 91	31:00:00	6.00
Femur		27	16 - 91	00:27:00	16.00
Femur	Singh and Gunberg (1970)	33	39 - 87 (62.3)	33:00:00	3.24 - 5.01
Mandible		52	39 - 87 (64.3)	52:00:00	2.55 - 3.83
Tibia		33	39 - 87 (62.30	33:00:00	3.02 - 4.59
Fibula	Stout and Stanley (1991)	36	13 - 102 (59.6)	21:15:00	14.52 - 18.45
Radius		36	13 - 102 (59.6)	21:15:00	15.87 - 17.97
Tibia		36	13 - 102 (59.6)	21:15:00	14.84 - 18.86
Rib	Stout *et al.* (1994)	59	11 - 88 (39.9)	N/A	10.43
Femur	Thompson (1979)	113	30 - 97 (72.1)	64:52:00	7.07 - 8.65
Humerus		29	30 - 97 (68)	N/A	6.21 - 8.52
Tibia		113	30 - 97 (72.1)	N/A	7.58 - 9.52
Ulna		31	30 - 97 (69.4)	N/A	7.89 - 10.57
Femur	Thompson (1981) *1	28	30 - 97 (33.7)	19:09:00	6.89
Tibia		22	21 - 78 (42.7)	17:05:00	3.85
Humerus		6	19 - 76 (49.6)	4:02:00	4.31
Tibia	Thompson and Galvin (1983)	64	17 - 53 (31.3)	56:08:00	8.52
Femur	Uytterschaut (1993)	20	17 - 92 (53.7)	N/A	6.51
Tibia		20	17 - 92 (53.7)	N/A	6.29
Femur	Walker (1990)	173	18 - 90+ (52.3)	90:83:00	13.80 - 16.72
Femur	Wantanabe *et al.* (1998)	108	0 - 92 (49.6)	72:26:00	4.88 - 6.39
Rib	Xi and Ren (2002)	86	20 - 70	86:00:00	4.14
Humerus	Yoshino *et al.* (1994)	40	23 - 80 (47.6)	40:00:00	6.1-9.28
Femur	Zhu (1983) *4	35	5 - 86 (39.1)	29:06:00	1.51 - 13.80

*[1] SEE not provided in study but sufficient information present to calculate SEE
*[2] Table lists the published sample sizes and uses these values in all statistical analyses; however, personal communication with the author revealed these values were incorrect for the individual elements. Correct totals are as follows: femur (n= 9), humerus (n =30), radius (n = 15) and tibia (n = 7). Average age of each group was also provided through personal communication and was not used in any statistical analysis because it was not published in the original article
*[3] SEE from Stout *et al.* (1996) equation
*[4] SEE reported in Kimura (1992)

3.2.2 Sampling Theory

It is well established that when sample size is small, the sample variance (s^2) is less likely to be representative of the variance within the population (σ^2) from which it was drawn. The SEE is essentially the standard deviation (s) of the sampled values from the corresponding predicted values (rather than the mean) with one less degree of freedom (df) for simple regression (df = n – 1 – p; where p is the number of predictors). Thus, as sample size increases, the sample SEE will converge on the 'true' level of the population. Sampling theory, based upon Cochran's theorem (Cochran 1934), reveals the relation between sample and population variance follows a chi-square (χ^2) distribution with n-1 degrees of freedom:

$$\chi^2 = \frac{[(n-1)]s^2}{\sigma^2}$$

Equation 3.2

Solving this equation for an unknown sample variance yields:

$$s^2 = \sigma^2 \frac{\chi^2}{n-1}$$

Equation 3.3

(Wolberg 1976)

Where n-1 represents the degrees of freedom. Thus, using the appropriate χ^2 values it is possible to predict the relation between n and SEE assuming σ^2 is known. To illustrate this point, we assumed the mean SEE of the two largest studies (Table 3.1), 10.59 years, reflects the square root of the 'true' population variance. From there we calculated the 95% confidence intervals of SEE(s) using n-2 degrees of freedom.

3.2.3 Simulation

To provide an intuitive demonstration of the relation between n and SEE, we generated a simulated population of 50,000 individuals of random age between 20 and 90 years (Figure 3.1). Simulated histomorphometric 'ages' were generated as normally distributed random error about chronological age in which the standard deviation of this error was again set to reflect the assumed population SEE in years (10.59 years). Two thousand 'studies' of random sizes (3 - 400 individuals) were simulated and the resulting SEE calculated. The minimum size of three was employed to ensure that at least one degree of freedom remained for calculating SEE.

3.3 Results

The mean reported SEE from the literature was 8.63 years and the standard deviation was 3.81 years (range: 1.51 - 16.48 years). The mean sample size was 59 and ranged from five to 328 specimens (Table 3.1). Based upon sampling theory the 95% confidence intervals for SEE created a funnel-shaped distribution (Figure 3.2) which converged on the population SEE value (set to 10.59 years). Representative 95% confidence intervals for samples of 10, 50, and 150 individuals were ± 4.2, 1.7 and 1.0 years, respectively. The results from the simulation mirrored the funnel-shaped pattern obtained via sampling theory (Figure 3.1).

Notably, for those studies in Table 3.1 that reported age range (n = 56), we detected a significant positive correlation between age range and the reported SEE ($p = .026$, $r^2 = .088$). As age range increased, the SEE increased (Figure 3.3). Although regression could not be run on all elements individually (e.g. clavicle and mandible), for those elements represented by at least three studies (e.g. femur and rib), no significant relation was detected between age range and SEE. When the relation between average age of a sample and SEE was examined no significant

linear relation was detected (p = .198, r^2 = .035). Finally, using an independent t-test no significant differences were found between the average SEE of individual element types (e.g. femur vs. tibia). This can be seen in Figure 3.4.

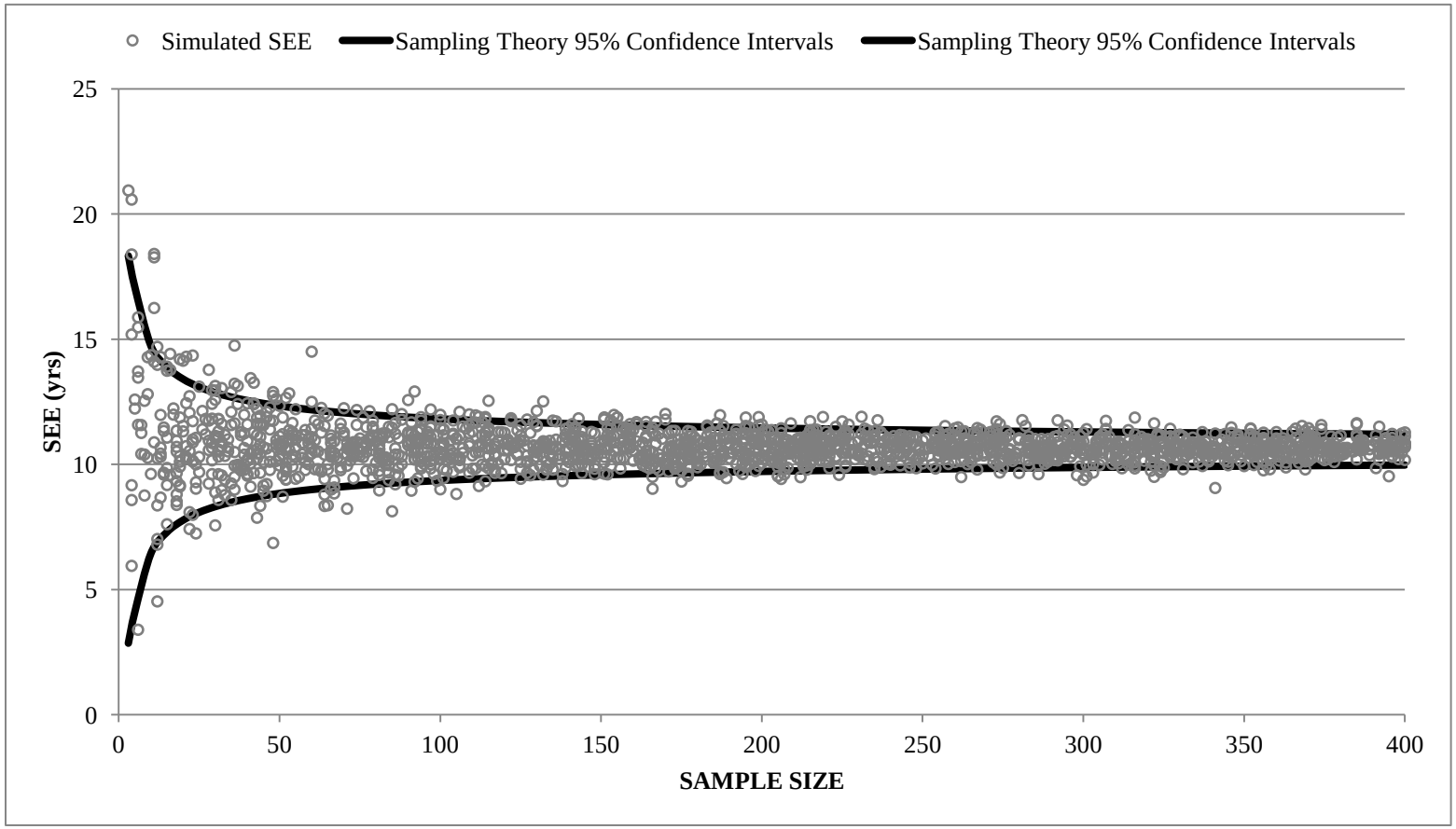

Figure 3.1: Sampling theory distribution 95% confidence intervals (s = 10.59 years) and scatter plot of Standard Error of the Estimates from the simulated model

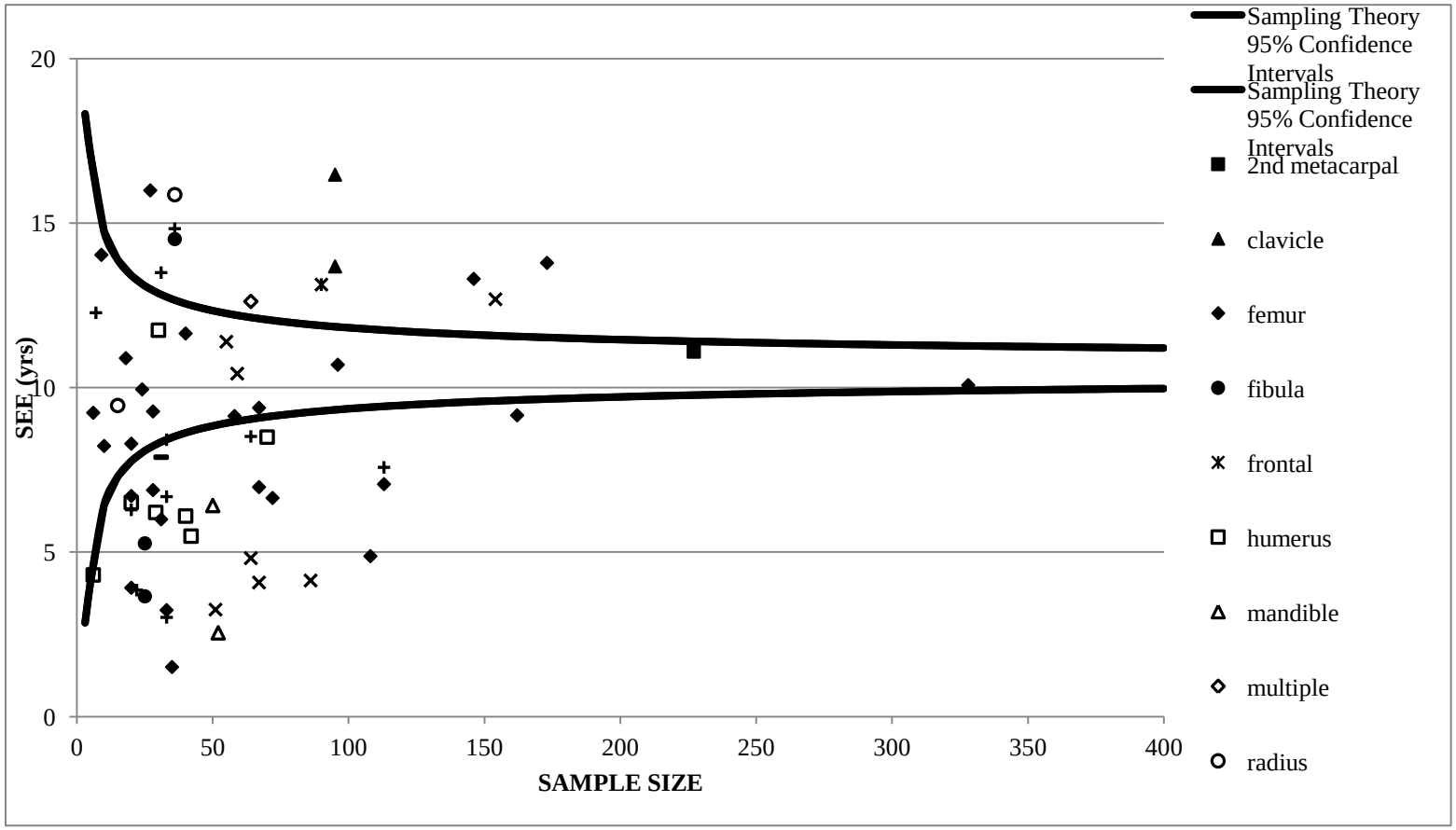

Figure 3.2: Sampling theory distribution 95% confidence intervals (s = 10.59 years) and scatter plot of reported Standard Error of the Estimates from the literature.

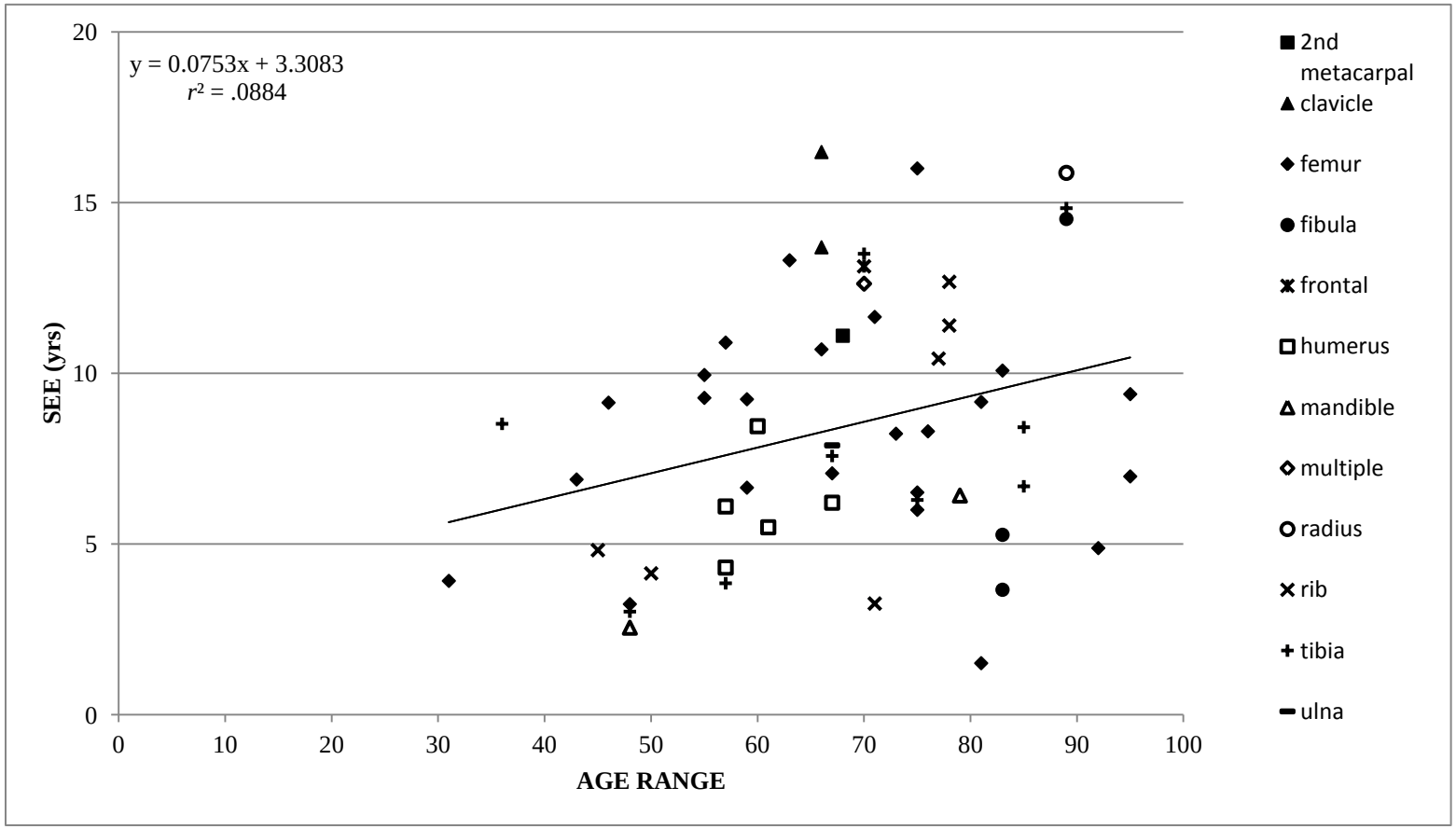

Figure 3.3: Scatter plot of the relation between age range and Standard Error of the Estimate (n= 56, p = .026, r^2 = .088)

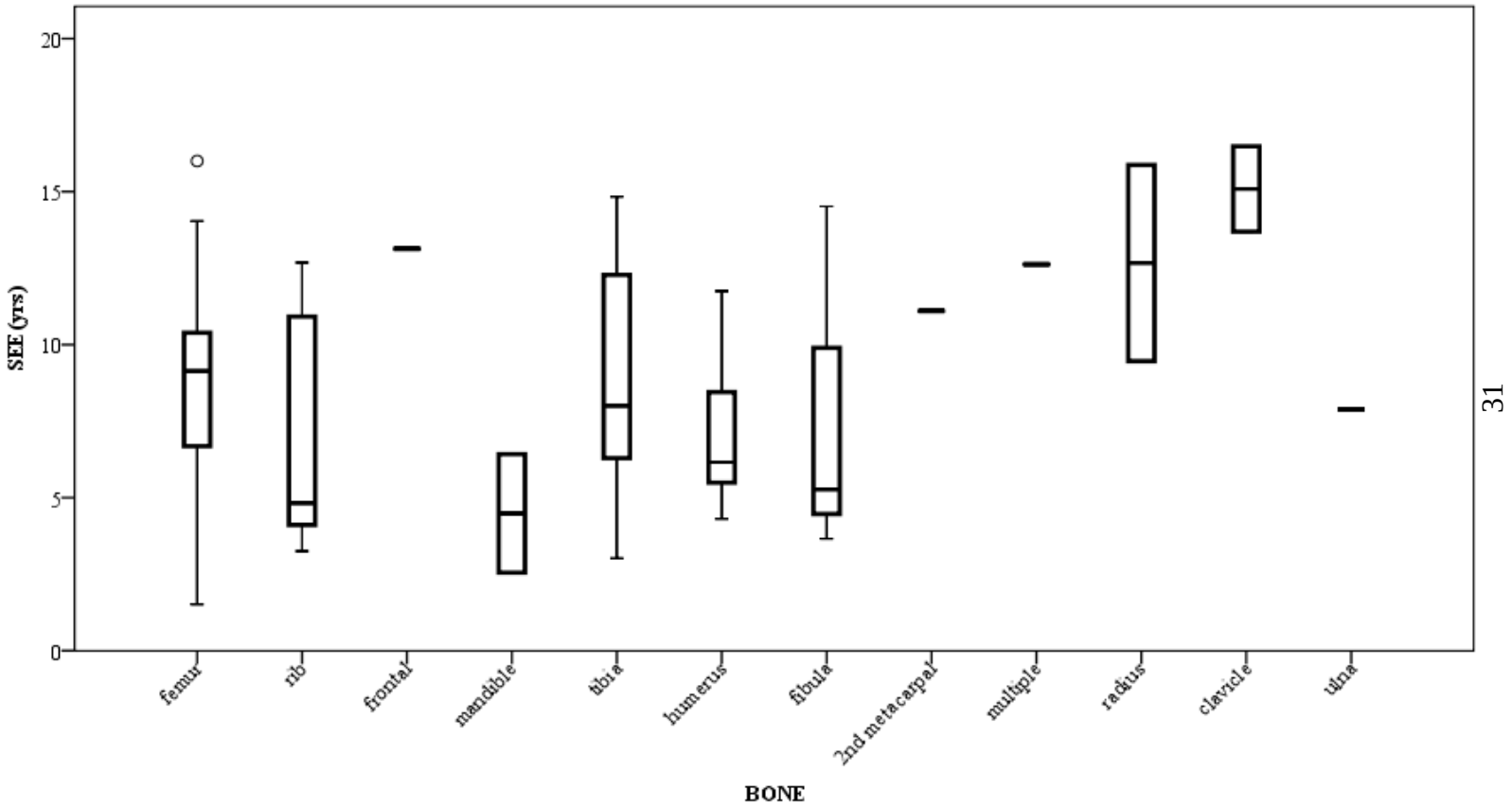

Figure 3.4: Box plot of individual skeletal elements and the Standard Error of the Estimate. Note the outlier in the femur where SEE was 16.00 years (Samson and Branigan, 1987)

3.4 Discussion and Conclusion

Although, the need for larger samples has been discussed by many (Bouvier and Ubelaker 1977; Crowder 2005; Lazenby 1984; Pfeiffer 1985; Walker, Lovejoy and Meindl 1994), sample sizes employed in the generation of histomorphometric aging methods have often been very small. Looking to the related literature, the effect of insufficient sample size is not fully appreciated. Bouvier and Ubelaker (1977) and Lazenby (1984) note that as sample size increases the variability of a sample tends to increase, thereby increasing the SEE. This suggests a linear relation between the two values. As we have illustrated, the relation between sample size and SEE is not linear. Standard error of the estimate becomes more variable as sample size decreases and this random variation lies both above and below the level of the 'true' population variance. This makes meaningful comparisons of different approaches developed within and between skeletal elements very difficult when small samples are involved. As indicated by our literature review there is a large degree of variation within the reported SEE for any given skeletal element. For example, SEE values for the femur and rib are highly variable ranging from 1.51 - 16.00 yrs and 3.26 - 12.68 yrs, respectively (Figure 3.4). From the data available, it is not possible to definitively ascertain whether this intra-element variation is due to differences between the populations sampled, the methodology employed, and/or random error associated with insufficient sampling.

Returning to the comparison of femoral aging approaches in our introduction, a review of Ahlqvist and Damsten's method, by Bouvier and Ubelaker (1977) further complicates matters as they found that when the sample size was increased from 20 to 40, the SEE increased from ±6.71 years to ±11.65 years (recall Kerley's original value was ±9.39 years; n = 67). While the question of which method is better in terms of predictive precision is certainly a valid one, we do

not believe that enough information exists to provide a definitive answer. This problem is further compounded when comparing different skeletal elements that have been analyzed with different methodologies. As noted above, no significant difference was found between skeletal elements and SEE. In the event that a choice needs to be made, we would strongly advocate the use of methods developed on larger sample sizes.

This raises the question: how large is large enough? When using regression to detect a relation many different 'rules of thumb' for minimum sample size have been suggested within the literature. For example, Tabachnick and Fidell (1996) suggest that the minimum sample size that should be used to detect a linear relation is $50 + 8p$, where p is the number of independent variables. Green (1991) notes that the formula $50 + 8p$ is only accurate when a small number of predictor variables are used ($p \leq 7$). Moreover, Tabachnick and Fidell (1989; 1996) strongly advocate using sample sizes greater than 100 whenever possible to avoid errors that accompany small sample size. Nunnally (1967) has similarly suggested that a sample of at least 100 is necessary to demonstrate a relation with little bias. Maxwell (2000) notes that when using regression to detect relations, sample sizes are often too small (100 or less) to truly detect a meaningful relation; and therefore he highly recommends that sample sizes greater than 140 be used. When using regression to make predictions (e.g., age estimates) even larger sample sizes are recommended, preferably on the order of several hundred. This is especially important when using more than one predicting variable (Guadagnoli and Velicer 1988; Maxwell 2000; Nunnally 1967; Nunnally and Bernstein 1994). As Nunnally and Bernstein (1994) note, prediction equations resulting from larger sample sizes are more likely to be stable because the estimates produced from these equations are less likely to result from chance. Our review of the literature revealed a mean sample size of 59 and it is notable that 84% (53/63) of the regression formulae

included in our analysis were based upon fewer than 100 individuals. Provided the SEE value we employed in our calculations (10.59 years) is an appropriate representation of human populations, it takes at least 150 individuals to develop a SEE which itself has a 95% confidence interval of ± 1.0 years or less. It should also be noted that there are diminishing gains with increasing sample size and it seems reasonable to advocate the use of sample sizes in the range of 150 - 200 individuals. If the true population SEE value is less than 10.59 years, which certainly may be the case for different sub-populations and/or skeletal elements, the confidence interval of the SEE will converge more quickly. As Figure 3.1 demonstrates, several studies fall well below the 95% confidence curves predicted at 10.59 years. This could be due to a number of factors including the use of a less variable sample set, a better experimental methodology, and/or chance. For example, as we noted above, methods with smaller age ranges tend to have lower SEE values, which could indicate less variation within the sample; however, while presenting an encouraging starting point, such low-lying points are difficult to interpret - particularly with such small sample sizes. Low-lying points for larger samples would provide more compelling evidence of a more precise approach. The relatively low number of points lying above the 95% confidence curves is encouraging as it suggests population level SEE values are on the order of 10 years or less. That said, a reporting bias against apparently poorer results could not be ruled out.

Ideally, it is beneficial to have a small SEE, but it is important to recognize that SEE is only meaningful if the sample it was generated from is representative of the population it is trying to describe. An important aspect in ensuring a sample is representative of its population is having a sample of an adequate size. It is untenable to expect an aging technique developed on a very limited sample to be representative of the larger population for which its use is ultimately

intended. Histomorphometric aging can be a valuable tool in physical anthropology; yet, few studies have been based on samples of sufficient size to enable confidence in the reported precision. There are only six studies based upon samples of ~150 specimens or more, representing only three skeletal elements (see Figure 3.1). This greatly limits our ability to make definitive comparisons between different methodologies using various skeletal elements. Our primary purpose here is not to criticize the methods and techniques used in histomorphometric aging, but to call attention to the effect of sample sizes on the reported level of precision and advocate the pursuit of more larger-scale studies. In the case of comparing different skeletal elements and methodological approaches, it would be ideal to employ standardized samples.

Given the results presented in this chapter it was concluded that developing a formula to predict age at death through the combination of histology and high-resolution micro-CT could not be resolved due to the limited sample size this study would be conducted on (n = 32). It is important to note, however, that the these results do not mean to suggest that histological studies investigating the age-related differences using smaller samples cannot provide valuable information, only that developing age-regression formulae on small sample sizes is inappropriate. Therefore, the focus of this thesis was shifted to evaluating the effect osteon orientation has on the geometric parameters of the histological features of cortical bone in attempt to better understand the relation between these variables and age. The results of this study are presented and discussed in Chapter 4.

CHAPTER FOUR
DETERMINANTS OF OSTEON GEOMETRIC PARAMETERS AND THEIR RELATION WITH AGE IN CORTICAL BONE

4.1 Introduction

Early bone histology pioneer, Anthony van Leeuwenhoeck (1677), was likely the first to produce a three-dimensional (3D) hand-drawn rendering of the microstructure of cortical bone. He described cortical bone as a collection of longitudinal and radial "pipes." Van Leeuwenhoeck created the rendering from a square piece of bone viewed under a microscope, which can only provide a limited depth of field. Until recently 2D techniques were predominantly used to view the microstructure within cortical bone; however, recent innovations in micro-CT imaging have made it possible to view the microstructure in 3D. These initial studies revealed that the network of the microstructure was much more complex than originally described by Leeuwenhoeck (Arhatari *et al.* 2011; Basillais *et al.* 2007; Cooper *et al.* 2004; Cooper *et al.* 2007a; Cooper *et al.* 2003; Mohsin, Taylor and Lee 2002; Stout *et al.* 1999; Tanck *et al.* 2006); nevertheless, the general description of the microstructure used today remains very similar to van Leeuwenhoeck's early description. The longitudinal pipes he described, now known as Haversian systems (secondary osteons) - after Clopton Havers who was the first to describe secondary osteons in 1691 - form the basic structural unit of bone.

4.1.1 Literature Review

Secondary osteons (hereafter osteons) are formed through remodelling, the primary means of skeletal maintenance. Remodelling is achieved through a process in which the basic multicellular unit (BMU) composed of osteoclasts (bone destroying cells) and osteoblasts (bone forming cells), removes microscopic regions of old bone and replaces them with new bone. As

this process takes place, new osteons subsequently replace and overlap old osteons, forming an interconnected network of osteonal canals.

Histology, the study of microscopic tissues, has principally been used to assess the microstructure of cortical bone. This 2D technique allows for the visualization and quantitative analysis of the specific histological details (such as osteon shape or size) within the microstructure. Using this technique, characteristic age-related differences have been identified and hypothesized to occur as a result of the remodelling process. These differences have largely been described in terms of the osteon geometry (for example, circularity and area).

Currey (1964) and Britz *et al.* (2009) have observed that osteon circularity increases with age. Therefore, younger individuals have increasingly elongated and/or irregularly shaped osteons. As osteons become more circular with age, they have also been shown to decrease in size (Currey 1964), indicating a possible relation between osteon area and age, an observation that has been extensively noted within the literature (Britz *et al.* 2009; Burr, Ruff and Thompson 1990; Currey 1964; Ericksen 1991; Iwamoto, Oonuki and Konishi 1978; Kerley 1965; Martin, Pickett and Zinaich 1980; Singh and Gunberg 1970; Thompson and Galvin 1983; Ural and Vashishth 2006; Watanabe *et al.* 1998; Yoshino *et al.* 1994).

Despite the fact that histological investigations can provide valuable information on the cross-sectional geometry of osteons, these investigations share one inherent limitation: they are 2D in nature. Bone is a 3D structure, in which the microstructure is composed of an elaborate, interconnected, network of canals (Stout *et al.* 1999). Furthermore, the fact that bone continually renews itself throughout life, adds a fourth, temporal, dimension (Cooper *et al.* 2007a; Cooper *et al.* 2003) .

Early attempts to investigate the microstructural system of cortical bone have noted the

complexity (as recently defined by Cooper *et al.* [2003] as the number of branching points within the canal network) of its architecture (Cohen and Harris 1958; Kragstrup and Melsen 1983; Tappen 1977). Nonetheless, the extent of branching within the network was not recognized until Stout *et al.* (1999) generated the first 3D computer-assisted renderings. They qualitatively described the network of Haversian systems as a complex pattern of interconnected, branching networks that cannot be fully realized through 2D techniques.

The application of micro-CT has made it possible for the microstructure of the osteonal canals to be visualized as well as quantified in 3D (Bousson *et al.* 2001; Bousson *et al.* 2004; Cooper *et al.* 2004; Cooper *et al.* 2007a; Cooper *et al.* 2003; Wachter *et al.* 2001). Many of the initial studies investigating the 3D microstructure of cortical bone using micro-CT have similarly noted the complexity of the canal networks (Arhatari *et al.* 2011; Basillais *et al.* 2007; Cooper *et al.* 2004; Cooper *et al.* 2007a; Cooper *et al.* 2003; Mohsin, Taylor and Lee 2002; Tanck *et al.* 2006). The complexity of the canals has also recently been quantified and shown to increase with age (Cooper *et al.* 2007a; Cooper *et al.* 2003).

While the initial application of micro-CT on cortical bone used a scan resolution of only 30 μm (Wachter *et al.* 2001), continuing advancements in the technology have allowed more recent studies to achieve scan resolutions as high as 1.7 μm (Arhatari *et al.* 2011). Nevertheless, the specific details of osteon geometry cannot be consistently visualized or quantitatively evaluated at lower resolutions; and therefore, micro-CT is still limited in its application of characterizing the age-related processes regarding the geometry of osteons.

Although, quantitative analysis of the 3D space of osteon canals is possible using micro-CT, the orientation of osteons has only been qualitatively described in actual bone. Osteons are generally described as being obliquely aligned along the dominant loading trajectories (Ascenzi,

Andreuzzi and Kabo 2004; Black, Mattson and Korostoff 1974; Hert, Fiala and Petrtyl 1994; Lanyon and Bourn 1979; Nomura *et al.* 2003; Petrtýl, Heřt and Fiala 1996; Rho, Kuhn-Spearing and Zioupos 1998), and have been found to gradually become more longitudinal as they move towards the neutral loading axis (Petrtýl, Heřt and Fiala 1996). Petrtýl *et al.* (1996) have also noted that the osteons in unloaded bones are either irregularly or longitudinally oriented, concluding that osteon orientation is guided by strain and/or stress.

Computational modelling has proposed mechanisms to explain the possible association between loading and osteon orientation. These studies have proposed that strain, the ratio of deformation that results from loading (Frost 1997; Lanyon and Bourn 1979), guides the direction of BMU development. (Burger, Klein-Nulend and Smit 2003; Smit and Burger 2000; Smit, Burger and Huyghe 2002; van Oers *et al.* 2008a). In further support for this theory, van Oers *et al.* (2008b) demonstrated that when bone is unloaded, BMUs become randomly oriented.

Although computer simulated modelling can potentially explain the mechanisms that guide the direction of BMUs, the orientation of osteons in 3D has not been quantitatively evaluated in actual bone. Despite the fact that the many studies have described the age-related differences in the microstructure of cortical bone, these studies are predominatly-2D investigations, and cannot provide information on how the differences in orientation may be related to the geometric parameters of osteons. Therefore, the relation between osteon orientation and osteon geometry (circularity, and aspect ratio) remains unknown.

As previously noted, Britz *et al.* (2009) have shown that osteon circularity increases with age. Operating under the widely held assumption that osteons are cylindrical, they predicted that the increasing circularity truly reflects differences in the orientation of osteons. Following their

hypothesis, it would hold that the age related differences observed in osteon geometry in 2D, such as increasing circularity, results from differences in osteon orientation in 3D (Figure 4.1).

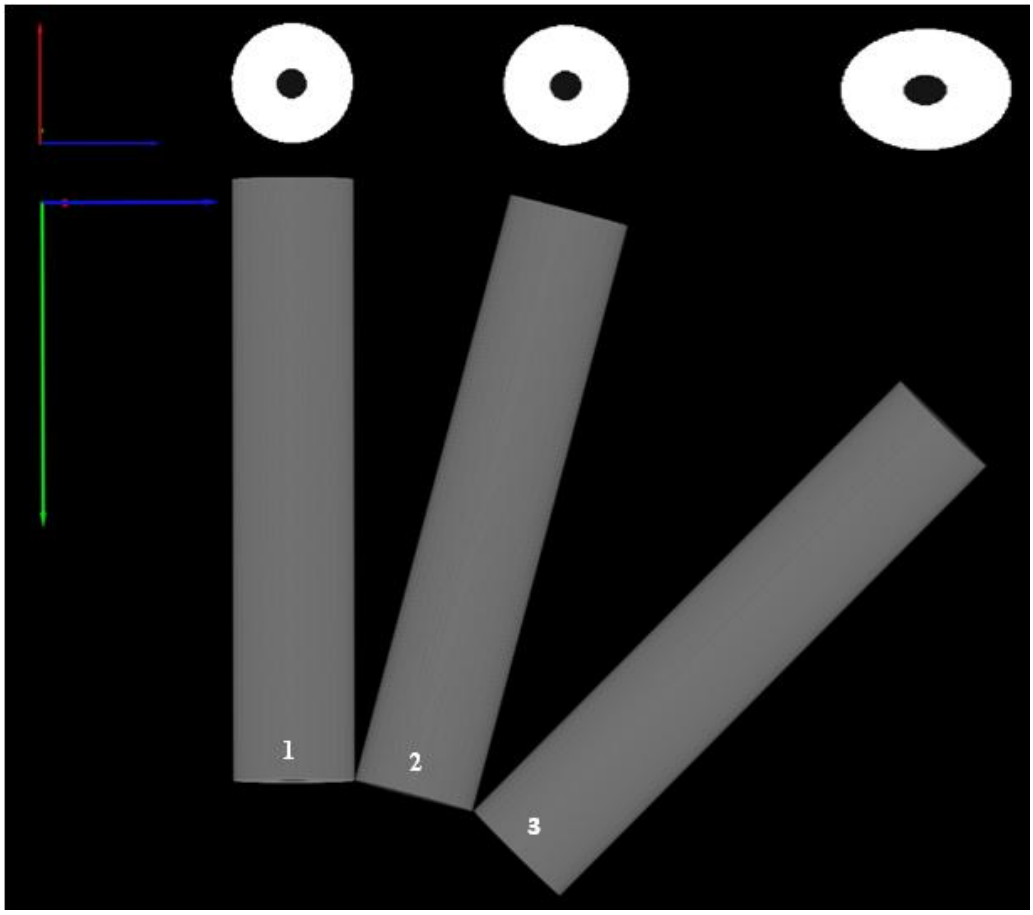

Figure 4.1: If truly cylindrical, longitudinal (cylinder 1) osteons should be circular in their cross sections, while those osteons that are obliquely orientated (cylinder 3) should have cross sections that are elongated. Axes of rotation are also shown: z-axis (green), y-axis (blue), and x-axis (red).

4.1.2 Objectives

Investigations into the remodelling process within the microstructure of cortical bone are restricted when utilizing histology alone, since histology only provides a 2D perspective on a 3D structure. Recent advancements in micro-CT provide an opportunity to investigate osteon orientation in 3D. The integration of histology, with micro-CT allows for the quantitative evaluation of the relation between osteon geometric parameters in 2D and osteon orientation in 3D. To my knowledge, this is the first study to combine 2D and 3D technologies for the purposes of quantitatively investigating the relation between osteon orientation and osteon geometry.

In an attempt to better understand the age-related differences that have been observed within the microstructure of cortical bone and operating under the widely held assumption that osteons are cylindrical, two questions were addressed. **First, does the orientation of osteons in 3D determine osteon geometric parameters visualized in 2D?** Specifically, I tested the hypothesis that the irregular/elongated shaped osteons visualized in a 2D cross-section are associated with deviations in osteon orientation from the longitudinal axis. I predicted that longitudinally orientated osteons would have circular cross-sections and that obliquely orientated osteons would have elongated cross-sections.

Second, can the differences in 3D osteon orientation explain the age-related differences observed in 2D osteon geometry? To address this objective I tested the hypothesis that the age-related differences observed in osteon geometry result from differences in osteon orientation. I predicted that the circular cross-sections associated with older ages result from longitudinally oriented osteons. If this hypothesis is correct, then I also expect osteon orientation to be associated with age.

4.2 Materials and Methods

4.2.1 Experimental Subjects

The femoral specimens used in the present study were obtained from the Melbourne Femur Collection (MFC). These specimens were collected from the Victorian Institute of Forensic Medicine (VIFM) in Melbourne Australia. The VIFM is currently one of the world's largest and best-documented collections from a modern population. The MFC is comprised of individuals whose remains, upon family consent, were donated at the time of autopsy. Next-of-kin questionnaires were completed and those individuals who were known to have medical conditions and/or known to have taken medications that affect bone were not sampled (Clement 2005). A sub-sample of 32 female (20 to 87 years) right femoral-midshaft specimens, collected from 1990 to 2003, was selected for analysis. This study was conducted with ethics approval from the VIFM (EC26/2006), the University of Melbourne (HREC 980139), and the University of Saskatchewan (Bio# 08-46).

The femoral diaphysis has been the most commonly studied region when assessing age-related differences in cortical bone for both 2D (Britz *et al.* 2009; Hennig and Cooper 2011; Robling and Stout 2000) and 3D techniques (Cooper *et al.* 2006; Cooper *et al.* 2007a; Cooper *et al.* 2007b). The anterior femur, which principally experiences tensile loading, was specifically selected as the region of interest (ROI) for this study. Using this region reduced the potential variation in the geometry and orientation of osteons that may be related to various modes of strain experienced within other regions of the femur (Szivek, Benjamin and Anderson 2000). Specimens were originally obtained as complete diaphyseal rings along the bone's long axis and subsequently cut into 5mm blocks from the anterior region (Figure 4.2) (Cooper *et al.* 2006).

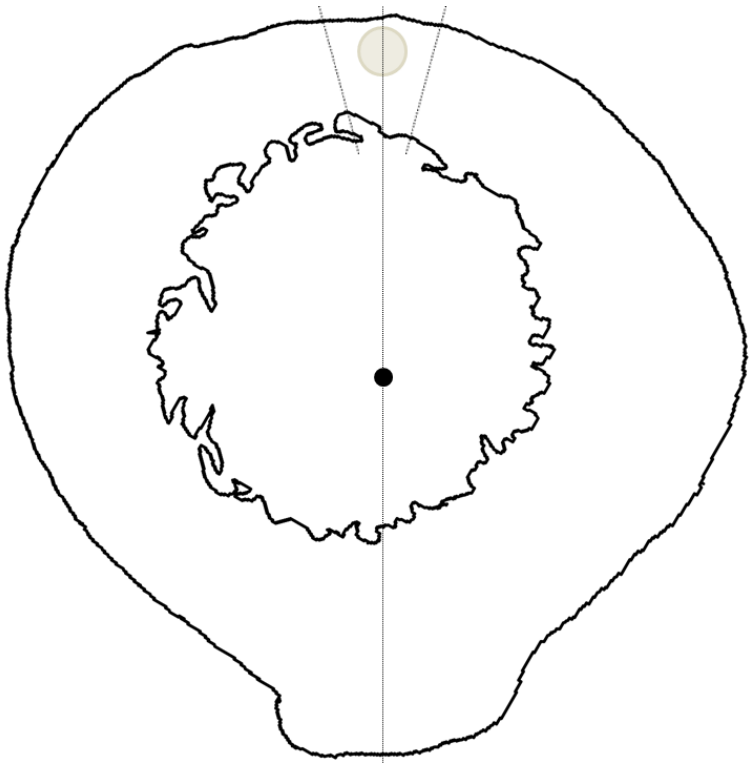

Figure 4.2: Figure demonstrating the placement of the ROI along the periosteal surface of the anterior region. The axis of the centroid (black dot) is the midpoint of the posteriorly located *linea aspera* and was used to locate the anteriorly placed ROI.

4.2.2 Two-Dimensional Analysis

4.2.2.1 Histological Section

Histological ground sections were created using a technique adapted from Frost (1958). Hereafter, histological sections are referred to as sections and individual scan images are referred to as slices in accordance with Kuhn *et al.* (1990). Sections were cut to approximately 150 µm, hand lapped to 50 µm with 2000 Grit 3M sandpaper, and sonicated (Bransonic ultrasonicator; Emerson Electric Co.; Danbury, CT) for several minutes to remove sandpaper residue.

Sections were mounted and imaged at 20X magnification with a modular microscopy platform (Motic BA400; Motic Group Co., LTD.; Richmond BC). Using a motorized microscope stage (OptiscanII; Prior Scientific; Rockland, MA) to help reduce error, tiled images of the entire section were created with the attached PaxCam2 and complimentary image database software V.7.4 (MIS, Inc.; Villa Park, IL.).

4.2.2.1.1 Image analysis

The tiled images were imported into ImageJ software platform (v.1.43u, NIH; http://rsb.info.nih.gov/ij/) and manually matched to an appropriate micro-CT slice (note: perfect matches could not be achieved as a result of slight variations in imaging and sectioning planes). Once matched, 3mm circular ROIs were selected from the primary axis of the periosteal surfaces (Figure 4.2). Individual osteons were outlined using ImageJ's built-in editor and an interactive LCD tablet (Cintiq 12WX, Wacom co. Ltd., Japan). Osteon outlines were recorded separately for all ROIs. These outlines served as the basis for the calculation of the averages of each geometric parameter for individual specimens. Osteons were outlined according to Britz *et al.* (2009). In brief, all osteons within the ROI with a clearly defined cement line were manually outlined. Osteons where ≥75% of the cement line was visible and where the remainder could be

inferred were also outlined. Osteons near the boundaries of the ROI were only outlined if the entire canal was within the ROI boundary and ≥75% of the cement line was visible.

4.2.2.1.1.1 Primary Measures

The osteon geometric parameters of osteon circularity and aspect ratio were measured in ImageJ (ImageJ: v.1.43u, NIH; http://rsb.info.nih.gov/ij/). Osteon circularity (On.Cr., unitless) and aspect ratio (AR, unitless) were selected because they are self-normalizing measures and are not affected by the size of the osteon.

Osteon circularity measures how circular an object is from the outline of the osteon (Figure 4.3). This formula is written as:

$$\text{Circularity} = 4\pi\left(\frac{\text{Area}}{(\text{Perimeter})^2}\right)$$

Equation 4.1

Values approaching zero represent increasingly elongated/irregular shapes while values of one represent perfect circles.

Aspect ratio measures how circular an object is from the ratio between the minor and major axes of the ellipse of best fit. For the purposes of this thesis, the inverse of the aspect ratio was used (Figure 4.3). Formula written as:

$$\text{Aspect Ratio} = \frac{\text{Minor Axis}}{\text{Major Axis}}$$

Equation 4.2

Similar to osteon circularity, scores of zero represent increasingly elongated ellipses, and scores approaching one represent a circular shape.

While osteon circularity and aspect ratio can both be used to describe the circularity of an object, it is important to highlight that they are different parameters. Osteon circularity is a measurement of the compactness of a shape and is directly measured from the outline of the osteon. Aspect ratio, however, is a measurement of the ratio between the minor and major axes and is measured from the ellipse of best fit (Figure 4.3).

4.2.2.1.1.2 Secondary Measures

Osteon angle (theta) is the angular rotation of the 2D outline about the x-axis. It is measured from the centroid of the ellipse of best fit as the angle between the major axis and a line running parallel to the x-axis (Figure 4.4b). Theta angles ranged from 0° to 180° but were transformed to range from 0° to 90° and represent the circumferential (0°) and radial (90°) directions.

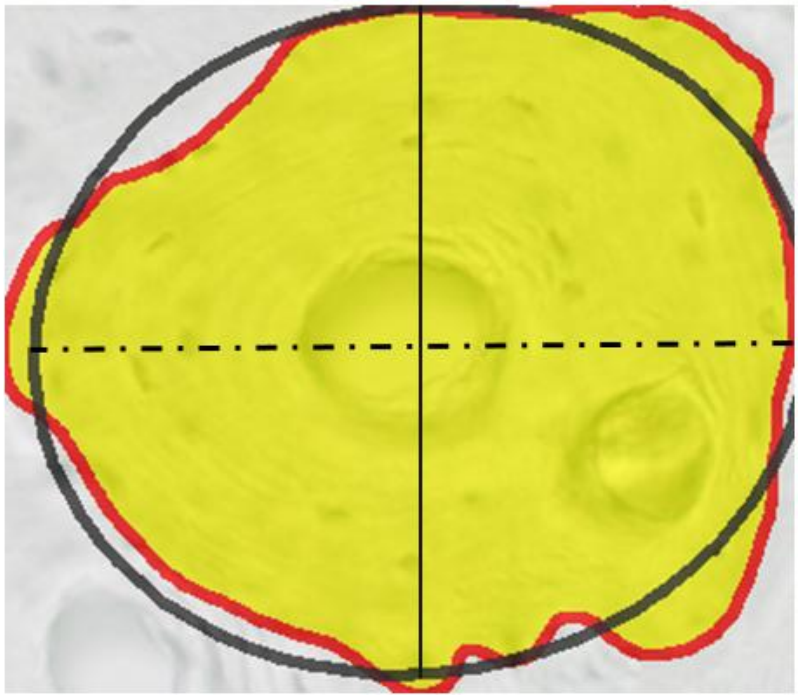

Figure 4.3: Figure of an outlined osteon with the ellipse of best fit. Solid line represents the minor axis. Dashed line represents the major axis. Circularity was calculated from the outline of the cement line (red). Aspect ratio was calculated from the ratio between the minor and major axes.

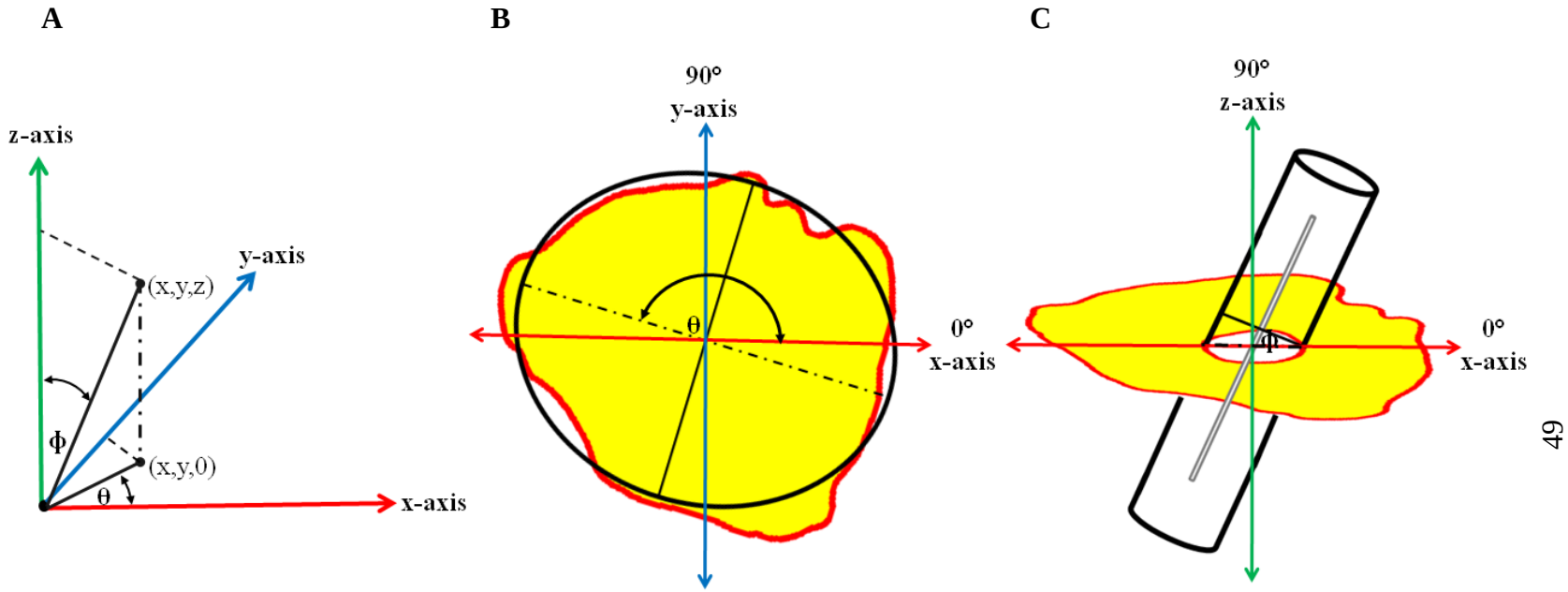

Figure 4.4**:** A**:** Image showing the axes of rotation of theta (θ) and phi (ϕ) along the Cartesian coordinate system. Theta was measured from the x-axis (red) and phi was measured from the z-axis (green). B: Schematic demonstrating how osteon angle (theta) was measured. The solid red line represents the line parallel to the x-axis from which theta was measured. Note the circumferential direction (0°) runs along the x-axis and the radial direction (90°) runs along the y-axis. C: Schematic demonstrating how osteon orientation (phi) was measured. Note the longitudinal direction (90°) runs along the z-axis and the horizontal direction (0°) runs along the x-axis. Solid lines represent the minor axis. Dashed lines represent the major axis.

4.2.3 Three-Dimensional Analysis

4.2.3.1 Imaging

Volume renders for this study were created from the micro-CT data collected from specimens that were previously scanned by Cooper *et al.* (Cooper *et al.* 2006; Cooper *et al.* 2007a). These scans were created using a SkyScan 1072 micro-computed tomograph (Kontich, Belgium) - 7µm isotropic voxel size. Their scan protocol included a rotation through 180° at a rotation step of 0.23°. The X-ray settings were standardized to 100 kV and 100 µA with an exposure time of 7.5 s per frame. To reduce noise, six-frame averaging was used. Each scan took approximately 12 hours.

I obtained matching ROIs for the 3D data using CT Analyser 1.10.1.0 software package (SkyScan, Aartselaar, Belgium). One hundred slices from these ROIs were used to create volume renders of the canals in Amira 5.3.3 (Visage Imaging Inc. Berlin, Germany). At a 7 µm resolution (slice thickness), the total depth (z-dimension) of the render was 700 µm, which was specifically chosen to ensure that the length of the canals were more than twice the approximate diameter of an average osteon - 200 µm to 300 µm (Bousson *et al.* 2000; Britz *et al.* 2009; Robling, Castillo and Turner 2006). Each volume render was skeletonized and subsequently edited using the filament editor extension in Amira.

4.2.3.1.1 Image Analysis

The orientation of the canals was measured in ImageJ. A custom macro was used to straighten and calculate the orientation of each canal (from the skeletonised lines) through trigonometric functions, based on the known 3D coordinates of each line. Osteon orientation (phi) is the measured angular rotation of the osteonal canal about the z-axis (Figure 4.4c). The orientation of each osteon was measured along the horizontal axis, where 0° represents a canal

running along the horizontal plane and angles approaching 90° represent canals that are longitudinal. The orientation of individual canals were measured with both positive and negative phi values, but for the purpose of this study, absolute values were used and therefore all orientations range from 0° to 90°.

4.2.4 Two-Dimensional and Three-Dimensional Data Analysis

The ROIs of the histological section were imported into Amira and superimposed into the middle of each volume render (Figure 4.5). The 3D volume renders of each specimen were manipulated so that the canals of the render matched the corresponding osteonal canals of the histological section. Once straightened, skeletonizations of the volume renders were imported back into Amira where the appropriate lines of the renders were manually matched to the corresponding osteon outlines (Figure 4.6). These matches served as the basis for the statistical comparison between the 3D data and the 2D data.

To eliminate potential sources of error in the editing process of the skeletonizations, osteons were excluded from analysis if the corresponding straightened line did not run through the outline of the matching osteon. Osteons with more than one line passing through were included in the analysis only if the secondary line was clearly distinguished from the primary line as a branching point. Furthermore, any canal with an orientation below 45° was considered a Volkmann's canal and was excluded from analysis. For a detailed description of the study's step-by-step protocol, refer to Appendix II.

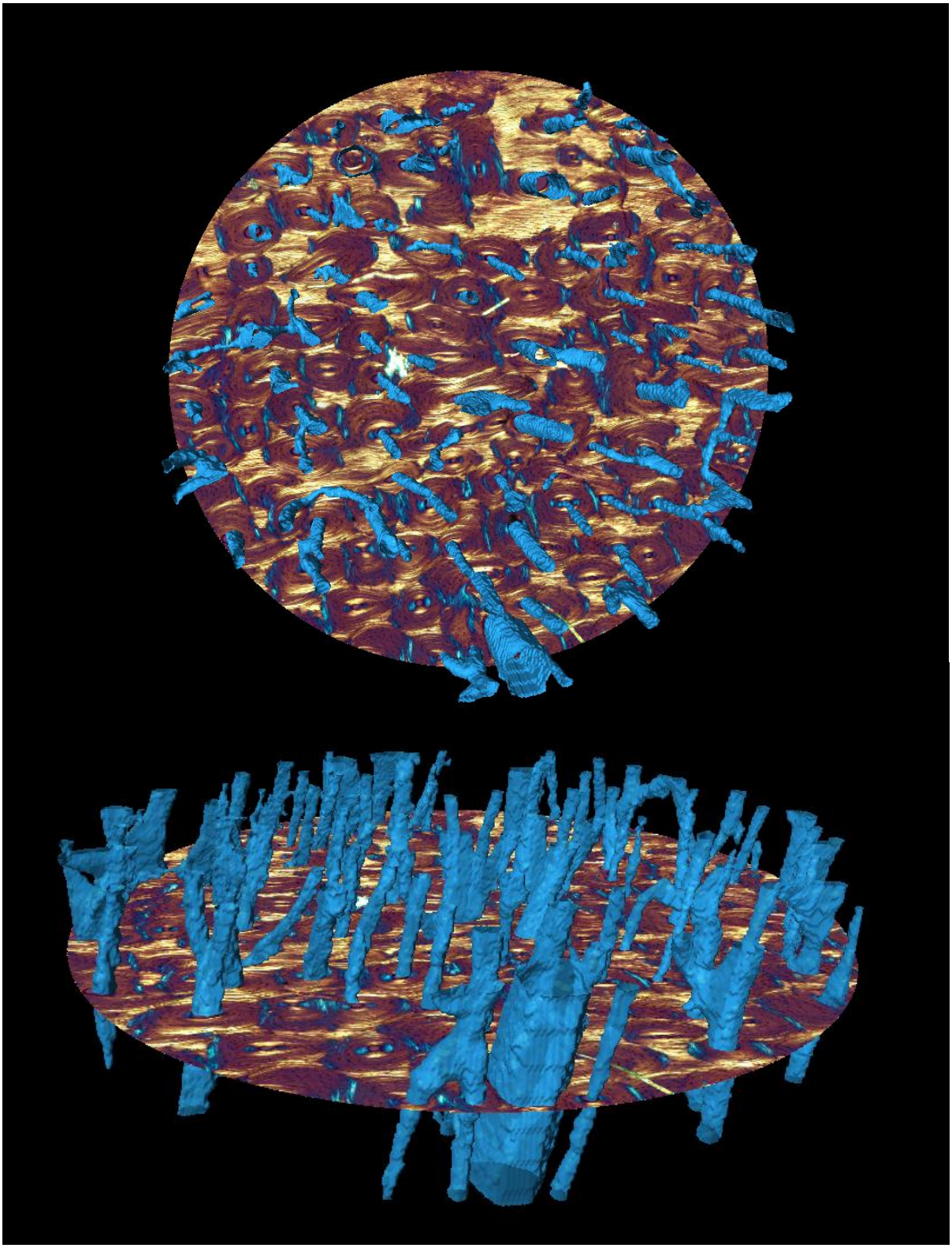

Figure 4.5: Histological section superimposed into the middle of the volume render. Fifty slices have been placed above and below the histological section (21 yrs, female). To: longitudinal view. Bottom: oblique view.

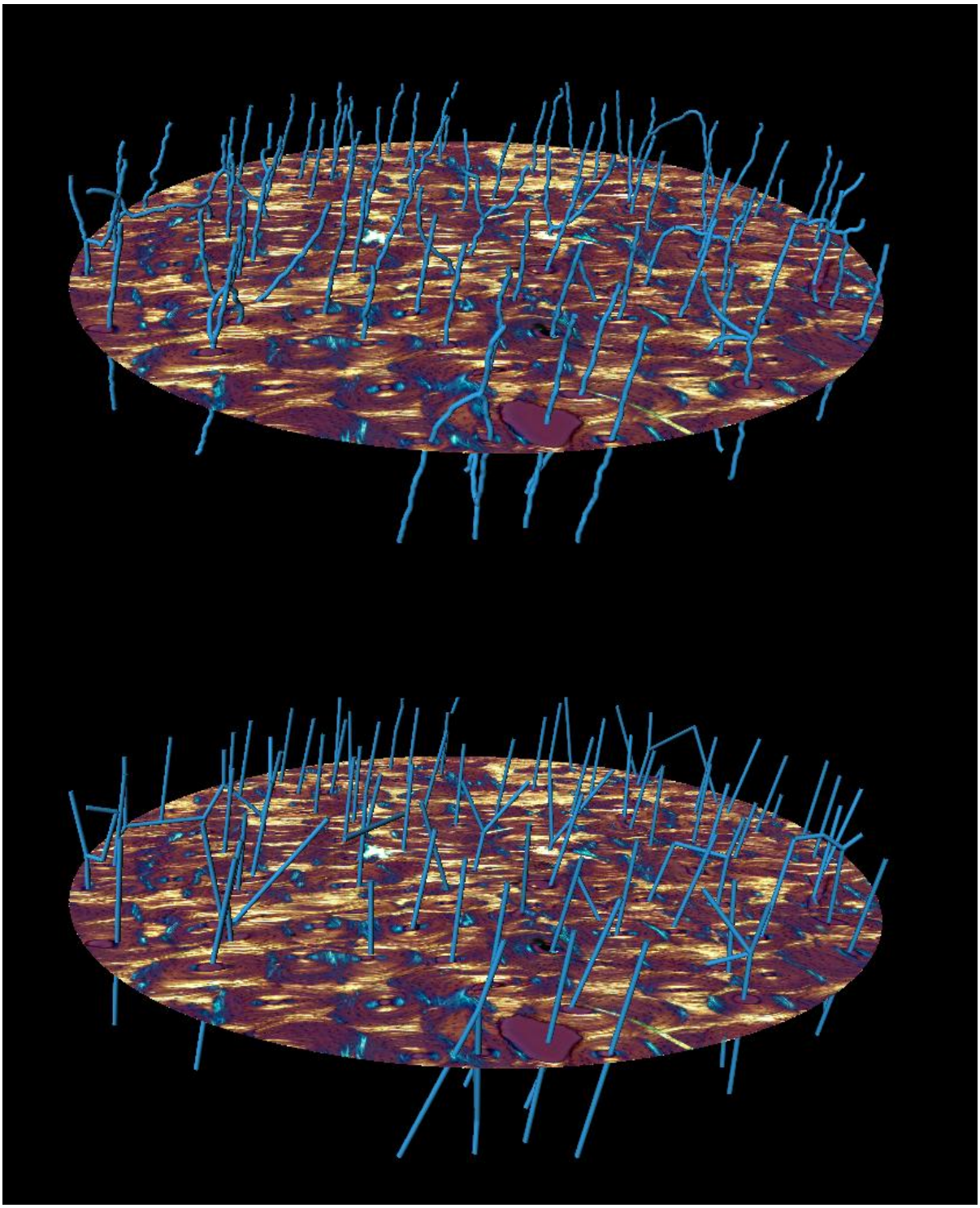

Figure 4.6: Histological section superimposed into the middle of the volume renders. Fifty slices have been placed above and below the histological section (21 yrs, female). Top: skeletonization from the volume render. Bottom: straightened lines from skeletonization.

4.2.5 Statistics

All statistics were calculated using SPSS 19.0 (SPSS Inc, Chicago, IL). The mean values of each variable were calculated for individual specimens and employed for all analyses. Komologorov-Smirnov 1-sample tests determined that the mean values for all parameters were normally distributed. Significance level for all analyses was set to the standard $p < .05$.

Regression analysis was used to examine the relation between orientation and osteon geometry. I hypothesized that osteon orientation (phi) predicts osteon shape. Assuming cylindricality of osteons, the orientation (phi) of osteons should determine their geometry. Therefore, as osteons become longitudinally orientated in 3D their cross-sections in 2D should become circular. Once the major axis was solved for (see Appendix III), osteon circularity (Equation 4.3) and aspect ratio (Equation 4.4) were predicted and their relation to osteon orientation (phi) estimated (Figure 4.7) (Appendix III)

$$\text{Circularity} \propto \pi^2 \left(\frac{(\text{Minor Axis})^2}{\sin\phi\,(\text{Perimeter})^2} \right)$$

Equation 4.3

$$\text{Aspect ratio} \propto \sin\phi$$

Equation 4.4

Univariate analysis of covariance was then used to investigate the relation of 2D osteon geometry against age and osteon orientation as covariates in order to investigate whether orientation independent of age could explain the differences in osteon geometric parameters. Partial eta-squared ($\eta^2_{partial}$) values were used to describe the relative amount of variance

accounted for by each factor/covariate. If cylindrical, the differences in orientation should then explain the age-related differences in the geometric parameters of osteons that have been previously observed. Since I predicted that the associated age-related increases in the circularity of osteons result from increases in osteon orientation (phi), I expect to see a relation between osteon orientation and age. Consequently, as age increases, osteons will become increasingly longitudinal and therefore, have circular cross-sections whereas the osteon of younger individuals will be more obliquely orientated with elongated cross-sections (Figure 4.7).

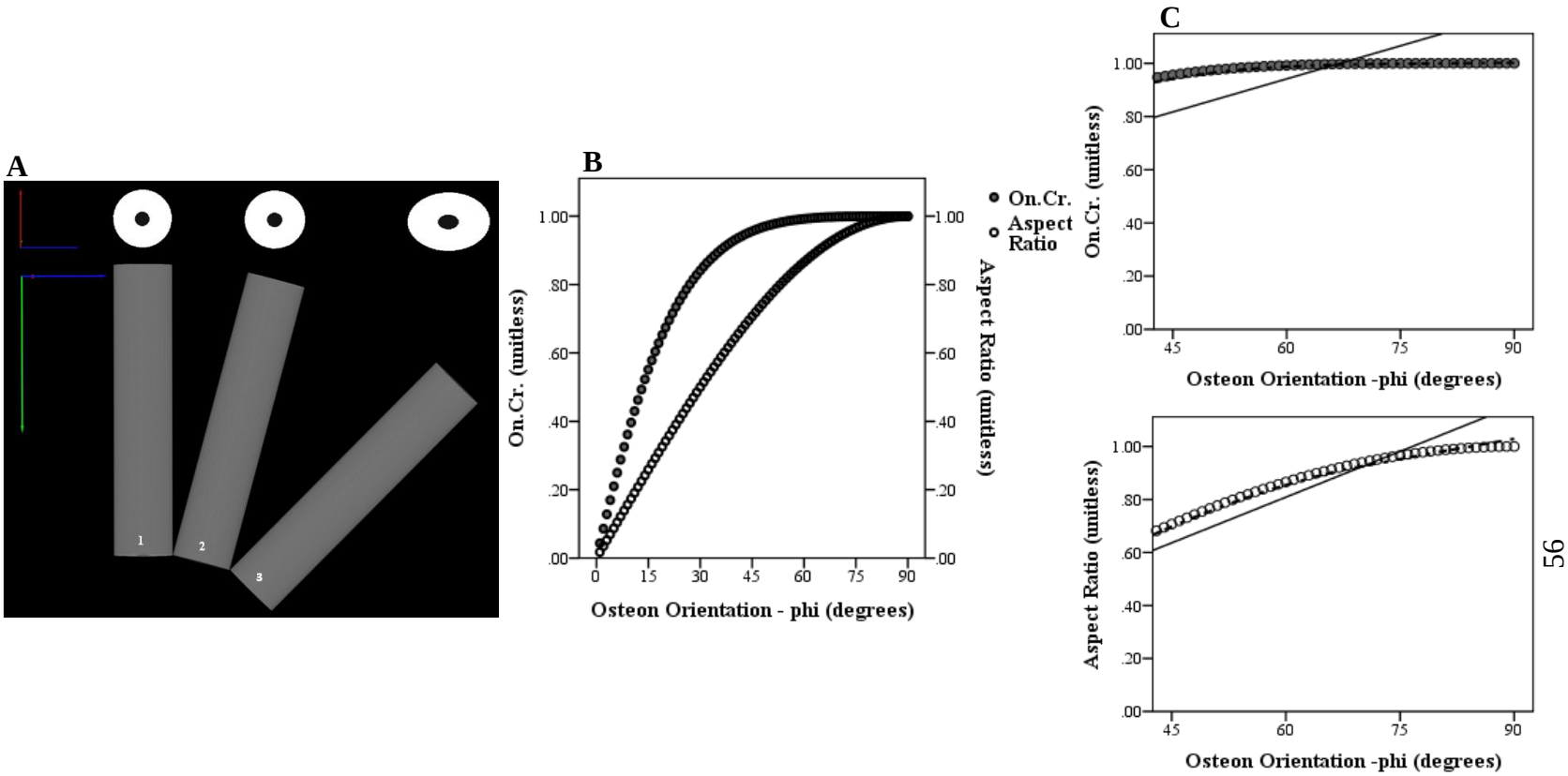

Figure 4.7: A: Assuming osteons are cylinders, the orientation can be used to predict geometric parameters. Osteons that are longitudinal (cylinder 1) have circular cross-sections, while osteons that are more obliquely orientated (cylinder 3) have elongated cross-sections. The axes of rotation are also shown: z-axis (green), y-axis (blue), and x-axis (red). Figures B and C demonstrate the expected relations between phi and osteon circularity and aspect ratio. Minor Axis /sin ϕ was used to determine the major axis. Using a standard minor axis as a diameter (250 μm), osteon circularity and aspect ratio could be predicted from estimating the major axis. Note these relations are not linear. Solid black line represents linear line of best fit. Dashed black line represents loess line of best-fit. Phi in Figure C represents range of degrees used in analysis. Anything below 45° was assumed to be a Volkmann's canal and discarded from analysis

4.3 Results

4.3.1 Summary Statistics

Four of the 32 histological sections could not be matched to a micro-CT slice and were excluded from the analysis. Additionally, one specimen with only primary canals (specimen VIFM_035) was also removed from analysis. Twenty-seven specimens, 20 to 86 years (mean 50.46 years; SD 22.17 years), and 1,408 osteons were analyzed in this study (Figure 4.8). Summary statistics of 2D and 3D parameters are provided in Table 4.1. Images of individual specimens and their osteon outlines are presented in Appendix IV.

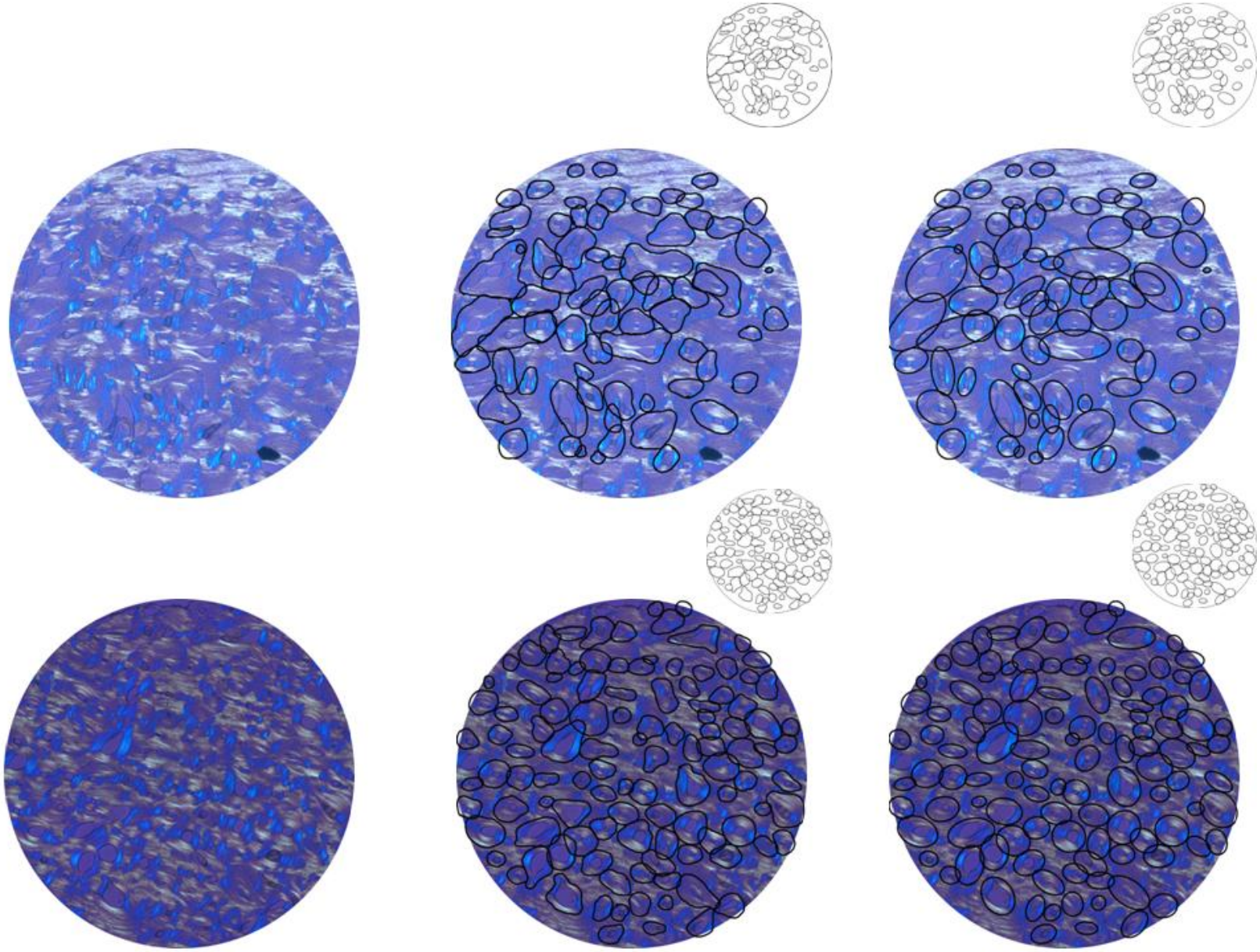

Figure 4.8: Example of ROIs from a younger (top, 33 yrs) and older (bottom, 86 yrs) female specimen. ROIs analyzed (left), the outlined osteons within the ROI (middle) and the ellipse of best-fit (right). Periosteal surface is up.

Table 4.1: Summary statistics of 2D and 3D parameters from mean values

	Sample (n)	**Range**	**Minimum (mean)**	**Maximum (mean)**	**Mean**	**Standard Deviation**
Age	27	66	20	86	51.48	22.38
Osteon Circularity	27	0.13	0.72	0.85	0.79	0.04
Aspect Ratio	27	0.18	0.59	0.77	0.70	0.05
Osteon Angle - theta (degrees)	27	36.28	15.44	51.72	30.09	9.43
Osteon Orientation - phi (degrees)	27	9.89	74.06	83.95	79.08	2.33

4.3.2 Primary Measures

4.3.2.1 Objective One

The raw data in Figure 4.9a illustrates the relation between osteon orientation (phi) and osteon circularity and aspect ratio. A significant negative correlation was found between osteon orientation (phi) and both osteon circularity and aspect ratio ($p = .016$, $r^2 = .211$; $p = .020$, $r^2 = .198$, respectively - Figure 4.9b). Thus, osteons became increasingly circular as their orientation (phi) became more oblique.

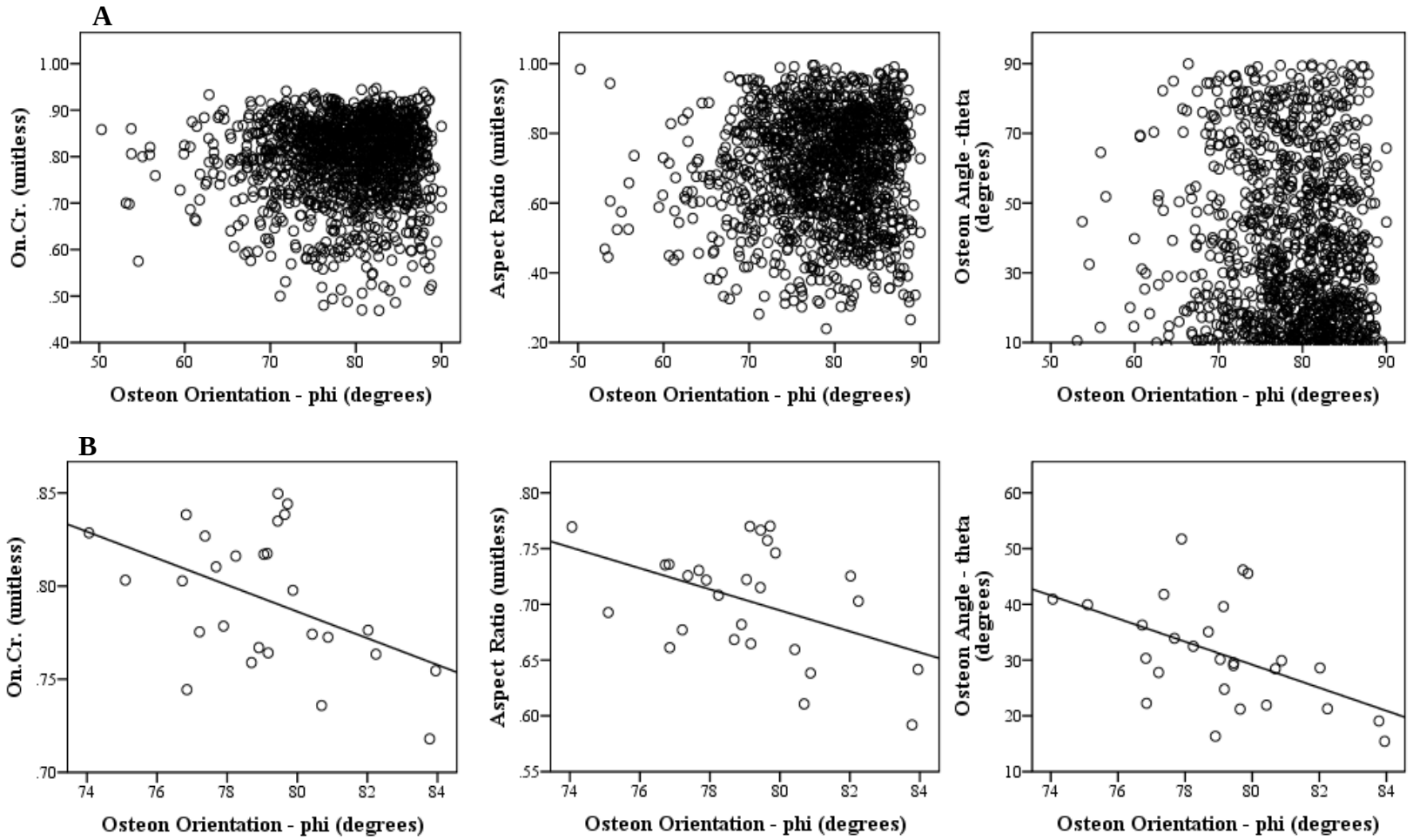

Figure 4.9: A: Scatter plot from the raw data showing the correlation of osteon orientation (phi) against the 2D geometric parameters (osteon circularity, aspect ratio, and osteon angle - theta). B: Scatter plot of the mean values demonstrating the correlation between phi and the 2D geometric parameters. Solid black line represents the line of best-fit. phi and On.Cr.: $p = .016$, $r^2 = .211$. phi and AR**:** $p = .020$, $r^2 = .198$. phi and theta: $p = .007$, $r^2 = .260$.

4.3.2.2 Objective Two

Univariate analysis of covariance revealed a significant positive correlation between age and both osteon circularity and aspect ratio ($p < .001$, $r^2 = .613$; $p < .001$, $r^2 = .523$) and signified that osteons became increasingly circular with age independent of osteon orientation (Figure 4.10). Age accounted for 51% of the variation of osteon circularity and 41% of the variation of aspect ratio. Table 4.4 demonstrates that when analyzed as covariate with age, osteon orientation (phi) was no longer significantly related to either osteon circularity or aspect ratio.

While the relation between osteon orientation (phi) and age was not statistically significant, the negative correlation approached significance ($p = .059$, $r^2 = .135$). The direction of the detected difference was unexpected. Osteons became more obliquely oriented as age increased. Figure 4.11 illustrates that there is a trend towards osteons moving away from the longitudinal plane as age increases.

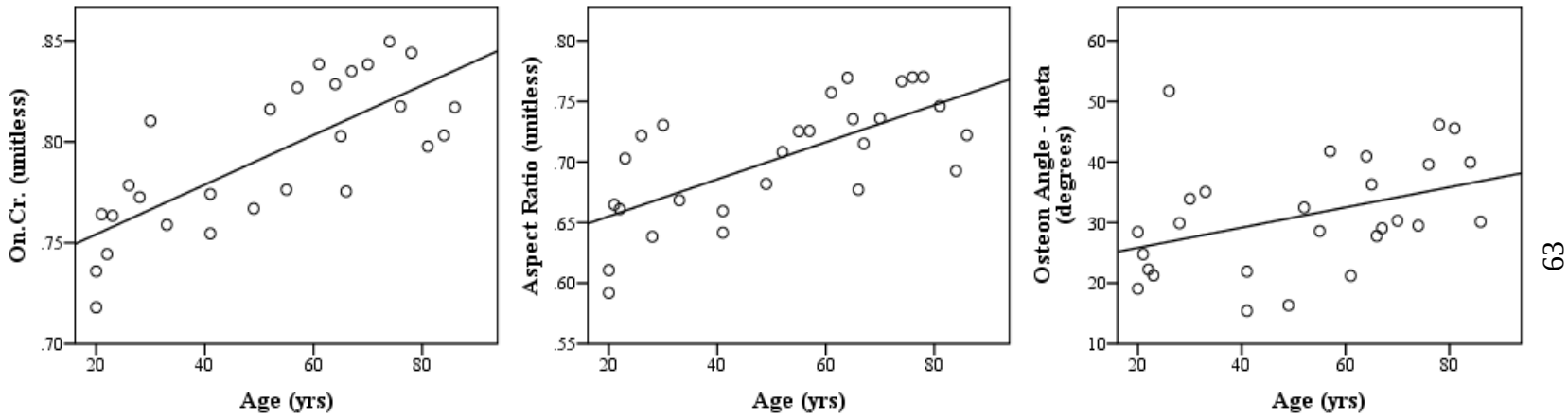

Figure 4.10: Scatter plots of the mean values demonstrating the correlation between age and the 2D geometric parameters. Solid black line represents the line of best fit. Age and On.Cr.: $p < .001$, $r^2 = .575$. Age and AR: $p < .001$, $r^2 = .481$. Age and theta: $p = .041$, $r^2 = .156$.

.

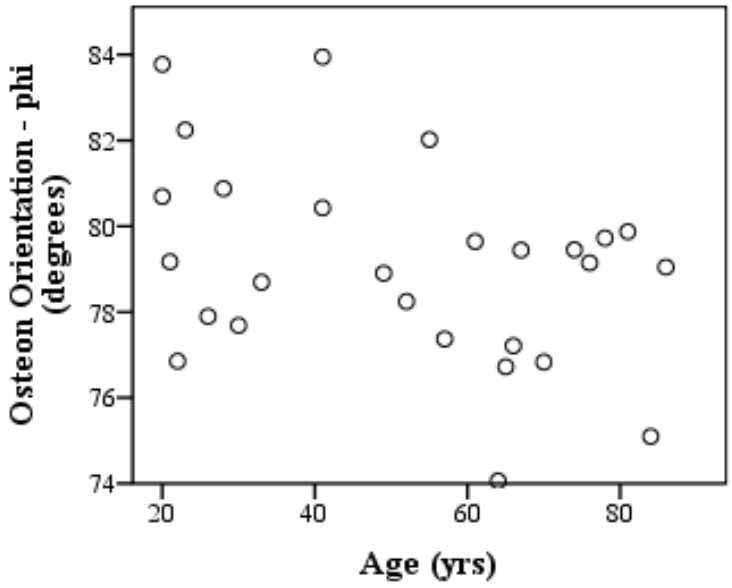

Figure 4.11: Scatter plot of the relation between age and osteon orientation (phi). Note this is not a significant relation. However, the relation approaches significance (age and phi: $p = .059$, $r^2 = .135$)

4.3.3 Secondary Measures

A significant negative correlation was also found between osteon orientation (phi) and osteon angle (theta) (p = .007, r^2 = .260). As osteons are rotated along the z-axis, they appear to be rotated along the x-axis as well. Figure 4.9b demonstrates that as osteons become more radially orientated along the x-axis they become more obliquely orientated along the z-axis.

A significant positive correlation was also detected between age and osteon angle (theta) (p = .041, r^2 = .156). Figure 4.12 illustrates that as age increased osteons also appeared to move away from the circumferential plane, becoming more radially orientated. To demonstrate the differences in osteon angle (theta) values with age, Figure 4.13 is divided into two age categories: young adult (20yrs - 49yrs) and old adult (50yrs - 89 yrs). Note that while the old age group had a high incidence of circumferential osteons, there was a progressive increase in the frequency of osteons that became more radially aligned. However, the results from the univariate analysis revealed that osteon orientation, not age, explains the rotation of osteon angle (theta) (p = .029, r^2 = .310 see Table 4.2) and accounted for 18% of the variance of osteon angle

Table 4.2: Summary statistics for univariate analysis. β represents the regression coefficient for each parameter. η^2_{partial} is the proportion of total variance accounted for by each variable

Variable	r^2	**Parameter**	β	**Sig**	η^2_{partial}
Osteon Circularity	. 613	Intercept	.993	.000	.580
		Age	.001	.000	.510
		Orientation (phi)	-.003	.139	.089
Aspect Ratio	.523	Intercept	1.003	.001	.381
		Age	.001	.000	.405
		Osteon Orientation (phi)	-.005	.159	.081
Osteon Angle (theta)	.310	Intercept	161.049	.013	.231
		Age	.101	.200	.068
		Osteon Orientation (phi)	-1.709	.029	.183

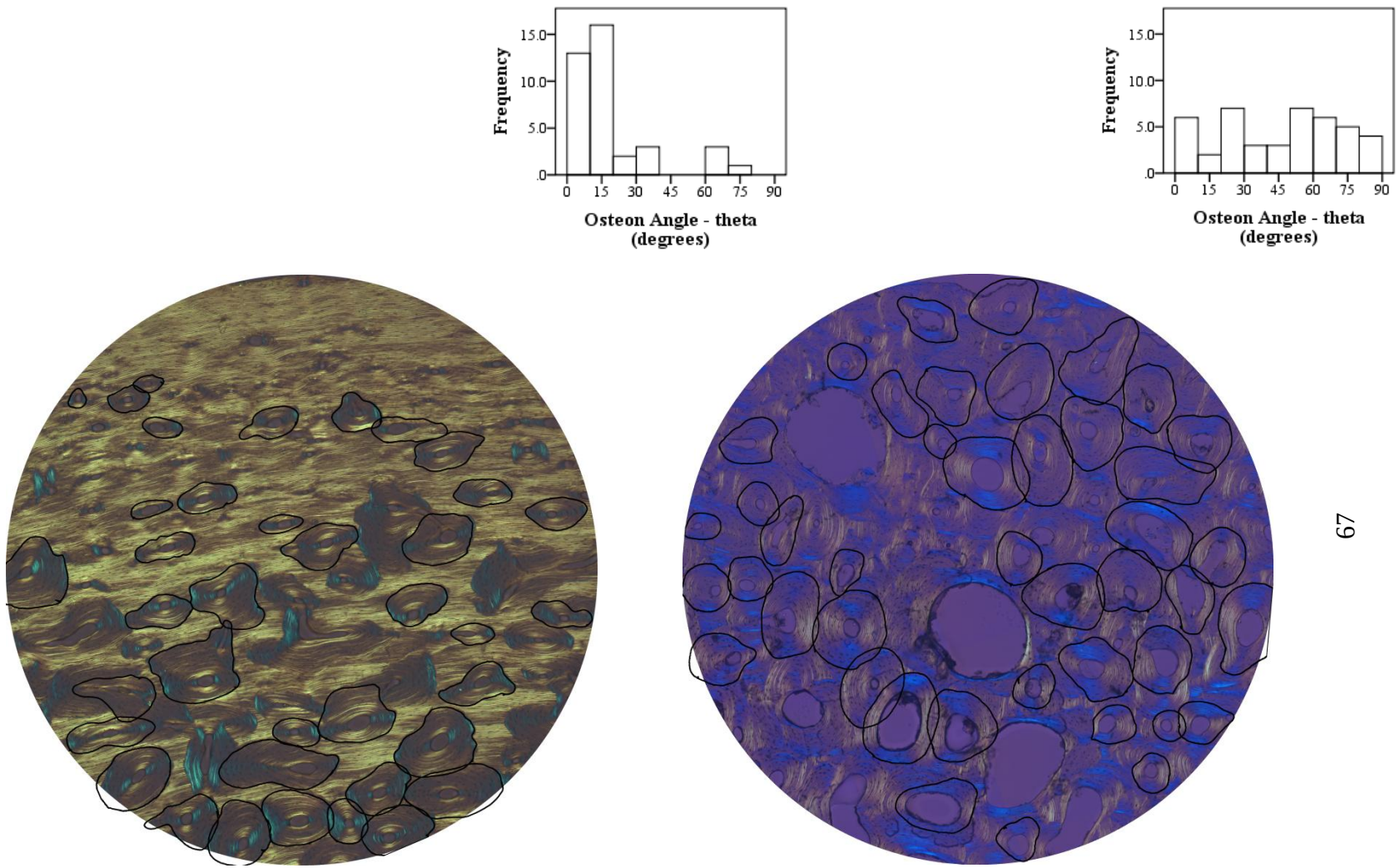

Figure 4.12: Example of osteon angle (theta) from a younger female (left, 20 yrs) and an older female (right, 78 yrs). Note: the outlines from the individual on the left are more circumferential in their orientation (major axis aligned along x-axis) than the outlines from the individual on the right, which are more radial in their orientations (major axis aligned along the y-axis). Histograms (top right corner) show the distributions of osteon angle (theta) for each individual. Periosteal surface is up.

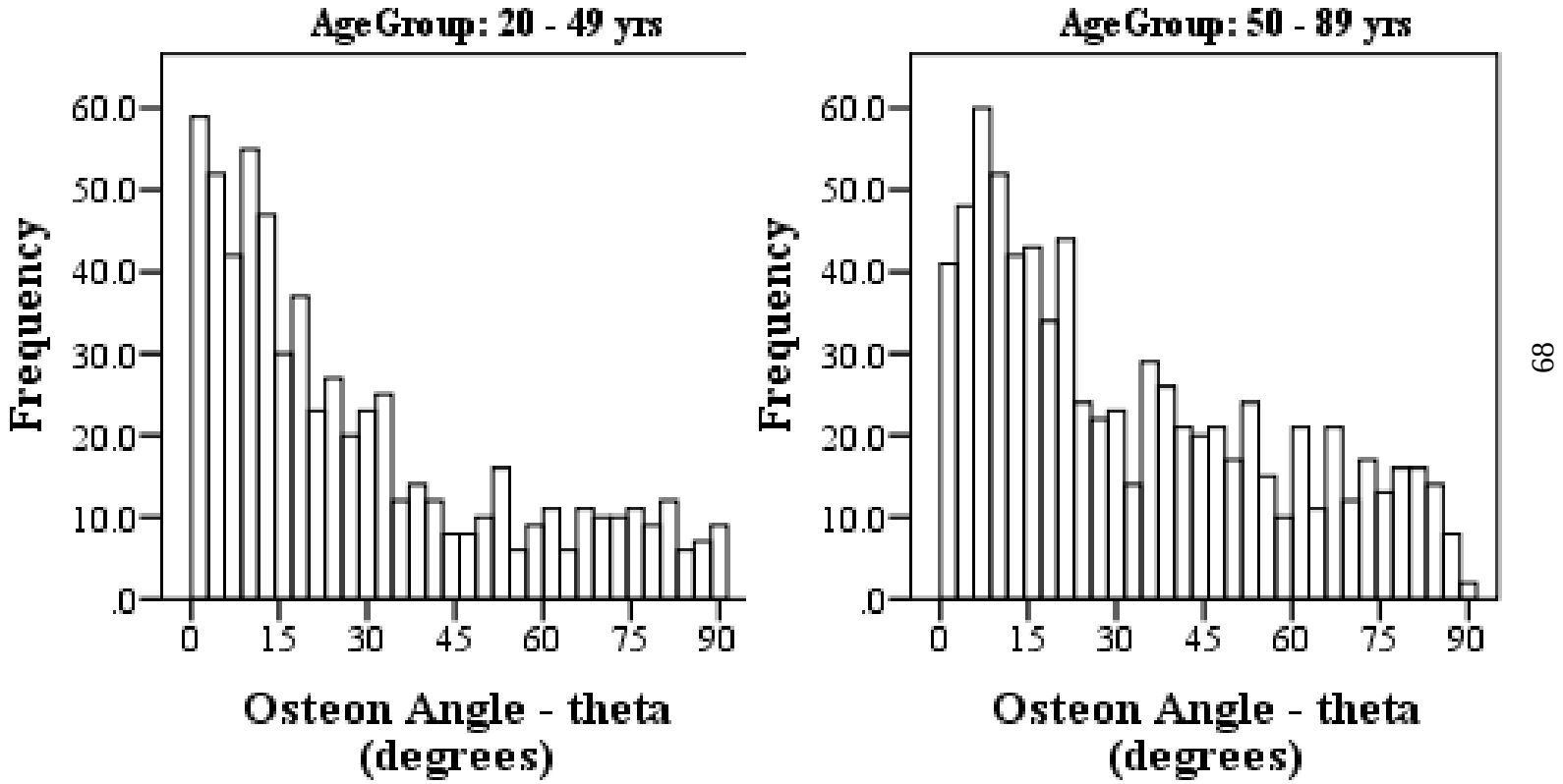

Figure 4.13: Histogram showing the distribution (raw data) of osteon angle (theta) by age group.

4.4 Discussion and Conclusion

I used two measures of circularity (osteon circularity and aspect ratio) to assess the relation of 2D osteon geometry to 3D osteon orientation (phi) and age. Both variables quantify the circularity of an object; however, they are different measurements. Osteon circularity is a direct measurement from the outline of the cement line and is therefore affected by the scalloped edges of the cement line. Aspect ratio is an indirect measurement from the ellipse of best-fit, which is estimated from the area of the outlined cementt line (Figure 4.3). To ensure that the ellipse of best-fit both was both an accurate and precise measurement, I evaluated the relation between osteon area and the estimated area from of the ellipse of best-fit (calculated from the major and minor axes) and found a perfect correlation ($p < 001$; r^2 1.00). Despite the differences between osteon circularity and aspect ratio, these measurements are very similar and prove to be closely related ($p < 001$; r^2 .758). Furthermore, the results presented here demonstrate that both measurements of circularity are similarly related to osteon orientation (phi) (Figure 4.9) and to age (Figure 4.10).

Osteons have generally been described as being roughly cylindrical. If this holds true, their orientation (phi) in 3D should influence their geometrical parameters visualized in 2D. The differences observed in the osteon geometry across the lifespan would therefore reflect differences in the orientation (phi) of osteons. However, my results demonstrate that using the orientation (phi) of an osteon to predict its geometry is not feasible. For example, the expected difference in aspect ratio from 84° to 74° was only -0.0332 (Figure 4.7). Yet, the actual difference observed from 84° to 74° in aspect ratio was 0.156. More importantly, the detected difference was opposite to what was predicted; as osteon orientation (phi) became obliquely orientated, their aspect ratio increased (not decreased), establishing that osteons do not have

circular cross-sections but rather elliptical cross-sections.

The results revealed that while both osteon circularity and aspect ratio were inversely related to osteon orientation (phi), their relation can likely be explained through the more dominant relation of both osteon circularity and aspect ratio to age (Table 4.3). Age was positively correlated to both osteon circularity and aspect ratio, signifying that osteons appear to become increasingly circular with age. Contrary to my predictions, age, not osteon orientation (phi), appears to be involved in determining the geometry of osteons.

Interestingly, the direction of the difference observed in osteon orientation (phi) was unexpected. As age increased osteons became obliquely orientated, not longitudinally orientated as was expected. I suggest that this can potentially be explained through the increasing complexity of the microstructure with advancing age. As remodelling progresses, older osteons are subsequently overlapped with newer osteons (Cooper *et al.* 2007a; Cooper *et al.* 2003; Currey 1964; Kerley 1965; Robling, Castillo and Turner 2006; Robling and Stout 2000). Subsequently, the coalescence between the individual canals increases, resulting in a progressive increase in the branching and interconnectivity within the canal networks (Chen *et al.* 2010; Cooper *et al.* 2007a; Cooper *et al.* 2003). I suggest that this increased interconnectivity and branching could play a role in the oblique orientations associated with age; as the complexity of the osteonal canal network increases the inclination of the canals required to maintain the interconnections and branching of the network may increase thereby resulting in the obliquely orientated osteons.

It has been well established that age-related bone loss along the endosteal surface, associated with an imbalance in remodelling, is accelerated during menopause. Along with accelerated remodelling, the porosity and coalescence of the canals is also said to increase along

this surface (Bousson *et al.* 2001; Feik, Thomas and Clement 1997) through a process described as trabecularization of the cortex, where cortical bone is gradually transformed into trabecular bone (Cooper *et al.* 2007a). While, the primary focus of this study was on the periosteal region, several of the specimens' cortices were remarkably thin, and consequently the entire cortex was within the 3mm ROI being studied. If the trabecularization of the cortex results in increased interconnectivity and the increased interconnectivity affects osteon orientation (phi), it becomes a potential variable to explain the obliqueness in osteon orientation (phi) with advancing age, especially in post-menopausal females where trabecularization of the cortex is most prevalent. This is important to consider given that the current sample is comprised of all females with half of the specimens over the age of 50 and likely post-menopausal. Future studies are therefore needed in order to evaluate the relation between the branching networks and osteon orientation along with what role menopause might play in this process.

The direction of strain has been proposed as guiding the direction of the orientation of an osteon (Hert, Fiala and Petrtyl 1994; Petrtýl, Heřt and Fiala 1996). In general, as individuals age, they become less active and their muscle mass begins to decline, resulting in less loading, and likely less strain, being placed on their bones (Frost 1997). It has been hypothesized that as loading decreases (but is not fully removed) osteons become longitudinally orientated and therefore, if truly cylindrical, osteons would consequently become increasingly circular (Figure 4.8).

The observed osteon orientations (phi) correspond with the previous findings from Heřt *et al.* (1994) who observed osteons to range from 0° to 15° (0° being longitudinal and 15° being equivalent to 85° within the present study). Thus, my results also support their conclusion that osteons are aligned along the dominant loading trajectories. However, my results also suggest

that osteons become obliquely orientated with advancing age, which implies that in order for strain to mediate bone adaptation and guide osteon orientation, the adaptive response to strain must be correlated with age. Lanyon (1984) has suggested mechanically related remodelling is initiated so that the architecture within bone can maintain suitable levels of strain. Frost (1987) has similarly proposed the mechanostat theory. This theory states that modelling operates to maintain the bone's strength and mass, whereas remodelling operates to maintain optimum levels of strain. Since, growth is dominant in younger individuals, modelling will also be dominant in order to maintain the bone's strength. Once growth ceases, remodelling becomes necessary to maintain the bone's ability to respond to the daily loads (Frost 1987; Lanyon 1984). I hypothesize that the density of bones during growth and modelling makes them less apt to respond to strain, resulting in longitudinally orientated osteons. Conversely, it follows that when remodelling is dominant and bones begin to lose density they would also become better optimized to respond to strain; thereby resulting in the increased interconnectivity and complexity within the canal network and ultimately obliquely orientated osteon.

It is clear from the results I have presented here that osteons are elliptical rather than cylindrical structures and that the differences seen in the geometric parameters of osteons across a lifespan are independent of osteon orientation. Nevertheless, the results did show that osteon orientation is inversely related to osteon circularity and aspect ratio (Figure 4.9). Thus as individuals age, osteons become increasingly oblique as well as increasingly circular. One possible explanation for this is the rotation of osteons along a second axis. My findings suggest that while osteons are being rotated along the z-axis (phi) they are also being rotated along the x-axis (theta), which I hypothosize is a result of the increased complexity (interconnectivity and branching) with age. Thus, the angle (theta) of osteons potentially becomes an integral part of

explaining the 2D shape of osteons. As the orientation of osteons in 3D moves away from the longitudinal axis, the osteon angle in 2D becomes increasingly radial. As an osteon is rotated along the x-axis, the major axis begins to align along the y-axis (moving towards 90°) and the minor axis, the x-axis (moving towards 0°).

My results indicate that osteons truly become more circular with age; however, the results also suggest that the appearance of increased circularity could potentially be inflated as a result of the projection of the elliptical cross-section onto the imaging/sectioning plane (Figure 4.14). For example, the individual with the most longitudinal osteon orientation (phi) - 83.95°, also had the most circumferential osteon angle (theta) - 15.44° and low circularity and aspect ratio values of 0.75 and 0.64, respectively. Conversely, the individual with the lowest osteon orientation (phi) - 74.06°, also had one of the most radial osteon angles (theta) - 40.92°, and high circularity and aspect ratio values of 0.83 and 0.77, respectively. Accordingly, my results suggest that as the 3D orientation (phi) of osteons became progressively oblique their projection along the 2D plane is also rotated, amplifying the appearance of circularity with age (Figure 4.14), lending further support to the findings that osteons are elliptical and not cylindrical.

A limitation of osteon angle (theta), however, must be addressed here: if an object is perfectly circular, theta is no longer a meaningful measurement. When the major and minor axes become equal, no true point of reference to measure the angle exists. The results presented here suggest that osteons are truly becoming more circular with age, independent of osteon orientation (phi) and osteon angle (theta). Therefore, these results must be interpreted with caution since osteon angle (theta) becomes a less reliable measurement as circularity increases. Future work is needed to evaluate the potential effects that theta has on osteon geometry.

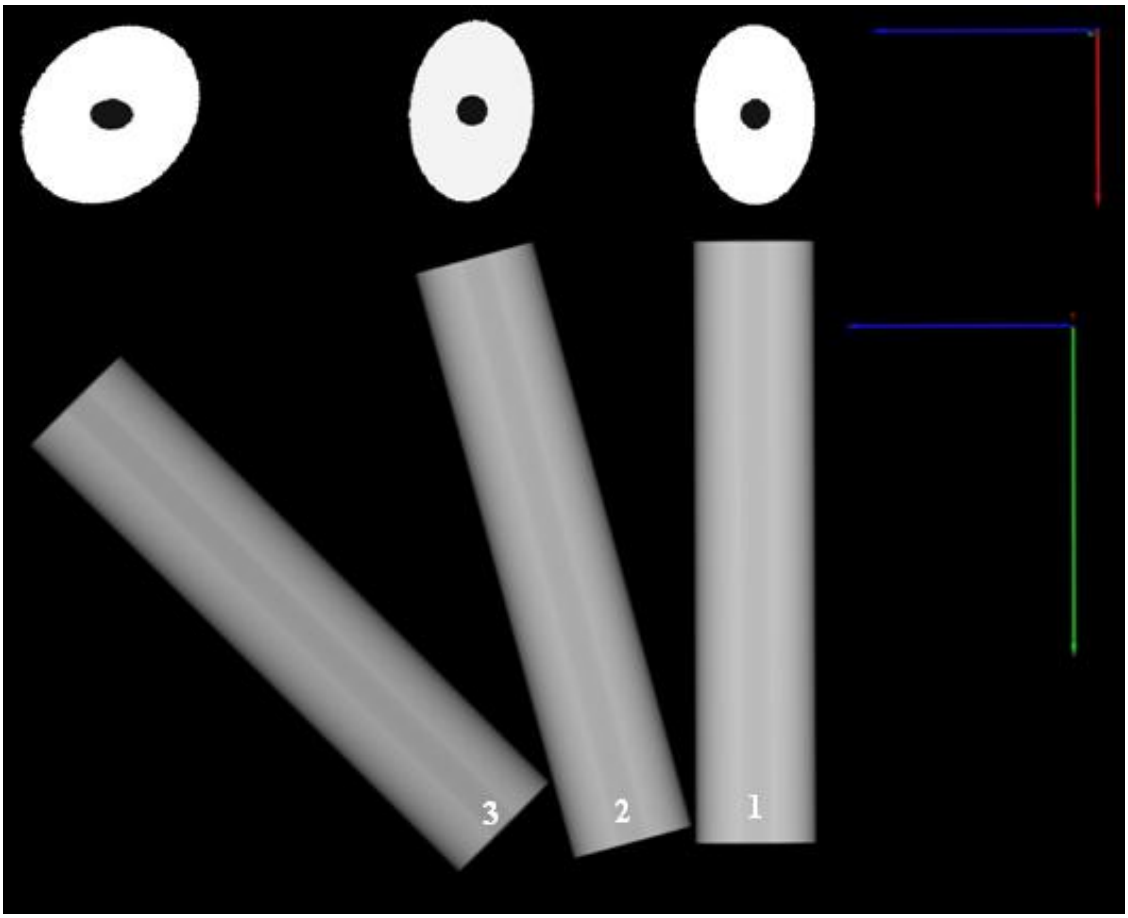

Figure 4.14: Schematic demonstrating how differences in the orientation of osteons (phi) and osteon angle (theta) can give the appearance of circularity. To match the results, cylinder 3 is rotated along 74° along the z-axis (green) and 41° about the x-axis (red). Cylinder 2 is rotated 84° along the z-axis (green) and 15° about the x-axis (red). Cylinder 1 is not rotated along any axis. The cross-sections are shown in the 2D plane with the y-axis (blue) and x-axis (red).

In summary, the orientation (phi) of osteons in 3D cannot be used to determine the geometry of osteons in 2D. Thus, orientation does not explain the age-related differences observed within the microstructure of cortical bone. The results establish that osteons are not cylindrical structures but rather elongated and/or irregularly shaped structures. This is especially prevalent in younger individuals. I propose that while the observed increase in circularity of osteons with age is a true phenomenon, the differences in the circularity of osteon can also be attributed to the rotation of osteons along both the z-axis and x-axis. As an osteon is rotated along the z and x-axes, the appearance of circularity is magnified as a result from the projection of the elliptical cross-section onto the imaging/sectioning plane. This was the first study to investigate the relation between osteon geometry in 2D and the osteon orientation (phi) in 3D. I have illustrated that the combination of these techniques is extremely valuable when investigating the age-related differences in bone. It is clear from the results presented here that the relation between these variables is much more complex than currently recognized. Therefore, further research is need, using a larger standardized sample, to investigate the effects of age, osteon orientation (phi), and osteon angle (theta) on the geometry of osteons.

CHAPTER FIVE
SUMMARY

5.1 Introduction

5.1.1 Overview of Thesis

It has been the objective of this thesis to integrate 2D histology and high-resolution micro-CT to investigate the microstructure of cortical bone in an attempt to produce an age estimation formula and quantitatively evaluate the relation of osteon geometry to osteon orientation. With recent innovations that allow cortical bone to be captured in 3D using micro-CT, our understanding of the remodelling process have been greatly improved. To my knowledge, this was the first study to incorporate both 2D and 3D technologies to assess the relation between these measures. Analysis of the 2D and 3D data did not lead to the development of an age estimation formula. Nevertheless, the incorporation of these techniques can provide a more extensive and revelatory view of the microstructure of cortical bone, thereby providing a greater understanding of the relation between adaptation and age. Using a multidisciplinary approach, the concepts presented in this thesis have the potential to influence several different fields of research such as physical anthropology and various fields of medicine.

5.2 Chapter Three

In this study, simulated histomorphometric ages were generated to reflect the assumed population's SEE in years. The results from the simulation revealed that SEE values will converge around 10 years once sample sizes reach ~150 specimens. While, histomorphometric aging techniques can be valuable to both forensic anthropology and archaeology, few studies use the recommended 150 specimens (Hennig and Cooper 2011). A considerable portion of the

variance in the reported precisions of histomorphometric aging methods can potentially be attributed to the use of small sample sizes. The results presented in Chapter 3 clearly demonstrate the effect small sample sizes can have on the reported SEE values for histological aging methods. Having histomorphometric aging techniques with small SEE values is of course ideal and beneficial; however, it is only beneficial and meaningful if the technique can be reliably applied to populations other than those for which it was developed. Thus, given the effect small sample sizes have on the reported SEE and the sample size that was used in this study, it was concluded that developing an age estimation formula using 2D and 3D techniques was no longer a feasible goal for this thesis.

5.3 Chapter Four

Computer generated 3D renderings of Tappen's (1977) serial sections revealed that cortical bone was composed of an elaborate interconnected microstructural system (Stout *et al.* 1999). While, the network of the interconnected branches, known as the Haversian systems, cannot be fully realized through 2D techniques, the canals can be visualized and quantified in 3D using micro-CT. Chapter 4 quantitatively evaluated the relation of 2D geometric parameters to 3D osteon orientation (phi) and age. Two questions were examined:

(1) does the orientation of osteons in 3D determine osteon geometric parameters visualized in 2D?

(2) can the differences in 3D osteon orientation explain the age-related differences observed in 2D osteon geometry?

In summary, I found that the 3D orientation (phi) of osteons does not account for the differences visualized in the 2D geometric parameters (osteon circularity and aspect ratio) of osteons. While an inverse relation was found between osteon orientation (phi) to both osteon

circularity and aspect ratio, these relations can likely be explained through the more dominant relation of circularity to age. I found that osteons became more circular as well as more obliquely orientated with age. Interestingly, while investigating a new geometric parameter, osteon angle (theta), I also found that osteons are rotated along the x-axis (theta) as well as the z-axis (phi). Therefore, as osteons increase in circularity with advancing age, the appearance of circularity is augmented by their projection along the sectioning plane as a result of their rotation along both the z-axis and the x-axis. My results from this study clearly establish that the shape of an osteon is not truly cylindrical but rather elliptical.

5.4 Future Directions

One of the goals of osteological research is to describe the age-related differences within the microstructure of cortical bone and identify processes that lead to unhealthy bones. I sought to explain the age-related differences seen in the microstructure of cortical bone through a combination of high-resolution micro-computed tomography and histology. Despite the fact that 2D techniques can provide quantitative information on the specific histological details, they cannot capture all the complexities of the microstructural network within cortical bone that 3D imaging can. Moreover, histological methods are ultimately destructive to bone, whereas 3D techniques though minimally invasive are less destructive than 2D histological techniques. In addition, 3D techniques, such as micro-CT and synchrotron radiation (SR) micro-CT, allow us to view the microstructure of bone from a completely new perspective, providing insights into age-related differences, such as the increasing complexity of the microstructure with advancing age (Cooper *et al.* 2007a; Cooper *et al.* 2003). More recently, studies using desktop micro-CT (Arhatari, *et al.* 2011) and SR micro-CT (Arhatari *et al.* 2011; Cooper *et al.* 2011) were able to identify borders of individual secondary osteons**.** Nevertheless, at lower resolutions 3D

techniques cannot consistently view the specific details of the geometric parameters of osteons that can be viewed using 2D techniques such as histology. Therefore, the combination of 2D and 3D techniques is ultimately the best way to gain a full understanding of the aging processes in bone. As technology improves, further gains can be expected in the study of bone microstructure.

The results presented in Chapter 4 demonstrate the usefulness of combining 2D and 3D techniques to evaluate age-related differences in the microstructure of cortical bone; however, given the limited sample size, the results should be taken as preliminary and investigated further. Studies using larger standardized sample sizes are required to elaborate on the results I have presented in this thesis. Given that larger sample sizes should better depict the relation between variables, the use of larger samples sizes (~150) is an important consideration in developing age-estimation formulae. More importantly, these equations must be tested on alternate samples before its validity and precision can be definitively determined.

My results clearly demonstrate that a strong correlation exists between age and circularity and support the previous findings of Brtiz *et al.* (2009) and Currey (1964). While many other age-related differences, such as osteon population density (OPD) are used to develop histomorphometric aging formulae, to my knowledge the relation between the circularity of osteons and age has not been used to develop a histomorphometric formula. Given the strength of this relation, I suggest that it should be considered when developing age estimation formulae.

While investigating osteon angle (theta), I noted that osteons are rotated along the x-axis becoming increasingly radial as osteon orientation (phi) is being rotated along the z-axis, moving away from the longitudinal plane. Given that my results demonstrate that osteons are not cylindrical, having an understanding of the relation of theta to these variables becomes

increasingly important. Looking at other measures of 3D orientations, such as theta in 3D, may also prove to be extremely valuable. However, as noted in Chapter 4, the difference observed in osteon angle (theta) may be confounded by the true increase in the circularity of osteons, making osteon angle (theta) a less reliable measure as circularity increases. Therefore, further investigations into how theta, in both 2D and 3D, relates to other geometric parameters of cortical bone are needed.

It is necessary to use 3D investigations in conjunction with 2D in order to further our understanding of how strain affects osteon geometry and osteon orientation (phi). Many studies have evaluated the effect strain has on the microstructure of cortical bone; nonetheless, the effect strain has on osteon geometry and orientation is not well understood. While it is difficult to directly measure strain levels in humans, animal models can be used. For example, in a series of studies using artiodactyls calcanei, Skedros *et al.* investigated the impact of strain on osteon size; (Skedros, Mason and Bloebaum 1994; Skedros, Mason and Bloebaum 2001; Skedros, Su and Bloebaum 1997). Additionally, while investigating regional variation in relation to strain, Skedros *et al.* found differences in osteon geometric parameters between areas experiencing different types of strain, such as compression versus tension (Skedros *et al.* 1994; Skedros, Mason and Bloebaum 1994; Skedros, Sorenson and Jenson 2007; Skedros, Su and Bloebaum 1997). Two of these studies noted that some areas that receive tensile forces were so habitually loaded that they were essentially in a state of chronic disuse (Skedros *et al.* 1994; Skedros, Mason and Bloebaum 1994). While variations in the 2D geometric parameters of osteons experiencing different types of strain have been discussed, the relation between 3D orientation (phi) and strain has not been evaluated. Repeating these studies using micro-CT would allow for the direct measurement of the various modes of strain (tension versus compression) on osteon

orientation (phi) and osteon geometry.

Regions experiencing different types of strain also need to be evaluated using 3D techniques. While the majority of studies focus on the anterior femur for both 2D (Britz *et al.* 2009; Hennig and Cooper 2011; Robling and Stout 2000) and 3D techniques (Cooper *et al.* 2006; Cooper *et al.* 2007a; Cooper *et al.* 2007b), investigations using other regions of the femur as well as other bones are necessary. Given that the results presented in this chapter suggest that the impact of strain is negligible until bones are fully optimized to endure strain, studies comparing the orientation (phi) of osteons in loaded bones to unloaded need to be completed so we can fully understand responsive changes to mechanical forces.

It is clear that there are many different factors affecting bone remodelling. Understanding how all these variables interact has proven difficult. Furthermore, my results indicate that the processes influencing bone remodelling and adaptation are much more complex than current theories explain. For example, the results presented in Chapter 4 suggest that younger individuals have longitudinally orientated osteons rather than obliquely orientated osteons. Studies investigating osteon orientation (phi) need to focus on the integration of methods using samples with well-documented medical histories in order to get a fully comprehensive understanding of age-related differences within the microstructure. One necessity in this area of research is the access and availability of proper modern-day collections. Therefore, more collections, such as the MFC, need to be created.

5.5 Conclusions

The results I have presented in this thesis provide new insights into utilizing larger more appropriate sample sizes when developing histomorphometric aging formulae. The majority of formulae have been developed on sample sizes that are too small and therefore do not truly

represent the populations variance. Thus, the development of standard measurement techniques on standardized samples sizes of at least 150 are necessary in order to truly characterize the populations variance and develop formulae that can precisely predict age at death within ±10 years.

The results from the analysis of data did not support my initial hypotheses:

(1) The orientation of osteons in 3D determines osteon geometric parameters visualized in 2D.

(2) The differences in 3D osteon orientation explain the age-related differences observed in 2D osteon geometry.

Nevertheless, I was able to quantitatively demonstrate that while osteons are more elliptical in their cross-sections than cylindrical, they do become more circular with advancing age independent of osteon orientation (phi). The results presented here have established the importance of employing both histology (2D) and high-resolution micro-CT (3D) in our endeavours to fully understand and explain bone adaptation and the remodelling processes at the microstructural level.

REFERENCES

Ahlqvist, J., and O. Damsten. 1969. "A modification of Kerley's method for the microscopic determination of age in human bone." *J Forensic Sci* 14(2):205-12.

Aiello, L. C., and T. Molleson. 1993. "Are Microscopic Ageing Techniques more Accurate than Macroscopic Techniques?" *J Archaeol Sci* 20:689-704.

Arhatari, B.D., D. M. L Cooper, C. D. L. Thomas, J. G. Clement, and A. G. Peele. 2011. "Imaging the 3D structure of secondary osteons in human cortical bone using phase-retrieval tomography." *Phys Med Biol* 56(16):5265.

Ascenzi, M. G., M. Andreuzzi, and J. M. Kabo. 2004. "Mathematical modeling of human secondary osteons." *Scanning* 26(1):25-35.

Aykroyd, R. G., D. Lucy, A. M. Pollard, and T. Solheim. 1997. "Technical note: regression analysis in adult age estimation." *Am J Phys Anthropol* 104(2):259-65.

Basillais, A., S. Bensamoun, C. Chappard, B. Brunet-Imbault, G. Lemineur, B. Ilharreborde, M.C. Ho Ba Tho, and C.L. Benhamou. 2007. "Three-dimensional characterization of cortical bone microstructure by microcomputed tomography: validation with ultrasonic and microscopic measurements." *J Orthop Sci* 12(2):141-48.

Bell, K. L., N. Loveridge, J. Reeve, C. D. L. Thomas, Sophie A. Feik, and J. G. Clement. 2001. "Super-osteons (remodeling clusters) in the cortex of the femoral shaft: Influence of age and gender." *Anat Rec* 264(4):378-86.

Bertram, J. E., and S. M. Swartz. 1991. "The 'law of bone transformation': a case of crying Wolff?" *Biol Rev Camb Philos Soc* 66(3):245-73.

Black, J., R. Mattson, and E. Korostoff. 1974. "Haversian osteons: size, distribution, internal structure, and orientation." *J Biomed Mater Res* 8(5):299-319.

Black, J., S. P. Richardson, R. U. Mattson, and S. R. Pollack. 1980. "Haversian osteons: longitudinal variation of internal structure." *J Biomed Mater Res* 14(1):41-53.

Bousson, V., A. Le Bras, F. Roqueplan, Y. Kang, D. Mitton, S. Kolta, C. Bergot, W. Skalli, E. Vicaut, W. Kalender, K. Engelke, and J. D. Laredo. 2006. "Volumetric quantitative computed tomography of the proximal femur: relationships linking geometric and densitometric variables to bone strength. Role for compact bone." *Osteoporosis Int* 17(6):855-64.

Bousson, Valérie, Catherine Bergot, Alain Meunier, Frédérique Barbot, Caroline Parlier-Cuau, Anne-Marie Laval-Jeantet, and Jean-Denis Laredo. 2000. "CT of the Middiaphyseal Femur: Cortical Bone Mineral Density and Relation to Porosity1." *Radiology* 217(1):179-87.

Bousson, Valérie, Alain Meunier, Catherine Bergot, Éric Vicaut, Maria Augusta Rocha, Maria Helena Morais, Anne-Marie Laval-Jeantet, and Jean-Denis Laredo. 2001. "Distribution of Intracortical Porosity in Human Midfemoral Cortex by Age and Gender." *J Bone Miner Res* 16(7):1308-17.

Bousson, Valérie, Françoise Peyrin, Catherine Bergot, Marc Hausard, Alain Sautet, and Jean-Denis Laredo. 2004. "Cortical Bone in the Human Femoral Neck: Three-Dimensional Appearance and Porosity Using Synchrotron Radiation." *J Bone Miner Res* 19(5):794-801.

Bouvier, M., and D. H. Ubelaker. 1977. "A comparison of two methods for the microscopic determination of age at death." *Am J Phys Anthropol* 46(3):391-4.

Britz, H. M., C. D. Thomas, J. G. Clement, and D. M. Cooper. 2009. "The relation of femoral osteon geometry to age, sex, height and weight." *Bone* 45(1):77-83.

Burger, E. H., J. Klein-Nulend, and T. H. Smit. 2003. "Strain-derived canalicular fluid flow regulates osteoclast activity in a remodelling osteon--a proposal." *J Biomech* 36(10):1453-9.

Burr, D. B., C. B. Ruff, and D. D. Thompson. 1990. "Patterns of skeletal histologic change through time: comparison of an archaic native American population with modern populations." *Anat Rec* 226(3):307-13.

Chen, H., X. Zhou, S. Shoumura, S. Emura, and Y. Bunai. 2010. "Age and gender-dependent changes in three-dimensional microstructure of cortical and trabecular bone at the human femoral neck." *Osteoporosis Int* 21(4):627-36.

Cho, H., S. D. Stout, R. W. Madsen, and M. A. Streeter. 2002. "Population-specific histological age-estimating method: a model for known African-American and European-American skeletal remains." *J Forensic Sci* 47(1):12-8.

Clement, J. G. 2005. "The Melbourne Femur Collection: the gift of tissue underpins important medical and forensic research." *VIFM Review* 3(Journal Article):7-11.

Cochran, W. G. 1934. "The distribution of quadratic forms in a normal system, with applications to the analysis of covariance." *Math Proc Cambridge* 30(02):178-91.

Cohen, J., and W. H. Harris. 1958. "The three-dimensional anatomy of haversian systems." *J Bone Joint Surg Am* 40-A(2):419-34.

Cooper, D. M. L., B. Erickson, A. G. Peele, K. Hannah, C. D. L. Thomas, and J. G. Clement. 2011. "Visualization of 3D osteon morphology by synchrotron radiation micro-CT." *J Anat* 219(4):481-89.

Cooper, D. M. L., J. R. Matyas, M. A. Katzenberg, and B. Hallgrimsson. 2004. "Comparison of microcomputed tomographic and microradiographic measurements of cortical bone porosity." *Calcif Tissue Int* 74(5):437-47.

Cooper, D. M. L., C. D. L. Thomas, J. G. Clement, and B. Hallgrímsson. 2006. "Three-dimensional microcomputed tomography imaging of basic multicellular unit-related resorption spaces in human cortical bone." *Anat Rec A Discov Mol Cell Evol Biol* 288A(7):806-16.

Cooper, D. M. L., C. D. L. Thomas, J. G. Clement, A.i L. Turinsky, C. W. Sensen, and B. Hallgrímsson. 2007a. "Age-dependent change in the 3D structure of cortical porosity at the human femoral midshaft." *Bone* 40(4):957-65.

Cooper, D. M. L., A. L. Turinsky, C. W. Sensen, and B. Hallgrímsson. 2003. "Quantitative 3D analysis of the canal network in cortical bone by micro-computed tomography." *Anat Rec B New Anat* 274B(1):169-79.

Cooper, D. M. L., A. Turinsky, C. Sensen, and B. Hallgrimsson. 2007b. "Effect of voxel size on 3D micro-CT analysis of cortical bone porosity." *Calcif Tissue Int* 80(3):211-9.

Crowder, C. 2005. "Evaluating the use of Quantitative Bone Histology to Estimate Adult Age at Death." Pp. 1-247: University of Totonto.

Currey, J. D. 1964. "Some Effects of Ageing in Human Haversian Systems." *J Anat* 98:69-75.

Curtis, J. M. 2003. "Estimation of Age at Death From the Microscopic Appearance of the Frontal Bone." Pp. 1-119: University of Indianapolis.

de Boef, M., and H. C. E. Larsson. 2007. "Bone microstructure: quantifying bone vascular orientation." *Can J Zool* 85(1):63-70.

DeHoff, R. T. 1983. "Quantitative serial sectioning analysis: preview." *J Microsc* 131(3):259-63.

Drusini, A. 1987. "Refinements of two methods for the histomorphometric determination of age in human bone." *Z Morphol Anthropol* 77(2):167-76.

Drusini, A., A. Volpe, and S. Dovigo. 1990. "Age determination in human adults by dental histology." *Z Morphol Anthropol* 78(2):169-74.

Dudar, J. C., S. Pfeiffer, and S. R. Saunders. 1993. "Evaluation of morphological and histological adult skeletal age-at-death estimation techniques using ribs." *J Forensic Sci* 38(3):677-85.

Ericksen, M. F. 1991. "Histologic estimation of age at death using the anterior cortex of the femur." *Am J Phys Anthropol* 84(2):171-9.

—. 1997. "Comparison of Two Methods of Estimating Age at Death in a Chilean Preceramic Population." *Int J Osteoarchaeol* 7(1):65-70.

Feik, S. A., C. D. L. Thomas, and J. G. Clement. 1997. "Age-related changes in cortical porosity of the midshaft of the human femur." *J Anat* 191(3):407-16.

Frost, H. M. 1958. "Preparation of thin undecalcified bone sections by rapid manual method." *Stain Technol* 33(6):273-7.

—. 1963. *Bone Remodelling Dynamics*. Springfield Illinios: Charles C Thomas Publisher.

—. 1973. *Bone Remodeling and its relationship to Metabolic Bone Diseases*. Springfiled Illinois: Charles C Thomas

—. 1987. "Bone "mass" and the "mechanostat": a proposal." *Anat Rec* 219(1):1-9.

—. 1997. "On Our Age-Related Bone Loss: Insights from a New Paradigm." *J of Bone Miner Res* 12(10):1539-46.

Goliath, Jesse. R. 2010. "Variation in Osteon Circularity and Its Impact on Estimating Age at Death." Pp. 1-42: Ohio State University.

Green, Samuel B. 1991. "How Many Subjects Does It Take To Do A Regression Analysis." *Multivar Behav Res* 26(3):499-510.

Guadagnoli, E., and W. F. Velicer. 1988. "Relation of sample size to the stability of component patterns." *Psychol Bull* 103(2):265-75.

Han, Seung-Ho, Sang-Hyun Kim, Yong-Woo Ahn, Gi-Yeong Huh, Dai-Soon Kwak, Dae-Kyoon Park, U. Young Lee, and Yi-Suk Kim. 2009. "Microscopic Age Estimation from the Anterior Cortex of the Femur in Korean Adults*." *J Forensic Sci* 54(3):519-22.

Hauser, R., D. Barres, M. Durigon, and L. Derobert. 1980. "[Identification using histomorphometry of the femur and tibia]." *Acta Med Leg Soc (Liege)* 30(2):91-7.

Hennig, C., and D. M. L. Cooper. 2011. "Brief communication: the relation between standard error of the estimate and sample size of histomorphometric aging methods." *Am J Phys Anthropol* 145(4):658-64.

Hert, J., P. Fiala, and M. Petrtyl. 1994. "Osteon orientation of the diaphysis of the long bones in man." *Bone* 15(3):269-77.

Hinton, P. R. 2004. *Statistics Explained 2nd ed*. New York: Routledge.

Hummel, S., and H. Schutkowski. 1993. "Approaches to the histological age determination of cremated human remains." Pp. 110-23 in *Histology of Ancient Bone*, edited by G. Grupe and A. N. Garland. New York: Springer-Verlag.

Iwamoto, S., E. Oonuki, and M. Konishi. 1978. "Study on the Age-Related Changes of the Compact Bone and the Age Estimation 2. On the Humerus." *Acta medica Kinki Univ* 3(Journal Article):203-08.

Jones, Anthony C., Bruce Milthorpe, Holger Averdunk, Ajay Limaye, Tim J. Senden, Arthur Sakellariou, Adrian P. Sheppard, Rob M. Sok, Mark A. Knackstedt, Arthur Brandwood,

Dennis Rohner, and Dietmar W. Hutmacher. 2004. "Analysis of 3D bone ingrowth into polymer scaffolds via micro-computed tomography imaging." *Biomaterials* 25(20):4947-54.

Jowsey, J. 1966. "Studies of Haversian systems in man and some animals." *J Anat* 100(Pt 4):857-64.

—. 1968. "Symposium on equine bone and joint diseases. Age and species differences in bone." *Cornell Vet* 58:Suppl:74-94.

Keough, N., E. N. L'Abbé, and M. Steyn. 2009. "The evaluation of age-related histomorphometric variables in a cadaver sample of lower socioeconomic status: implications for estimating age at death." *Forensic Sci Int* 191(1-3):114.e1-14.e6.

Kerley, E. R., and D. H. Ubelaker. 1978. "Revisions in the microscopic method of estimating age at death in human cortical bone." *Am J Phys Anthropol* 49(4):545-46.

Kerley, E.R. 1965. "The microscopic determination of age in human bone." *Am J Phys Anthropol* 23(2):149-63.

Kim, Yi-Suk, Deog-Im Kim, Dae-Kyoon Park, Je-Hoon Lee, Nak-Eun Chung, Won-Tae Lee, and Seung-Ho Han. 2007. "Assessment of Histomorphological Features of the Sternal End of the Fourth Rib for Age Estimation in Koreans*." *J Forensic Sci* 52(6):1237-42.

Kimura, K. 1992. "Estimation of age at death from second metacarpals." *Z Morphol Anthropol* 79(2):169-81.

Kragstrup, J., and F. Melsen. 1983. "Three-dimensional morphology of trabecular bone osteons reconstructed from serial sections." *Metab Bone Dis Relat Res* 5(3):127-30.

Kuhn, J. L., S. A. Goldstein, L. A. Feldkamp, R. W. Goulet, and G. Jesion. 1990. "Evaluation of a microcomputed tomography system to study trabecular bone structure." *J Orthop Res* 8(6):833-42.

Lanyon, L. E. 1984. "Functional strain as a determinant for bone remodeling." *Calcif Tissue Int* 36(0):S56-S61.

Lanyon, L. E., and S. Bourn. 1979. "The influence of mechanical function on the development and remodeling of the tibia. An experimental study in sheep." *J Bone Joint Surg Am* 61(2):263-73.

Lanyon, L. E., and C. T. Rubin. 1984. "Static vs dynamic loads as an influence on bone remodelling." *J Biomech* 17(12):897-905.

Lazenby, R. A. 1984. "Inherent Deficiencies in Cortical Bone Microstructural Age Estimation Techniques." *OSSA* 9(Journal Article):95-103.

Leeuwenhoeck, Anthony. 1677. "Microscopical Observations of the Structure of Teeth and other Bones: Made and Communicated, in a Letter by Mr. Anthony Leeuwenhoeck." *Phil Trans R Soc* 12(133-142):1002-03.

Maat, G. J. R., A. Maes, M. J. Aarents, and N. J. D. Nagelkerke. 2006. "Histological Age Prediction from the Femur in a Contemporary Dutch Sample*." *J Forensic Sci* 51(2):230-37.

Marotti, G. 1996. "The structure of bone tissues and the cellular control of their deposition." *Ital J Anat Embryol* 101(4):25-79.

Martin, R. B. 2000. "Toward a unifying theory of bone remodeling." *Bone* 26(1):1-6.

Martin, R. B., J. C. Pickett, and S. Zinaich. 1980. "Studies of skeletal remodeling in aging men." *Clin Orthop Relat Res* (149):268-82.

Martin, R.B. 2007. "Targeted bone remodeling involves BMU steering as well as activation." *Bone* 40(6):1574-80.

Maxwell, Scott E. 2000. "Sample size and multiple regression analysis." *Psychol Methods* 5(4):434-58.

Mohsin, S., D. Taylor, and T. C. Lee. 2002. "Three-dimensional reconstruction of Haversian systems in ovine compact bone." *Eur J Morphol* 40(5):309-15.

Mulhern, Dawn M., and Dennis P. Van Gerven. 1997. "Patterns of femoral bone remodeling dynamics in a medieval Nubian population." *Am J Phys Anthropol* 104(1):133-46.

Narasaki, S. 1990. "Estimation of age at death by femoral osteon remodeling: application if Thompson's core technique to modern Japanese." *J Anthropol Soc Nippon* 98(Journal Article):29-38.

Nomura, Tsutomu, Evan Gold, Michael P. Powers, Susumu Shingaki, and J. Lawrence Katz. 2003. "Micromechanics/structure relationships in the human mandible." *Dent Mater* 19(3):167-73.

Nor, F., R. F. Pastor, and H. Schutkowski. 2006. "Population specific equation for estimation of age: A model for known Malaysian population skeletal remains." *Malaysian J Forensic Pathol Sci* 1(Journal Article):15-28.

Nunnally, J. C. 1967. *Psychometric Theory 2nd ed*. New York: Mcgraw-Hill.

Nunnally, J. C., and I. H. Bernstein. 1994. *Psychometric Theory*. New York: McGraw-Hill.

Pearson, Osbjorn M., and Daniel E. Lieberman. 2004. "The aging of Wolff's “law”: Ontogeny and responses to mechanical loading in cortical bone." *Am J Phys Anthropol* 125(S39):63-99.

Petrtýl, M., J. Heřt, and P. Fiala. 1996. "Spatial organization of the haversian bone in man." *J Biomech* 29(2):161-69.

Pfeiffer, S. 1985. "Comparison of adult age estimation techniques, using an ossuary sample." *Can Rev Phys Anthropol* 4(Journal Article):13-17.

—. 1992. "Cortical bone age estimates from historically known adults." *Z Morphol Anthropol* 79(1):1-10.

Pfeiffer, Susan. 1998. "Variability in osteon size in recent human populations." *Am J Phys Anthropol* 106(2):219-27.

Pfeiffer, Susan, Christian Crowder, Lesley Harrington, and Michael Brown. 2006. "Secondary osteon and Haversian canal dimensions as behavioral indicators." *Am J Phys Anthropol* 131(4):460-68.

Pratte, D. G., and S. Pfeiffer. 1999. "Histological Age Estimation of a Cadaveral Sample of Diverse Origins." *Can Soc Forensic Sci* 32(Journal Article):155-67.

Recker, R.R. 1983. *Bone Histomophometry: Teachniques and Interprestation*. Bocal Raton, Florida: CRC PRess.

Ren, P., H. J. Xi, S. Yu, and et al. 2001. "Age determination by the histomorphometry of female ribs." *Chinese J Forensic Med* (Journal Article).

Renders, G. A. P., L. Mulder, L. J. Van Ruijven, and T. M. G. J. Van Eijden. 2007. "Porosity of human mandibular condylar bone." *J Anat* 210(3):239-48.

Rho, Jae-Young, Liisa Kuhn-Spearing, and Peter Zioupos. 1998. "Mechanical properties and the hierarchical structure of bone." *Med Eng Phys* 20(2):92-102.

Robling, A. G., A. B. Castillo, and C. H. Turner. 2006. "Biomechanical and molecular regulation of bone remodeling." *Annu Rev Biomed Eng* 8:455-98.

Robling, A. G., and S. D. Stout. 2000. "Histomorphometry of Cortical Bone." Pp. 187-213 in *Biological Anthropology of the Human Skeleton*, edited by M. A. Kattzenberg and S. R. Saunders. Canada: Wiley-Liss.

Rogers, N. L. 1996. "A Study of Histological Aging of the Human Clavicle." Knoxville: University of Tennessee.

Rother, V. P., G. Kruger, J. Mechlitt, and H. Hunger. 1978. "Histomorphometrische sowie regressions-und faktor-analytische Untersuchungen von Alternsveranderungen des Humerus." *Anat Anz* 144(Journal Article):346-65.

Rubin, C. T., and K. J. McLeod. 1994. "Promotion of bony ingrowth by frequency-specific, low-amplitude mechanical strain." *Clin Orthop Relat Res* (298):165-74.

Ruff, C., Br. Holt, and E. Trinkaus. 2006. "Who's afraid of the big bad Wolff?: "Wolff's law" and bone functional adaptation." *Am J Phys Anthropol* 129(4):484-98.

Samson, D., and K. Branigan. 1987. "A new method of estimating age at death from fragmentary and weathered bone." Pp. 101-08 in *Death, Decay, and Reconstruction. Approaches to Archeology and Forensic Science*, edited by A. Bodington, A. N. Garland, and R. C. Janaway. Manchester: Manchester University Press.

Singh, I. J., and D. L. Gunberg. 1970. "Estimation of age at death in human males from quantitative histology of bone fragments." *Am J Phys Anthropol* 33(3):373-81.

Skedros, J. G., R. D. Bloebaum, M. W. Mason, and D. M. Bramble. 1994. "Analysis of a tension/compression skeletal system: Possible strain-specific differences in the hierarchical organization of bone." *Anat Rec* 239(4):396-404.

Skedros, J. G., M. W. Mason, and R. D. Bloebaum. 1994. "Differences in osteonal micromorphology between tensile and compressive cortices of a bending skeletal system:

Indications of potential strain-specific differences in bone microstructure." *Anat Rec* 239(4):405-13.

—. 2001. "Modeling and remodeling in a developing artiodactyl calcaneus: a model for evaluating Frost's Mechanostat hypothesis and its corollaries." *Anat Rec* 263(2):167-85.

Skedros, J. G., S. M. Sorenson, and N. H. Jenson. 2007. "Are distributions of secondary osteon variants useful for interpreting load history in mammalian bones?" *Cells Tissues Organs* 185(4):285-307.

Skedros, J. G., S. C. Su, and R. D. Bloebaum. 1997. "Biomechanical implications of mineral content and microstructural variations in cortical bone of horse, elk, and sheep calcanei." *Anat Rec* 249(3):297-316.

Smit, Theo H., and Elisabeth H. Burger. 2000. "Is BMU-Coupling a Strain-Regulated Phenomenon? A Finite Element Analysis." *J Bone Miner Res* 15(2):301-07.

Smit, Theo H., Elisabeth H. Burger, and Jacques M. Huyghe. 2002. "A Case for Strain-Induced Fluid Flow as a Regulator of BMU-Coupling and Osteonal Alignment." *J Bone Miner Res* 17(11):2021-29.

Stout, S., and C. Crowder. 2012. "Bone Remodeling, Histomorphology, and Histomorphometry " Pp. 1-21 in *Bone Histology: An Anthropological Perspective*, edited by C. Crowder and S. Stout. Boca Raton, Florida: CRC Press.

Stout, S. D., B. S. Brunsden, C. F. Hildebolt, P. K. Commean, K. E. Smith, and N. C. Tappen. 1999. "Computer-assisted 3D reconstruction of serial sections of cortical bone to determine the 3D structure of osteons." *Calcif Tissue Int* 65(4):280-4.

Stout, S. D., W. H. Dietze, M. Y. Iscan, and S. R. Loth. 1994. "Estimation of age at death using cortical histomorphometry of the sternal end of the fourth rib." *J Forensic Sci* 39(3):778-84.

Stout, Sam D., and Robert R. Paine. 1992. "Histological age estimation using rib and clavicle." *Am J Phys Anthropol* 87(1):111-15.

Stout, Sam D., Marcello A. Porro, and Beatrice Perotti. 1996. "Brief communication: A test and correction of the clavicle method of Stout and Paine for histological age estimation of skeletal remains." *Am J Phys Anthropol* 100(1):139-42.

Stout, Sam D., and Sarah C. Stanley. 1991. "Percent osteonal bone versus osteon counts: The variable of choice for estimating age at death." *Am J Phys Anthropol* 86(4):515-19.

Szivek, J. A., J. B. Benjamin, and P. L. Anderson. 2000. "An experimental method for the application of lateral muscle loading and its effect on femoral strain distributions." *Med Eng Phys* 22(2):109-16.

Tabachnick, B., and L. Fidell. 1989. *Using Multivariate Statistics*. Cambridge: Harper & Row.

—. 1996. *Using Multivariate Statistics*. Cambridge: Harper & Row.

Tanck, E., G. Hannink, R. Ruimerman, P. Buma, E. H. Burger, and R. Huiskes. 2006. "Cortical bone development under the growth plate is regulated by mechanical load transfer." *J Antat* 208(1):73-79.

Tappen, N. C. 1977. "Three-dimensional studies of resorption spaces and developing osteons." *Am J Anat* 149(3):301-31.

Thompson, D. D. 1979. "The core technique in the determination of age at death of skeletons." *J Forensic Sci* 24(4):902-15.

—. 1981. "Microscopic determination of age at death in an autopsy series." *J Forensic Sci* 26(3):470-5.

Thompson, D. D., and C. A. Galvin. 1983. "Estimation of age at death by tibial osteon remodeling in an autopsy series." *Forensic Sci Int* 22(2-3):203-11.

Turner, C. H. 1998. "Three rules for bone adaptation to mechanical stimuli." *Bone* 23(5):399-407.

Ural, A., and D. Vashishth. 2006. "Interactions between microstructural and geometrical adaptation in human cortical bone." *J Orthop Res* 24(7):1489-98.

—. 2007. "Anisotropy of age-related toughness loss in human cortical bone: A finite element study." *J Biomech* 40(7):1606-14.

Uytterschaut, H. T. 1993. "Human bone remodelling and aging." Pp. 95-109 in *Histology of Ancient Human Bone*, edited by G. Grupe and A. N. Garland. New York: Springer-Verlag.

van Oers, René F. M., Ronald Ruimerman, Esther Tanck, Peter A. J. Hilbers, and Rik Huiskes. 2008a. "A unified theory for osteonal and hemi-osteonal remodeling." *Bone* 42(2):250-59.

van Oers, René F. M., Ronald Ruimerman, Bert van Rietbergen, Peter A. J. Hilbers, and Rik Huiskes. 2008b. "Relating osteon diameter to strain." *Bone* 43(3):476-82.

Wachter, N., P. Augat, G. Krischak, M. Mentzel, L. Kinzl, and L. Claes. 2001. "Prediction of cortical bone porosity in vitro by microcomputed tomography." *Calcif Tissue Int* 68(1):38-42.

Walker, R. A. 1990. "Assessments of cortical bone dynamics and skeletal age at death from femoral cortical histology." Pp. 1-222: Kent State University.

Walker, Robert A., C. Owen Lovejoy, and Richard S. Meindl. 1994. "Histomorphological and geometric properties of human femoral cortex in individuals over 50: Implications for histomorphological determination of age-at-death." *Am J Hum Biol* 6(5):659-67.

Wasserman, Nicholas, Brandon Brydges, Shane Searles, and Ozan Akkus. 2008. "In vivo linear microcracks of human femoral cortical bone remain parallel to osteons during aging." *Bone* 43(5):856-61.

Watanabe, Y., M. Konishi, M. Shimada, H. Ohara, and S. Iwamoto. 1998. "Estimation of age from the femur of Japanese cadavers." *Forensic Sci Int* 98(1-2):55-65.

White, T.D.; Folkens, P.A. 2005. *The Human Bone Maual*. Burlington, MA: Elsevier Inc.

Wolberg, J. 1976. *Prediction Analysis*. New Jersey: D Van Nostradn Company Inc.

Wolff, Julius. 1893. "Das Gesetz der Transformation der Knochen." *Dtsch med Wochenschr* 19(47):1222,24.

Xi, H. J., and P. Ren. 2002. "Age Determination by the Histomorphometry of Male Ribs." *Acta Antropol Sinica* 2(Abstract).

Yoshino, Mineo, Kazuhiko Imaizumi, Sachio Miyasaka, and Sueshige Seta. 1994. "Histological estimation of age at death using microradiographs of humeral compact bone." *Forensic Sci Int* 64(2-3):191-98.

Zhu, F. 1983. "Preliminary study of determination of bone age by microscopic method." *Acta Anthropol Sinica* 2(Abstract):142-51.

APPENDIX I

JOHN WILEY AND SONS LICENSE TERMS AND CONDITIONS

May 31, 2012

This is a License Agreement between Cheryl Hennig ("You") and John Wiley and Sons ("John Wiley and Sons") provided by Copyright Clearance Center ("CCC"). The license consists of your order details, the terms and conditions provided by John Wiley and Sons, and the payment terms and conditions.

All payments must be made in full to CCC. For payment instructions, please see information listed at the bottom of this form.

License Number	2882570682002
License date	Apr 05, 2012
Licensed content publisher	John Wiley and Sons
Licensed content publication	American Journal of Physical Anthropology
Licensed content title	Brief communication: The relation between standard error of the estimate and sample size of histomorphometric aging methods
Licensed content author	Cheryl Hennig, David Cooper
Licensed content date	Aug 1, 2011
Start page	658
End page	664
Type of use	Dissertation/Thesis
Requestor type	Author of this Wiley article
Format	Print and electronic
Portion	Full article
Will you be translating?	No
Order reference number	None
Total	**0.00 USD**

Terms and Conditions

TERMS AND CONDITIONS

This copyrighted material is owned by or exclusively licensed to John Wiley & Sons, Inc. or one of its group companies (each a "Wiley Company") or a society for whom a Wiley Company has exclusive publishing rights in relation to a particular journal (collectively WILEY"). By clicking "accept" in connection with completing this licensing transaction, you agree that the following terms and conditions apply to this transaction (along with the billing and payment terms and conditions established by the Copyright Clearance Center Inc., ("CCC's Billing and Payment terms and conditions"), at the time that you opened your Rightslink account (these are available at any time at http://myaccount.copyright.com)

Terms and Conditions

1. The materials you have requested permission to reproduce (the "Materials") are protected by copyright.

2. You are hereby granted a personal, non-exclusive, non-sublicensable, non-transferable, worldwide, limited license to reproduce the Materials for the purpose specified in the licensing process. This license is for a one-time use only with a maximum distribution equal to the number that you identified in the licensing process. Any form of republication granted by this licence must be completed within two years of the date of the grant of this licence (although copies prepared before may be distributed thereafter). The Materials shall not be used in any other manner or for any other purpose. Permission is granted subject to an appropriate acknowledgement given to the author, title of the material/book/journal and the publisher. You shall also duplicate the copyright notice that appears in the Wiley publication in your use of the Material. Permission is also granted on the understanding that nowhere in the text is a previously published source acknowledged for all or part of this Material. Any third party material is expressly excluded from this permission.

3. With respect to the Materials, all rights are reserved. Except as expressly granted by the terms of the license, no part of the Materials may be copied, modified, adapted (except for minor reformatting required by the new Publication), translated, reproduced, transferred or distributed, in any form or by any means, and no derivative works may be made based on the Materials without the prior permission of the respective copyright owner. You may not alter, remove or suppress in any manner any copyright, trademark or other notices displayed by the Materials. You may not license, rent, sell, loan, lease, pledge, offer as security, transfer or assign the Materials, or any of the rights granted to you hereunder to any other person.

4. The Materials and all of the intellectual property rights therein shall at all times remain the exclusive property of John Wiley & Sons Inc or one of its related companies (WILEY) or their respective licensors, and your interest therein is only that of having possession of and the right to reproduce the Materials pursuant to Section 2 herein during the continuance of this Agreement. You agree that you own no right, title or interest in or to the Materials or any of the intellectual property rights therein. You shall have no rights hereunder other than the license as provided for above in Section 2. No right, license or interest to any trademark, trade name, service mark or other branding ("Marks") of WILEY or its licensors is granted hereunder, and you agree that you shall not assert any such right, license or interest with respect thereto.

5. NEITHER WILEY NOR ITS LICENSORS MAKES ANY WARRANTY OR REPRESENTATION OF ANY KIND TO YOU OR ANY THIRD PARTY, EXPRESS, IMPLIED OR STATUTORY, WITH RESPECT TO THE MATERIALS OR THE ACCURACY OF ANY INFORMATION CONTAINED IN THE MATERIALS, INCLUDING, WITHOUT LIMITATION, ANY IMPLIED WARRANTY OF MERCHANTABILITY, ACCURACY, SATISFACTORY QUALITY, FITNESS FOR A PARTICULAR PURPOSE, USABILITY, INTEGRATION OR NON-INFRINGEMENT AND ALL SUCH WARRANTIES ARE HEREBY EXCLUDED BY WILEY AND ITS LICENSORS AND WAIVED BY YOU.

6. WILEY shall have the right to terminate this Agreement immediately upon breach of this Agreement by you.

7. You shall indemnify, defend and hold harmless WILEY, its Licensors and their respective directors, officers, agents and employees, from and against any actual or threatened claims, demands, causes of action or proceedings arising from any breach of this Agreement by you.

8. IN NO EVENT SHALL WILEY OR ITS LICENSORS BE LIABLE TO YOU OR ANY OTHER PARTY OR ANY OTHER PERSON OR ENTITY FOR ANY SPECIAL, CONSEQUENTIAL, INCIDENTAL, INDIRECT, EXEMPLARY OR PUNITIVE DAMAGES, HOWEVER CAUSED, ARISING OUT OF OR IN CONNECTION WITH THE DOWNLOADING, PROVISIONING, VIEWING OR USE OF THE MATERIALS REGARDLESS OF THE FORM OF ACTION, WHETHER FOR BREACH OF CONTRACT, BREACH OF WARRANTY, TORT, NEGLIGENCE, INFRINGEMENT OR OTHERWISE (INCLUDING, WITHOUT LIMITATION, DAMAGES BASED ON LOSS OF PROFITS, DATA, FILES, USE, BUSINESS OPPORTUNITY OR CLAIMS OF THIRD PARTIES), AND WHETHER OR NOT THE PARTY HAS BEEN ADVISED OF THE POSSIBILITY OF SUCH DAMAGES. THIS LIMITATION SHALL APPLY NOTWITHSTANDING ANY FAILURE OF ESSENTIAL PURPOSE OF ANY LIMITED REMEDY PROVIDED HEREIN.

9. Should any provision of this Agreement be held by a court of competent jurisdiction to be illegal, invalid, or unenforceable, that provision shall be deemed amended to achieve as nearly as possible the same economic effect as the original provision, and the legality, validity and enforceability of the remaining provisions of this Agreement shall not be affected or impaired thereby.

10. The failure of either party to enforce any term or condition of this Agreement shall not constitute a waiver of either party's right to enforce each and every term and condition of this Agreement. No breach under this agreement shall be deemed waived or excused by either party unless such waiver or consent is in writing signed by the party granting such waiver or consent. The waiver by or

consent of a party to a breach of any provision of this Agreement shall not operate or be construed as a waiver of or consent to any other or subsequent breach by such other party.

11. This Agreement may not be assigned (including by operation of law or otherwise) by you without WILEY's prior written consent.

12. Any fee required for this permission shall be non-refundable after thirty (30) days from receipt.

13. These terms and conditions together with CCC's Billing and Payment terms and conditions (which are incorporated herein) form the entire agreement between you and WILEY concerning this licensing transaction and (in the absence of fraud) supersedes all prior agreements and representations of the parties, oral or written. This Agreement may not be amended except in writing signed by both parties. This Agreement shall be binding upon and inure to the benefit of the parties' successors, legal representatives, and authorized assigns.

14. In the event of any conflict between your obligations established by these terms and conditions and those established by CCC's Billing and Payment terms and conditions, these terms and conditions shall prevail.

15. WILEY expressly reserves all rights not specifically granted in the combination of (i) the license details provided by you and accepted in the course of this licensing transaction, (ii) these terms and conditions and (iii) CCC's Billing and Payment terms and conditions.

16. This Agreement will be void if the Type of Use, Format, Circulation, or Requestor Type was misrepresented during the licensing process.

17. This Agreement shall be governed by and construed in accordance with the laws of the State of New York, USA, without regards to such state's conflict of law rules. Any legal action, suit or proceeding arising out of or relating to these Terms and Conditions or the breach thereof shall be instituted in a court of competent jurisdiction in New York County in the State of New York in the United States of America and each party hereby consents and submits to the personal jurisdiction of such court, waives any objection to venue in such court and consents to service of process by registered or certified mail, return receipt requested, at the last known address of such party.

Wiley Open Access Terms and Conditions

All research articles published in Wiley Open Access journals are fully open access: immediately freely available to read, download and share. Articles are published under the terms of the Creative Commons Attribution Non Commercial License. which permits use, distribution and reproduction in any medium, provided the original work is properly cited and is not used for commercial purposes. The license is subject to the Wiley Open Access terms and conditions:
Wiley Open Access articles are protected by copyright and are posted to repositories and websites in accordance with the terms of the Creative Commons Attribution Non Commercial License. At the time of deposit, Wiley Open Access articles include all changes made during peer review, copyediting, and publishing. Repositories and websites that host the article are responsible for incorporating any publisher-supplied amendments or retractions issued subsequently.
Wiley Open Access articles are also available without charge on Wiley's publishing platform, **Wiley Online Library** or any successor sites.

Use by non-commercial users

For non-commercial and non-promotional purposes individual users may access, download, copy, display and redistribute to colleagues Wiley Open Access articles, as well as adapt, translate, text- and data-mine the content subject to the following conditions:

 The authors' moral rights are not compromised. These rights include the right of "paternity" (also known as "attribution" - the right for the author to be identified as such) and "integrity" (the right for the author not to have the work altered in such a way that the author's reputation or integrity may be impugned).

 Where content in the article is identified as belonging to a third party, it is the obligation of the user to ensure that any reuse complies with the copyright policies of the owner of that content.

 If article content is copied, downloaded or otherwise reused for non-commercial research and education purposes, a link to the appropriate bibliographic citation (authors, journal, article title, volume, issue, page numbers, DOI and the link to the definitive published version on Wiley Online Library) should be maintained. Copyright notices and disclaimers must not be deleted.

 Any translations, for which a prior translation agreement with Wiley has not been agreed, must prominently display the statement: "This is an unofficial translation of an article that appeared in a Wiley publication. The publisher has not endorsed this translation."
Use by commercial "for-profit" organisations

Use of Wiley Open Access articles for commercial, promotional, or marketing purposes requires further explicit permission from Wiley and will be subject to a fee. Commercial purposes include:

- Copying or downloading of articles, or linking to such articles for further redistribution, sale or licensing;
- Copying, downloading or posting by a site or service that incorporates advertising with such content;

- The inclusion or incorporation of article content in other works or services (other than normal quotations with an appropriate citation) that is then available for sale or licensing, for a fee (for example, a compilation produced for marketing purposes, inclusion in a sales pack)

- Use of article content (other than normal quotations with appropriate citation) by for-profit organisations for promotional purposes

- Linking to article content in e-mails redistributed for promotional, marketing or educational purposes;

- Use for the purposes of monetary reward by means of sale, resale, licence, loan, transfer or other form of commercial exploitation such as marketing products

- Print reprints of Wiley Open Access articles can be purchased from: corporatesales@wiley.com

Other Terms and Conditions:

BY CLICKING ON THE "I AGREE..." BOX, YOU ACKNOWLEDGE THAT YOU HAVE READ AND FULLY UNDERSTAND EACH OF THE SECTIONS OF AND PROVISIONS SET FORTH IN THIS AGREEMENT AND THAT YOU ARE IN AGREEMENT WITH AND ARE WILLING TO ACCEPT ALL OF YOUR OBLIGATIONS AS SET FORTH IN THIS AGREEMENT.

v1.7

If you would like to pay for this license now, please remit this license along with your payment made payable to "COPYRIGHT CLEARANCE CENTER" otherwise you will be invoiced within 48 hours of the license date. Payment should be in the form of a check or money order referencing your account number and this invoice number RLNK500755284. Once you receive your invoice for this order, you may pay your invoice by credit card. Please follow instructions provided at that time.

Make Payment To:
Copyright Clearance Center
Dept 001
P.O. Box 843006
Boston, MA 02284-3006

For suggestions or comments regarding this order, contact RightsLink Customer Support: customercare@copyright.com or +1-877-622-5543 (toll free in the US) or +1-978-646-2777.

Gratis licenses (referencing $0 in the Total field) are free. Please retain this printable license for your reference. No payment is required.

APPENDIX II

II.I Steps for Histology

1) Cut histology sections to approximately 150 µm and hand grind down to approximately 100 µm and place sections in ultrasonicator for approximately 5 to 10 minutes

2) Mount specimen onto slide using a mounting medium and let set for at least 48 hours. Once mounting medium has set, the specimens can be imaged under the microscope. Tiled or stitched images can be created using an automated stage

a) Choose an appropriate magnification and adjust microscope settings such as lighting and white balance and focus specimen accordingly and capture images

3) Once a tiled/stitched image is created of the histological section, import both histology image and 3D scan data into ImageJ. Find the difference in size between the CT slice and histology section and create matching a 3mm regions of interest (ROI)

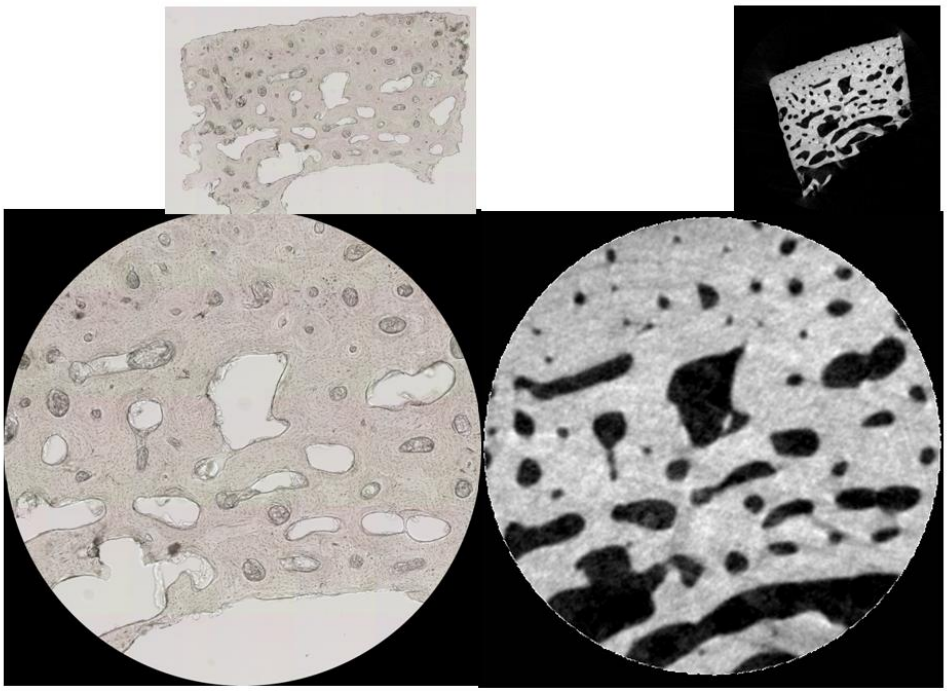

Figure II.1: Figure showing matching histology section and micro-CT slice

4) Create an new ROI set in ImageJ and trace osteons

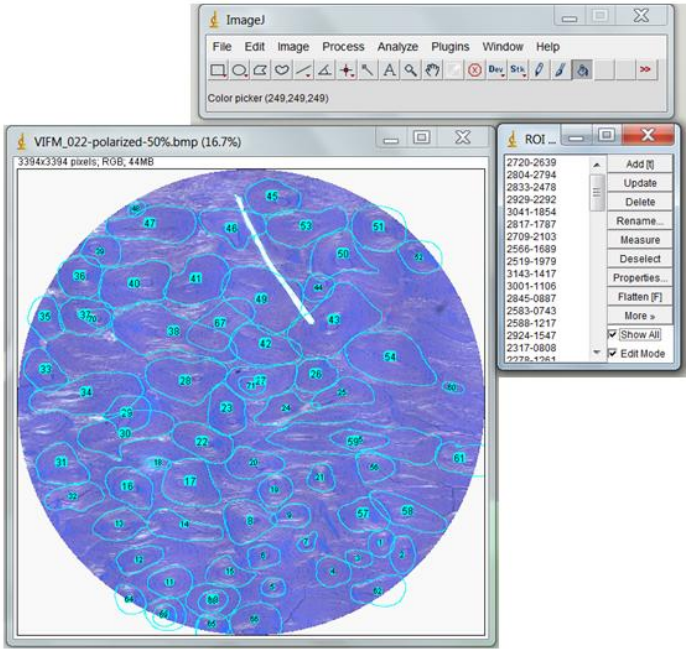

Figure II.2: Figure of ROI manager with histology section and outlined osteons in ImageJ.

5) Import image of histology section into Amira

II.II Steps for Micro-CT

1) Develop a scan and reconstruction protocol that works for your desired purpose (**NOTE:** steps and achievable resolutions will vary depending on the desktop micro-CT system you are using)

2) Import scan data and histology image into ImageJ and find the best matching scan slice to the histology section

3) Import scans into CT Analyser and crop the regions of interest.

4) Import scan data into Amira (choose appropriate x, y, and z dimensions based on the size difference of CT slices and histology sections) and choose an appropriate threshold to create the isosurface

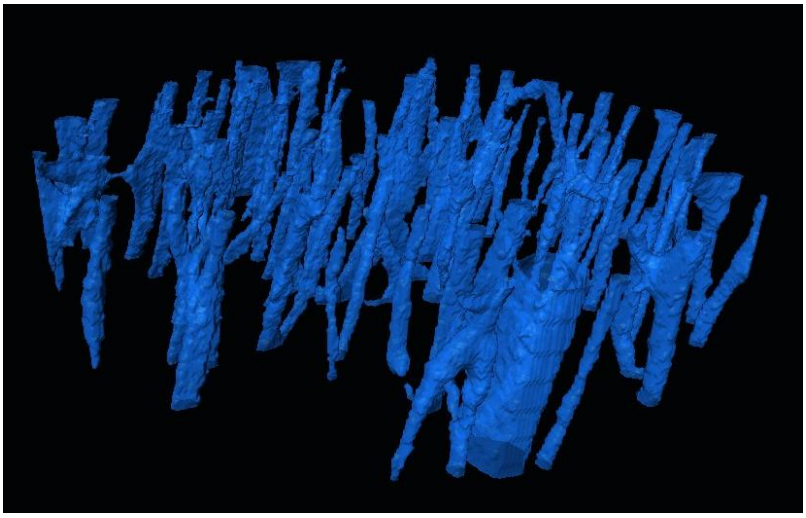

Figure II.3: isosurface of volume render in Amira

5) Create and edit the skeletonizations of the isosurface

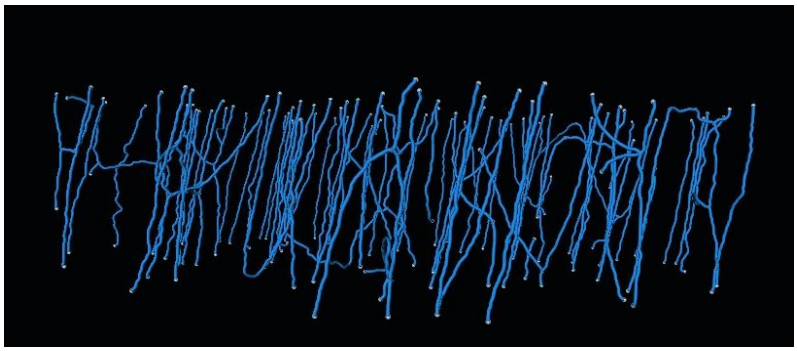

Figure II.4: Skeletonization from an isosurface in Amira

6) Rotate 3D render so that it aligns with the histology slice. (**NOTE**: You will need to do this for the skeletonizations and linesets as well).

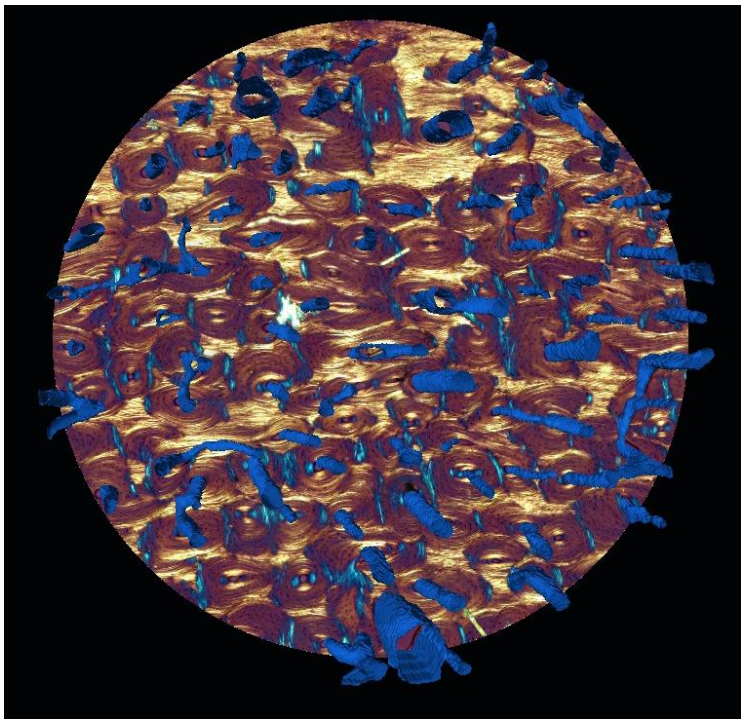

Figure II.5: Histology section superimposed into the isosurface of a volume renders

7) Create lineset from the skeletonizations (**NOTE:** you must do this after you edit the skeletonizations)

8) In ImageJ select install and run Text Skeleton V.10.1 macro

9) Import back into Amira and match the individual lines with the individual outlines of the ROI from ImageJ

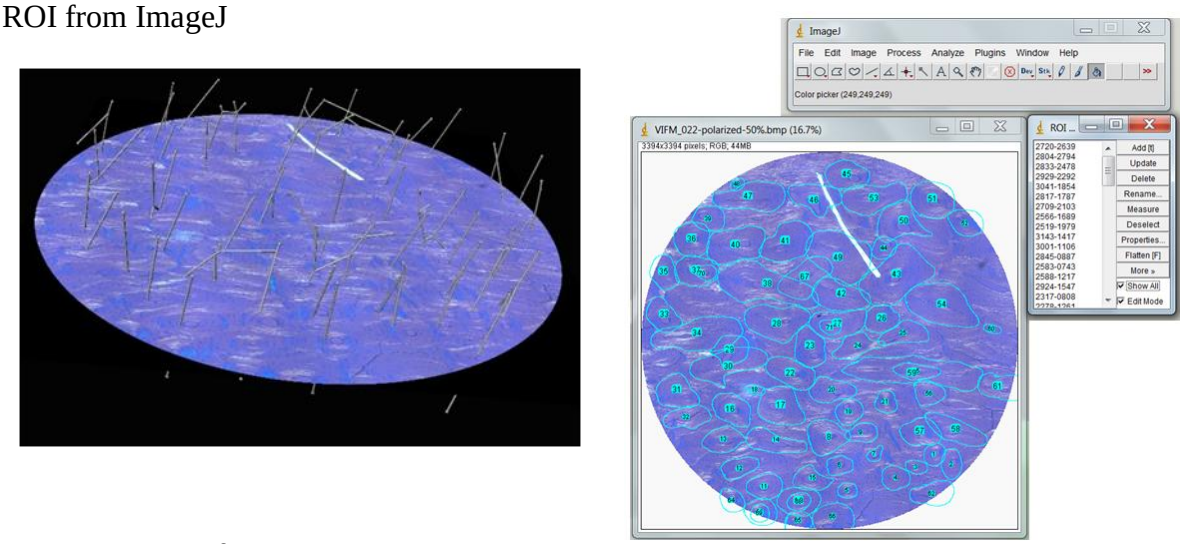

Figure II.6: Figure of lineset and outlined osteons. Use the individuals outlines created in ImageJ and match them to the appropriate line in Amira.

APPENDIX III

III.I Circularity

Underlying assumption: osteons are cylindrical structures

Let Area = Area of Ellipse

Let Perimeter = Perimeter of Ellipse

Circularity is calculated using the following equation:

$$\text{Circularity} = 4\pi\left(\frac{\text{Area}}{(\text{Perimeter})^2}\right)$$

Equation 4.1

Area is calculated by the equation:

$$\text{Area} = \pi\left(\frac{1}{2}\text{Minor Axis}\right)\left(\frac{1}{2}\text{Major Axis}\right)$$

But since

$$\text{Major Axis} = \frac{\text{Minor Axis}}{\sin\phi}$$

where the Minor Axis is an observable and measurable distance and sin ϕ is an observable and measureable angle,

Area can be written as:

$$\text{Area} = \pi * \left(\frac{1}{2}\text{Minor Axis}\right)\left(\frac{\frac{1}{2}\text{ Minor Axis}}{\sin\phi}\right)$$

Which can be simplified to:

$$\text{Area} = \pi\left(\frac{\frac{1}{4}\text{ (Minor Axis)}^2}{\sin\phi}\right)$$

Therefore, circularity can be expressed and simplified as follows:

$$\text{Circularity} = 4\pi\left(\frac{\text{Area}}{(\text{Perimeter})^2}\right)$$

Equation 4.1

$$\text{Circularity} = 4\pi\left(\frac{\left(\frac{\frac{1}{4}\pi\text{ (Minoir Axis)}^2}{\sin\phi}\right)}{(\text{Perimeter})^2}\right)$$

$$\text{Circularity} = 4\pi\left(\frac{\frac{1}{4}\pi\text{ (Minor Axis)}^2}{\sin\phi}\right)\left(\frac{1}{(\text{Perimeter})^2}\right)$$

$$\text{Circularity} = \left(\frac{1}{4}\right)4\pi\pi\left(\frac{(\text{Minor Axis})^2}{\sin\phi}\right)\left(\frac{1}{(\text{Perimeter})^2}\right)$$

$$\text{Circularity} = 1\pi^2\left(\frac{(\text{Minor Axis})^2}{\sin\phi\ (\text{Perimeter})^2}\right)$$

Thus, the final equation for circularity can be written as:

$$\text{Circularity} = \pi^2 \left(\frac{(\text{Minor Axis})^2}{\sin \phi \, (\text{Perimeter})^2} \right)$$

Equation 4.3

III.II Aspect Ratio

Underlying assumption: osteons are cylindrical structures.

The Aspect Ratio is calculated using the equation:

$$\text{Aspect Ratio} = \frac{\text{Minor Axis}}{\text{Major Axis}}$$

Equation 4.2

But since

$$\text{Major Axis} = \frac{\text{Minor Axis}}{\sin \phi}$$

AR can be expressed and simplified as follows:

$$\text{Aspect Ratio} = \frac{\text{Minor Axis}}{\left(\frac{\text{Minor Axis}}{\sin \phi} \right)}$$

$$\text{Aspect Ratio} = \text{Minor Axis} \left(\frac{\sin \phi}{\text{Minor Axis}} \right)$$

Therefore, the final equation for A_R can be presented as:

$$\text{Aspect Ratio} = \sin \phi$$

Equation 4.4

APPENDIX IV

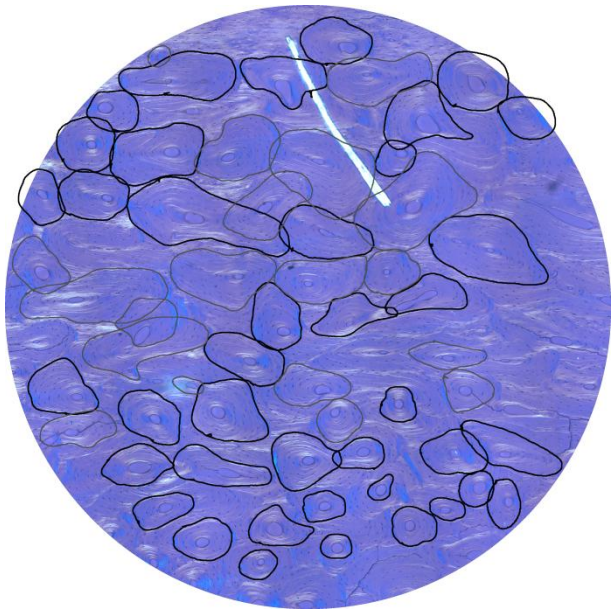

Figure IV.1: VIFM_022 (22 yrs) - above. The osteons that were included (black) and excluded (grey) from the analysis. Those osteons outlined in black were included in the analysis and had matching 3D data. These osteons had a single matching line passing through the outlined region. Those outlines in grey did not have matching 3D data or had multiple lines passing through and were therefore excluded from analysis

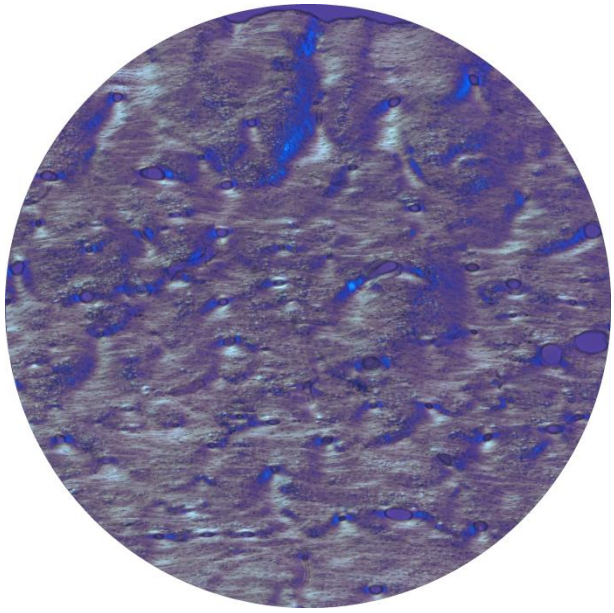

Figure IV.2: VIFM_035 (24 yrs). Note this specimen has all primary canals and was therefore not included in the analysis

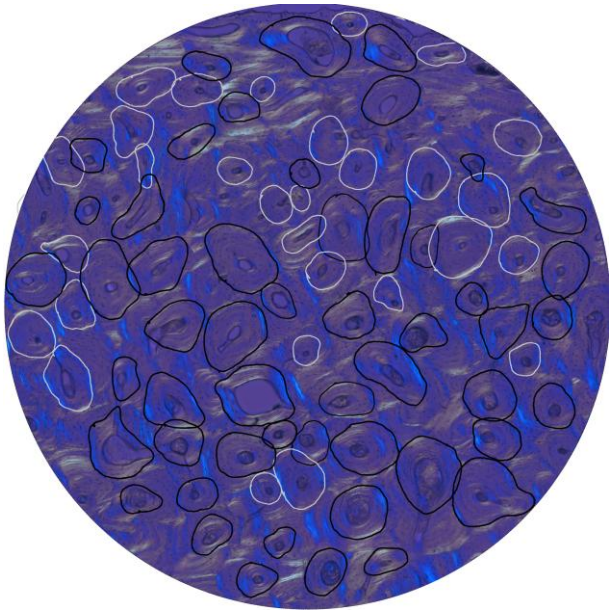

Figure IV.3: VIFM_053 (57 yrs) - above. The osteons that were included (black) and excluded (grey) from the analysis. Those osteons outlined in black were included in the analysis and had matching 3D data. These osteons had a single matching line passing through the outlined region. Those outlines in grey did not have matching 3D data or had multiple lines passing through and were therefore excluded from analysis

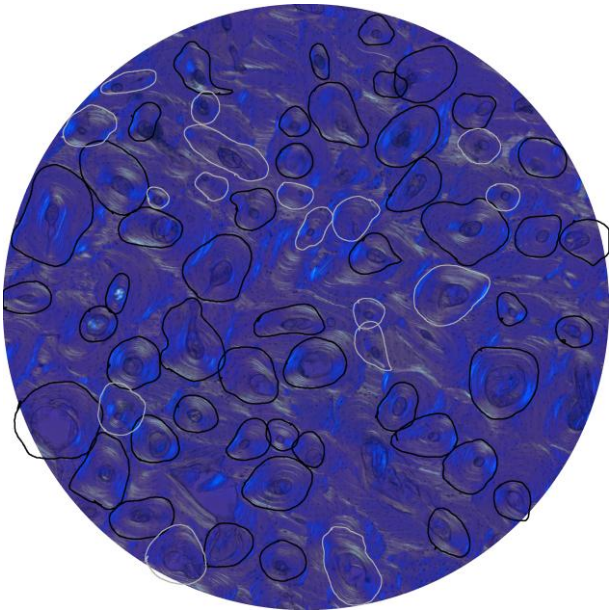

Figure IV.4: VIFM_056 (65 yrs) - above. The osteons that were included (black) and excluded (grey) from the analysis. Those osteons outlined in black were included in the analysis and had matching 3D data. These osteons had a single matching line passing through the outlined region. Those outlines in grey did not have matching 3D data or had multiple lines passing through and were therefore excluded from analysis

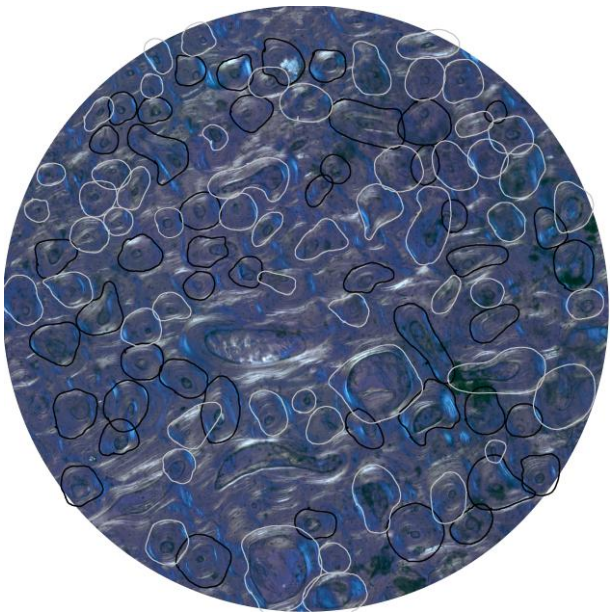

Figure IV.5: VIFM_063(64 yrs) - above. The osteons that were included (black) and excluded (grey) from the analysis. Those osteons outlined in black were included in the analysis and had matching 3D data. These osteons had a single matching line passing through the outlined region. Those outlines in grey did not have matching 3D data or had multiple lines passing through and were therefore excluded from analysis

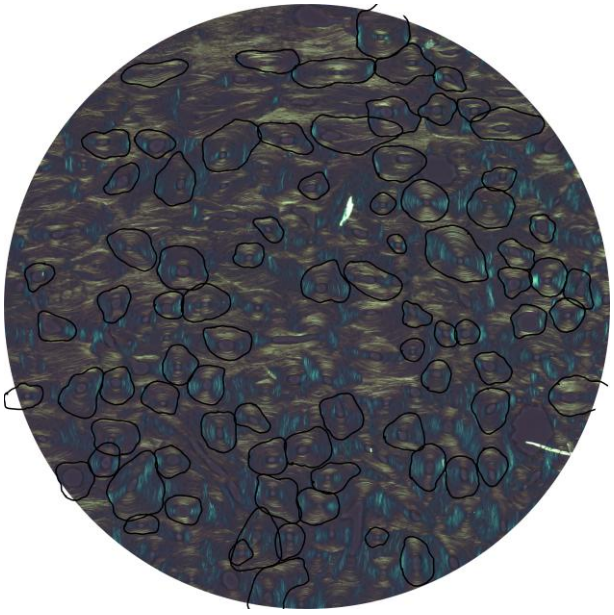

Figure IV.6: VIFM_081 (30 yrs) - above. The osteons that were included (black) and excluded (grey) from the analysis. Those osteons outlined in black were included in the analysis and had matching 3D data. These osteons had a single matching line passing through the outlined region. Those outlines in grey did not have matching 3D data or had multiple lines passing through and were therefore excluded from analysis

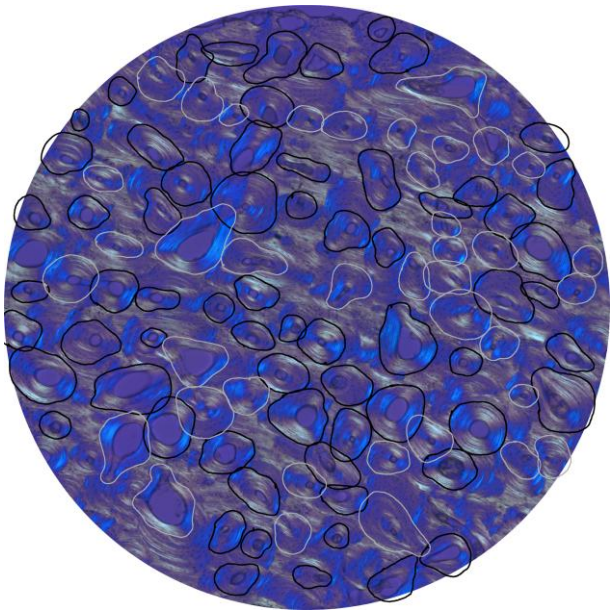

Figure IV.7: VIFM_094 (86yrs) - above. The osteons that were included (black) and excluded (grey) from the analysis. Those osteons outlined in black were included in the analysis and had matching 3D data. These osteons had a single matching line passing through the outlined region. Those outlines in grey did not have matching 3D data or had multiple lines passing through and were therefore excluded from analysis

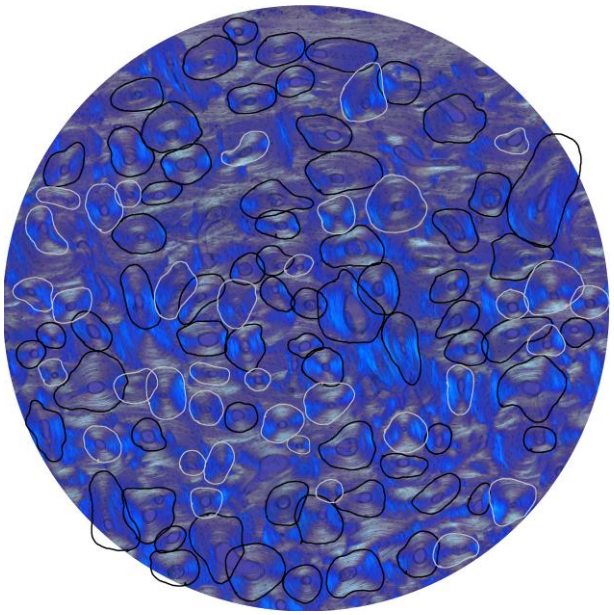

Figure IV.8: VIFM_109 (52yrs) - above. The osteons that were included (black) and excluded (grey) from the analysis. Those osteons outlined in black were included in the analysis and had matching 3D data. These osteons had a single matching line passing through the outlined region. Those outlines in grey did not have matching 3D data or had multiple lines passing through and were therefore excluded from analysis

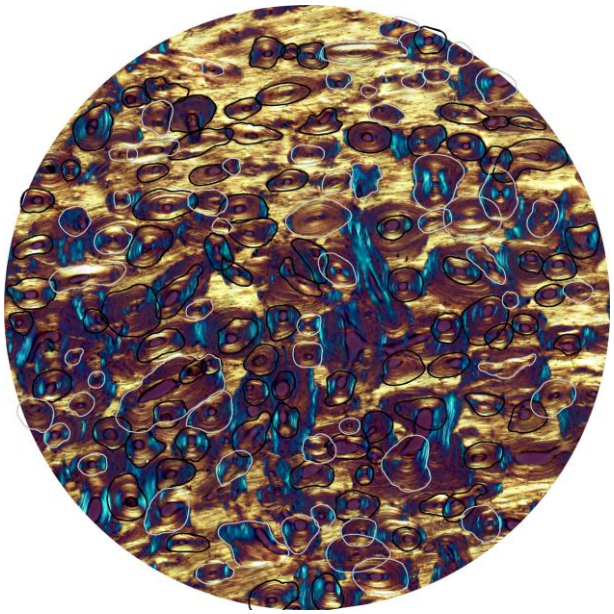

Figure IV.9: VIFM_113 (66 yrs) - above. The osteons that were included (black) and excluded (grey) from the analysis. Those osteons outlined in black were included in the analysis and had matching 3D data. These osteons had a single matching line passing through the outlined region. Those outlines in grey did not have matching 3D data or had multiple lines passing through and were therefore excluded from analysis

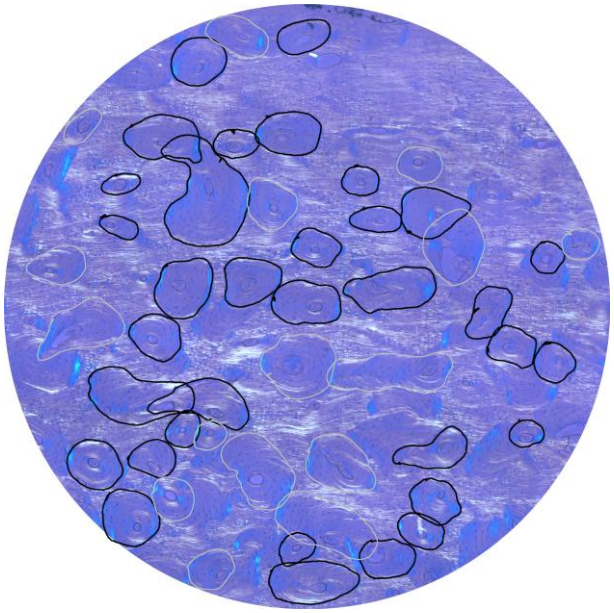

Figure IV.10: VIFM_117 (23 yrs) - above. The osteons that were included (black) and excluded (grey) from the analysis. Those osteons outlined in black were included in the analysis and had matching 3D data. These osteons had a single matching line passing through the outlined region. Those outlines in grey did not have matching 3D data or had multiple lines passing through and were therefore excluded from analysis

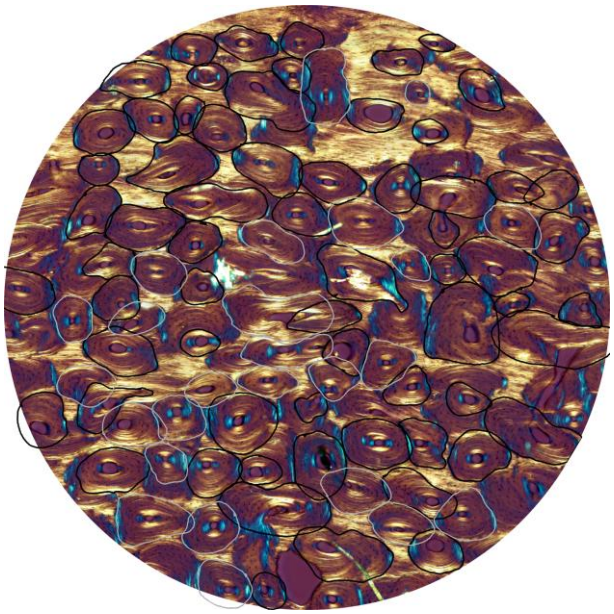

Figure IV.11: VIFM_126 (21 yrs) - above. The osteons that were included (black) and excluded (grey) from the analysis. Those osteons outlined in black were included in the analysis and had matching 3D data. These osteons had a single matching line passing through the outlined region. Those outlines in grey did not have matching 3D data or had multiple lines passing through and were therefore excluded from analysis

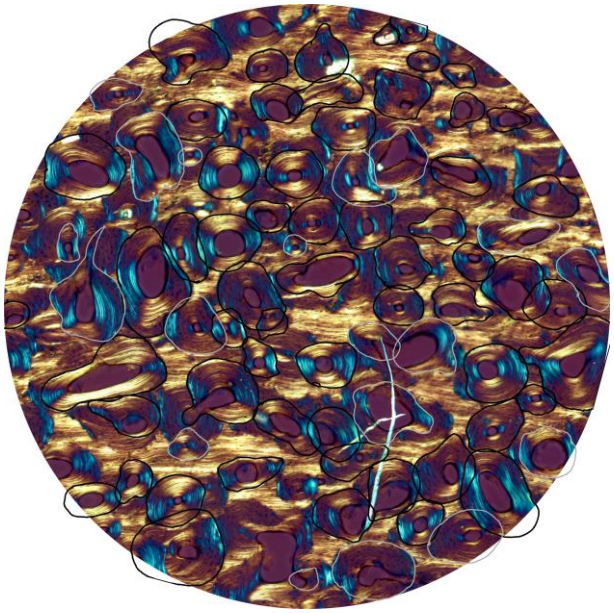

Figure IV.12: VIFM_127 (55 yrs) - above. The osteons that were included (black) and excluded (grey) from the analysis. Those osteons outlined in black were included in the analysis and had matching 3D data. These osteons had a single matching line passing through the outlined region. Those outlines in grey did not have matching 3D data or had multiple lines passing through and were therefore excluded from analysis

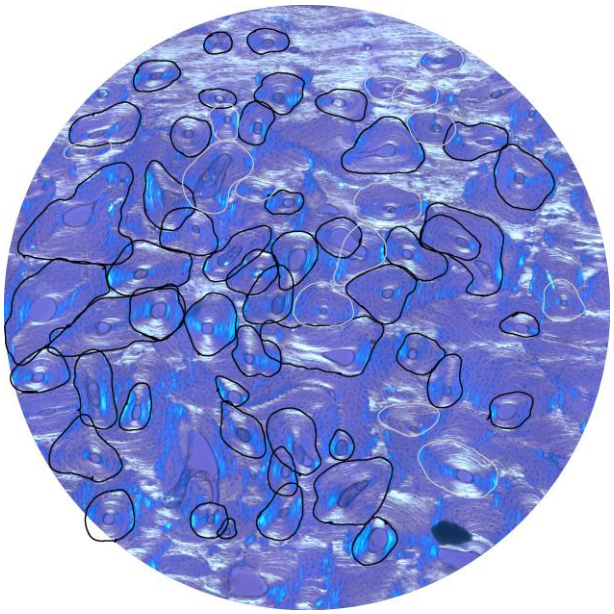

Figure IV.13: VIFM_128 (33 yrs) - above. The osteons that were included (black) and excluded (grey) from the analysis. Those osteons outlined in black were included in the analysis and had matching 3D data. These osteons had a single matching line passing through the outlined region. Those outlines in grey did not have matching 3D data or had multiple lines passing through and were therefore excluded from analysis

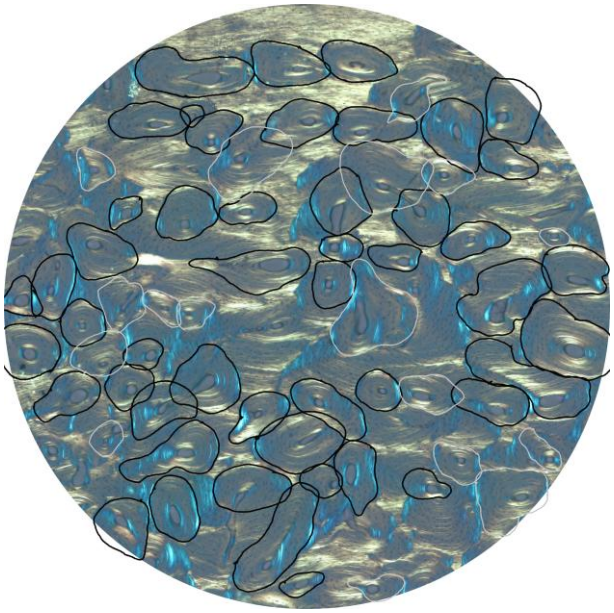

Figure IV.14: VIFM_134 (28 yrs) - above. The osteons that were included (black) and excluded (grey) from the analysis. Those osteons outlined in black were included in the analysis and had matching 3D data. These osteons had a single matching line passing through the outlined region. Those outlines in grey did not have matching 3D data or had multiple lines passing through and were therefore excluded from analysis

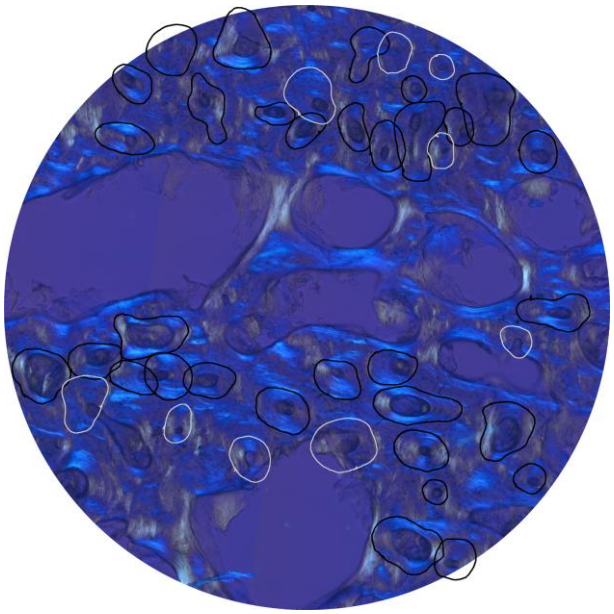

Figure IV.15: VIFM_140 (84yrs) - above. The osteons that were included (black) and excluded (grey) from the analysis. Those osteons outlined in black were included in the analysis and had matching 3D data. These osteons had a single matching line passing through the outlined region. Those outlines in grey did not have matching 3D data or had multiple lines passing through and were therefore excluded from analysis

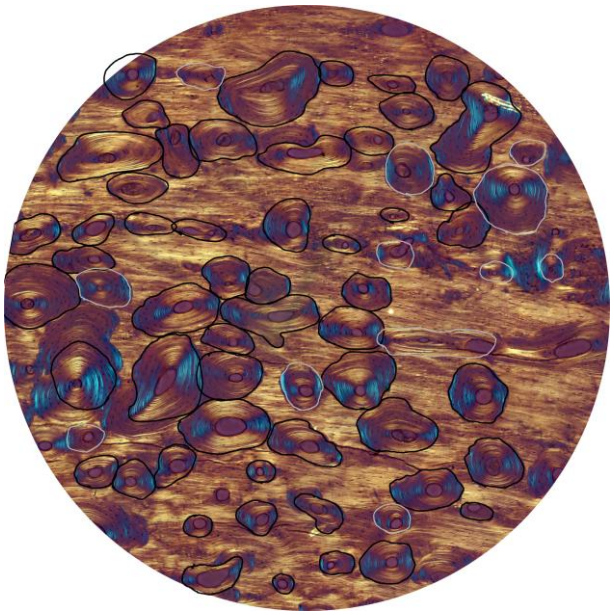

Figure IV.16: VIFM_156 (41 yrs) - above. The osteons that were included (black) and excluded (grey) from the analysis. Those osteons outlined in black were included in the analysis and had matching 3D data. These osteons had a single matching line passing through the outlined region. Those outlines in grey did not have matching 3D data or had multiple lines passing through and were therefore excluded from analysis

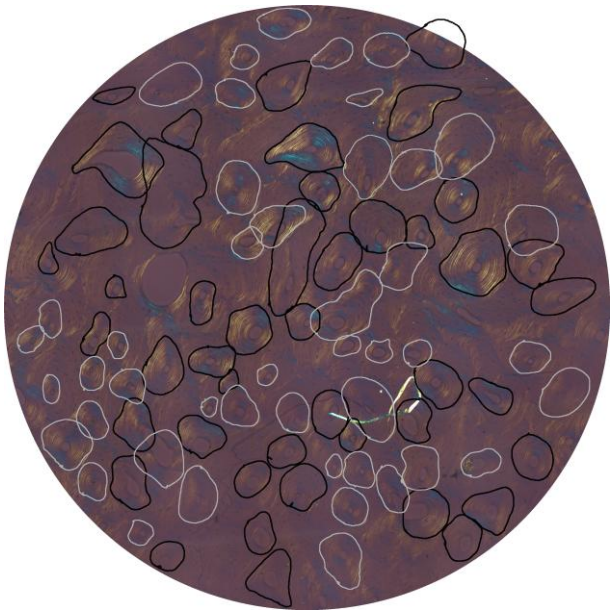

Figure IV.17: VIFM_172 (26yrs) - above. The osteons that were included (black) and excluded (grey) from the analysis. Those osteons outlined in black were included in the analysis and had matching 3D data. These osteons had a single matching line passing through the outlined region. Those outlines in grey did not have matching 3D data or had multiple lines passing through and were therefore excluded from analysis

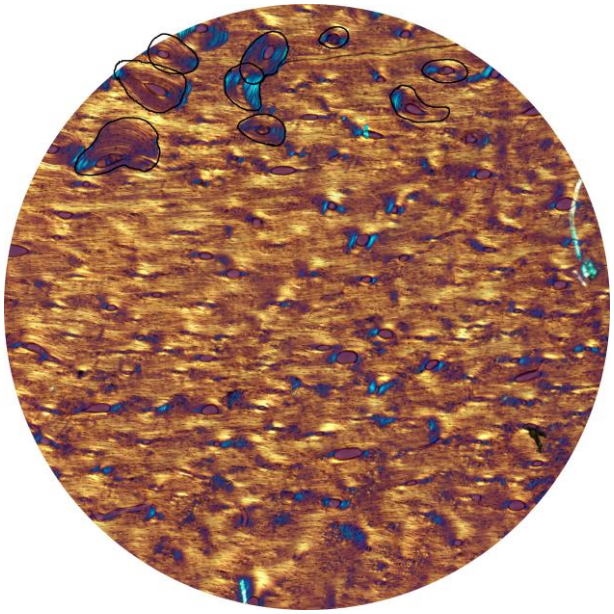

Figure IV.18: VIFM_189 (20 yrs) - above. The osteons that were included (black) and excluded (grey) from the analysis. Those osteons outlined in black were included in the analysis and had matching 3D data. These osteons had a single matching line passing through the outlined region. Those outlines in grey did not have matching 3D data or had multiple lines passing through and were therefore excluded from analysis

Figure IV.19: VIFM376 (67 yrs) - above. The osteons that were included (black) and excluded (grey) from the analysis. Those osteons outlined in black were included in the analysis and had matching 3D data. These osteons had a single matching line passing through the outlined region. Those outlines in grey did not have matching 3D data or had multiple lines passing through and were therefore excluded from analysis

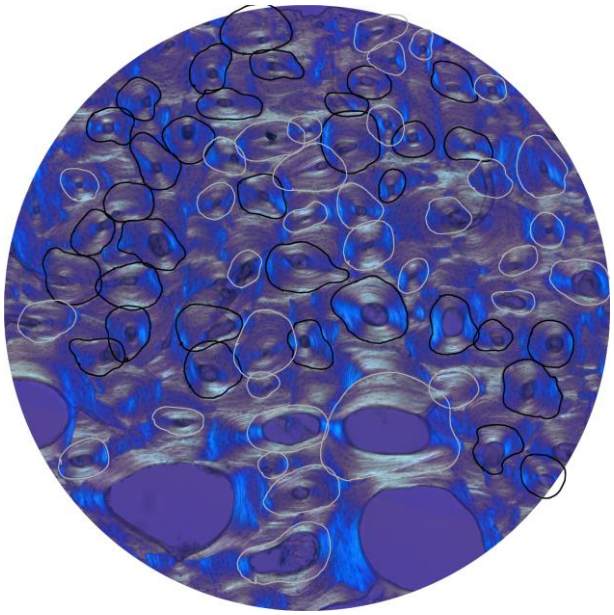

Figure IV.20: VIFM_399 (70 yrs) - above. The osteons that were included (black) and excluded (grey) from the analysis. Those osteons outlined in black were included in the analysis and had matching 3D data. These osteons had a single matching line passing through the outlined region. Those outlines in grey did not have matching 3D data or had multiple lines passing through and were therefore excluded from analysis

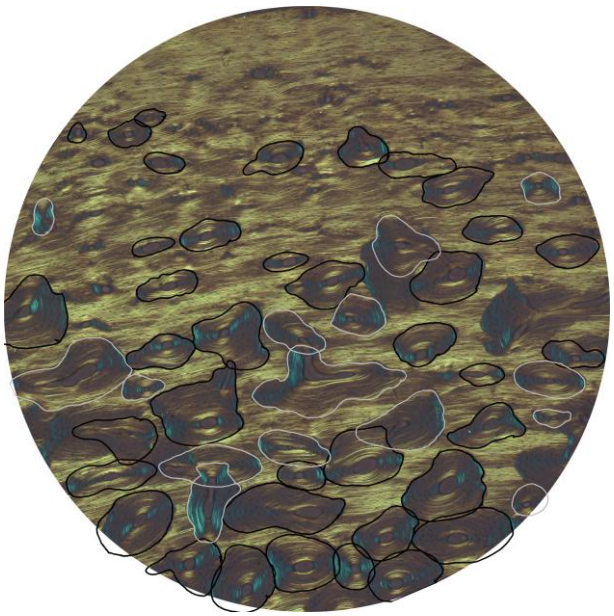

Figure IV. 21: VIFM_406 (20 yrs) - above. The osteons that were included (black) and excluded (grey) from the analysis. Those osteons outlined in black were included in the analysis and had matching 3D data. These osteons had a single matching line passing through the outlined region. Those outlines in grey did not have matching 3D data or had multiple lines passing through and were therefore excluded from analysis

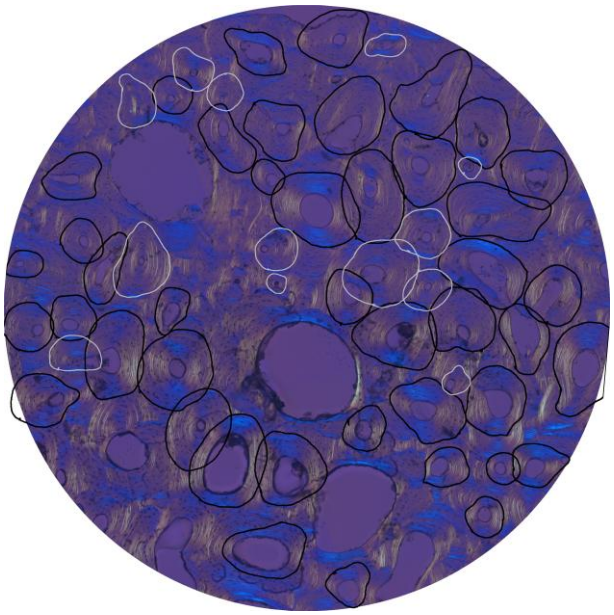

Figure IV.22: VIFM_411 (78 yrs) - above. The osteons that were included (black) and excluded (grey) from the analysis. Those osteons outlined in black were included in the analysis and had matching 3D data. These osteons had a single matching line passing through the outlined region. Those outlines in grey did not have matching 3D data or had multiple lines passing through and were therefore excluded from analysis

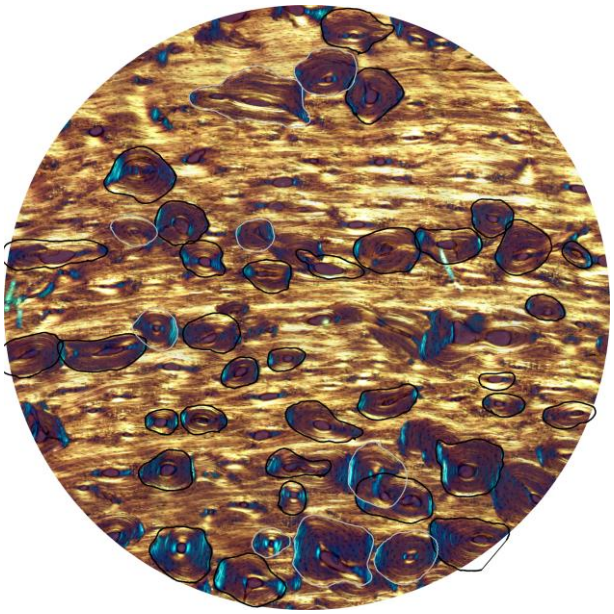

Figure IV.23: VIFM_412 (41 yrs) - above. The osteons that were included (black) and excluded (grey) from the analysis. Those osteons outlined in black were included in the analysis and had matching 3D data. These osteons had a single matching line passing through the outlined region. Those outlines in grey did not have matching 3D data or had multiple lines passing through and were therefore excluded from analysis

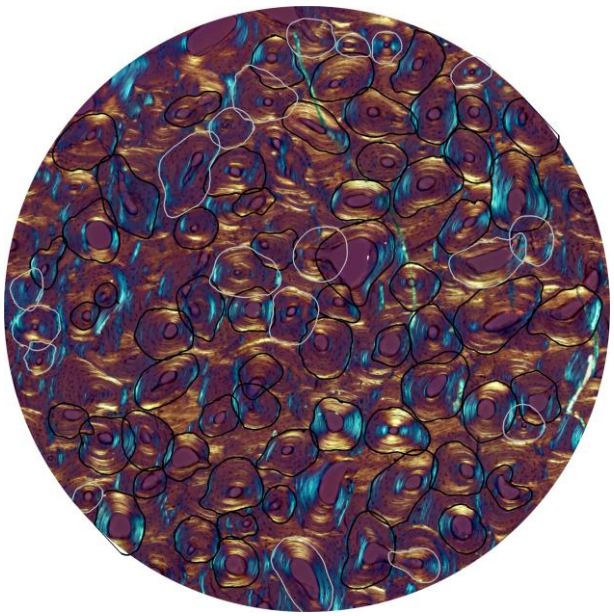

Figure IV.24: VIFM_412 (41 yrs) - above. The osteons that were included (black) and excluded (grey) from the analysis. Those osteons outlined in black were included in the analysis and had matching 3D data. These osteons had a single matching line passing through the outlined region. Those outlines in grey did not have matching 3D data or had multiple lines passing through and were therefore excluded from analysis

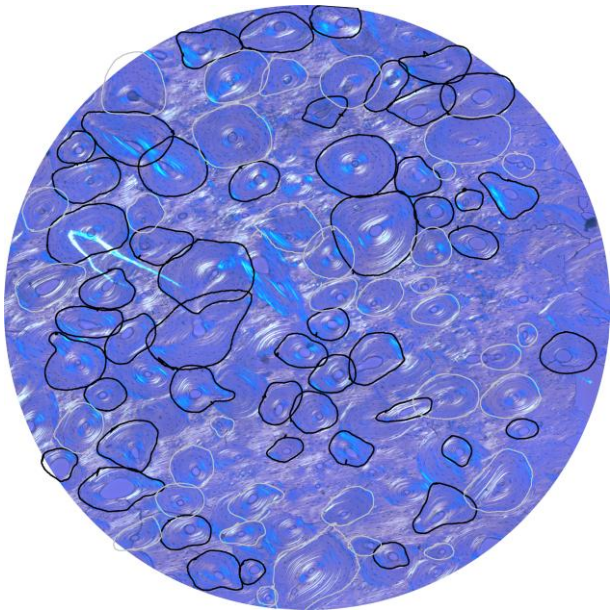

Figure IV.25: VIFM_432 (49 yrs) - above. The osteons that were included (black) and excluded (grey) from the analysis. Those osteons outlined in black were included in the analysis and had matching 3D data. These osteons had a single matching line passing through the outlined region. Those outlines in grey did not have matching 3D data or had multiple lines passing through and were therefore excluded from analysis

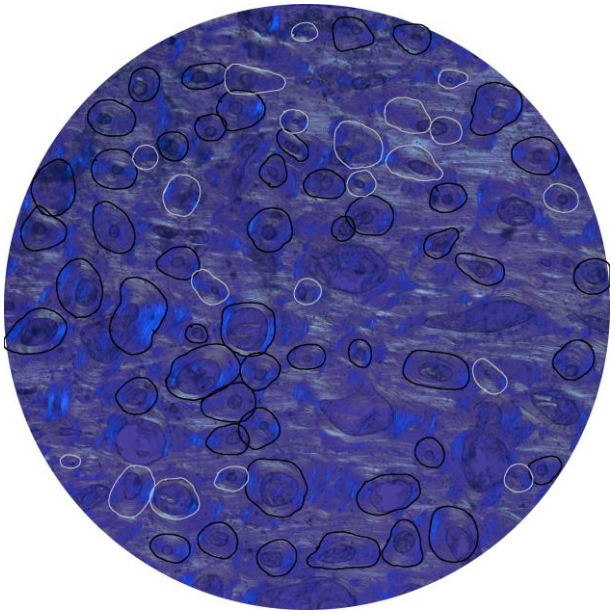

Figure IV.26: VIFM_436 (74 yrs) - above. The osteons that were included (black) and excluded (grey) from the analysis. Those osteons outlined in black were included in the analysis and had matching 3D data. These osteons had a single matching line passing through the outlined region. Those outlines in grey did not have matching 3D data or had multiple lines passing through and were therefore excluded from analysis

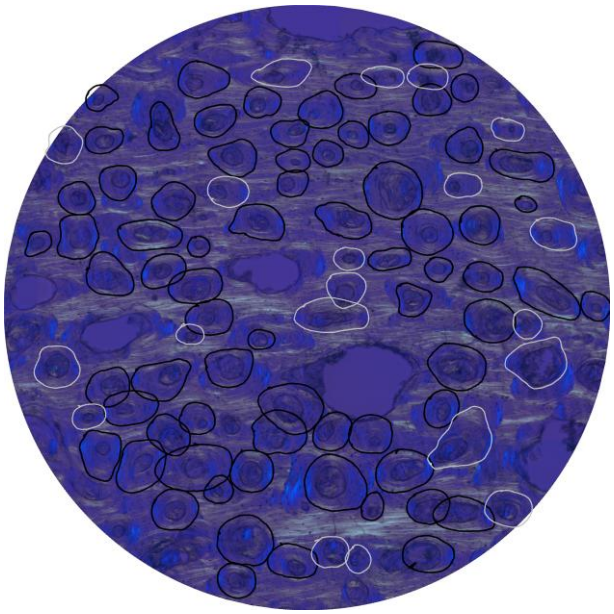

Figure IV.27: VIFM_439 (61 yrs) - above. The osteons that were included (black) and excluded (grey) from the analysis. Those osteons outlined in black were included in the analysis and had matching 3D data. These osteons had a single matching line passing through the outlined region. Those outlines in grey did not have matching 3D data or had multiple lines passing through and were therefore excluded from analysis

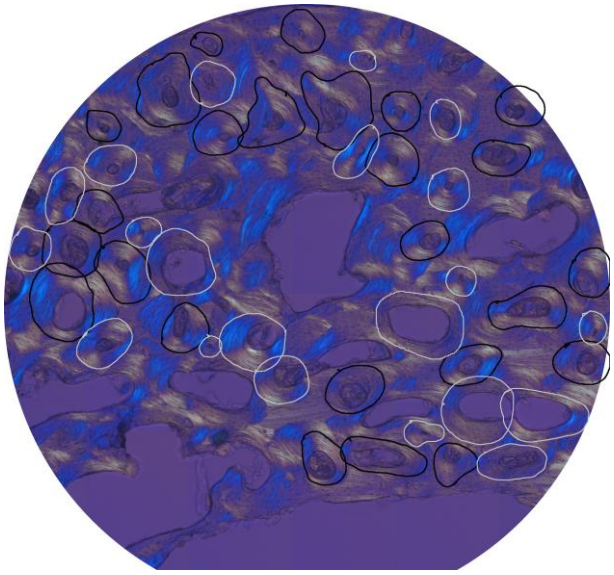

Figure IV.28: VIFM_496 (76 yrs) - above. The osteons that were included (black) and excluded (grey) from the analysis. Those osteons outlined in black were included in the analysis and had matching 3D data. These osteons had a single matching line passing through the outlined region. Those outlines in grey did not have matching 3D data or had multiple lines passing through and were therefore excluded from analysis